UNIVERSITÀ
DEGLI STUDI
FIRENZE

DOCTORAL PROGRAMME IN INDUSTRIAL ENGINEERING

XXXIV

Development of a hierarchical architecture for real-time autonomous vehicle control

SSD ING/IND-14

Doctoral Candidate

Margherita Montani

Supervisors

PhD. Prof. Renzo Capitani

PhD. Eng. Claudio Annicchiarico

Dean

Prof. Giampaolo Manfrida

Years 2018/2021

to my child

Summary

The autonomous driving is one of the automotive research challenges of the last years, and even if a lot of technologies steps forward have been taken, it remains an open research issue.

So, the aim of this PhD thesis was to improve the current level of dynamic control of an autonomous car using commercial hardware and sensor technologies and respecting their functioning constraints.

The research focused on the development and implementation of different logic layers inside the autonomous car framework.

The first step was to develop an algorithm to localize the vehicle and estimate the car speeds. In this way, the signals required for the correct operation of the control architecture are added to the input signals provided by the sensors. Two of the most adopted technologies were tested. However, the estimation errors made were too high to guarantee the desired level of operation of the control systems. Therefore, based on the characteristics and issues given by the design of these systems, we developed a vehicle speeds estimator consisting of a combination of both. In this way, even in high non-linear dynamic conditions, the errors on the estimation were reduced, improving the car localization and functioning of the control algorithms.

Then, an on-line Path Planning was developed able to define the performances that maximize the car speed in a known track. The focuses were: to ensure a real-time trajectory calculation (updating it with the current vehicle dynamics and environmental conditions); and allow computational cost compatible with the correct functioning of the other systems involved. For this reason, it was chosen an optimization algorithm that allows to maintain a linear cost function simplifying the car model and limiting the computational times. However, in order to ensure the most correct representation of vehicle dynamics a more accurate modelling of the car GG-V has been implemented as constraint equations.

Once defined the trajectory, a high-level controller was developed to track the dynamic performances provided by the Path Planning. So, was implemented an algorithm that ensures a feed-back control of the Steering Wheel Angle (SWA), accelerator and brake pedal by dividing the later dynamic model from the longitudinal one. In addition, was added a feed-forward control that tracks the lateral and longitudinal acceleration calculated by the planner. Thus, the performances tracking delay and the feed-back control modelling errors were reduced.

Finally, to enhance the lateral and longitudinal stability, an Electronic Stability System (ESC) and Anti-lock Brake System (ABS) controls are developed with the aim of improve the current commercial systems performances. About the lateral stability control, a tracking controller was implemented to define the brake input

corrections that must be added to the ones established by the Trajectory Tracking to follow reference yaw rate and side slip angle. Instead, to ensure that the wheels don't lock, a discrete control allows the wheels to follow a target longitudinal speed. In this way, it was found that comparing with the standard ABS the tuning process takes less time and the brake performances are increased, in terms of reduction of the brake distance; and increased stability during full braking manoeuvres.

The different layers ware developed independently achieving their own performance improvement and then are integrated together with specific interfaces. Furthermore, two mathematical modelling types were made starting from available experimental data: a sensor characterization to ensure the input signals have their delays, noise and sample time; and a transfer function model of the Brake-By-Wire system developed by Meccanica 42 srl, to ensure actuation outputs delay and constraints. Thus, the real exchange of signals between the architecture developed and the vehicle model is ensured, and the correct operation of the controls once implemented in the car is verified.

A real-time static simulator placed at Meccanica 42 srl is used to develop and test the architecture and compare the performances obtained with the ones of a driver. The results showed that: it was possible to obtain an optimisation and tracking of the trajectory that update in real-time taking into account the current dynamic conditions; some good improvements were achieved both with regard to the estimation of the states and the stability of the vehicle; and it was possible to integrate the various layers together guaranteeing satisfactory dynamic performance even if worse than the individual one.

Preface

Nowadays, along with the pollution effects on our planet a central role is given to those technologies that aim to improve people's well-being and safety.

The automotive sector had been lagging behind in these aspects compared to other industries, which is why in the last years there has been a growing impulse towards a zero emission, zero road fatalities future. Thus, autonomous driving has been undertaken opening up wide ways for research, not only in the industrial sector but also in the urban and civil one.

Driven by the curiosity to learn more about the study and development of these technologies within the automotive world and the development possibilities still necessary to improve the current level of safety and automation available, I have tried to make a little contribution to bring us closer to the scenario in which the number of road accidents will be reduced and passengers will be able to travel safely.

This work has been made possible thanks to the support, cooperation and guidance I have received from my tutors and the continuous exchange of ideas with my fellow PhD students and thesis students. For this reason I would like to thank all of them for the skills acquired and the results obtained.

Contents

List of Figures

List of Tables

Chapter 1

Introduction

In the last years, the autonomous driving has become the declared goal of many automotive and high-tech companies such as BMW, Toyota, Volvo, Tesla, Apple, Google, Nvidia. In addition, local and state governments are setting incentives and smart city areas to enable companies to test and improve the systems developed.

Fostering the birth and making the possibility of a fully autonomous car transport scenario was the need to reduce the number of road fatalities that in the European Union (EU) arrived to fifty road deaths per million inhabitants. In fact, in the 2019, the EU has declared to incentive projects that allow to achieve the target of zero road fatalities in the 2050 [1]. Being the most of the road accidents due to human factors as drivers distractions or inabilities, a scenario in which vehicles are able to control themselves with specific actions and communicate with each other, could allow the elimination of the road fatalities percentage given by the human side.

By the design point of view, an autonomous car must be able to replace and improve the performance of a human driver. Thus, it needs of different software logic that can be divided in 4 main layers:

- **Perception**: surrounding environment perception;
- **Localization**: dynamic conditions estimation and vehicle localization in the world map;
- **Planning**: definition of the trajectory and decisions that have to be make;
- **Control**: actuation input definition to follow the predefined choices and ensure stability.

The technology boost that allowed the development of autonomous driving was the increasing of the electrical and electronic components inside car. The possibility given by By-Wire (BW) devices of using Controller Area Network(CAN) messages to actuate braking and steering systems opens the view to a big programming and control possibilities. In addition, the growth of Artificial Intelligence (AI) to elaborate and understand images and video, as well as manage different signal types has allowed to consider the car like a system able to read what surrounding it and on this decided what to do.

Besides a benefit from the point of view of people safety, the autonomous driving ensures a wide range of advantages, such as: a reduction in pollutant

emissions thanks to a better traffic congestion; the possibility for people with physical limitations to move independently; and the possibility for people of saving their time, dedicating themselves to work or pleasure activities, during the trip without worrying about the road.

To better define the steps made in the autonomous driving research, in the 2014, the Society of Automotive Engineers (SAE) has made a classification [2] (revised in the 2021) in which the automation level of a car is defined by some characteristics:

- **Level 0-No driving automation**: The performance by the driver of the entire Dynamic Driving Task (DDT), even when enhanced by active safety systems;
- **Level 1-Driver assistance**: The sustained and Operational Design Domain (ODD)-specific execution by a driving automation system of either the lateral or the longitudinal vehicle motion control subtask of the DDT (but not both simultaneously) with the expectation that the driver performs the remainder of the DDT;
- **Level 2-Partial driving automation**: The sustained and ODD-specific execution by a driving automation system of both the lateral and longitudinal vehicle motion control subtasks of the DDT with the expectation that the driver completes the Object and Event Detection and Response (OEDR) subtask and supervises the driving automation system;
- **Level 3-Conditional driving automation**: The sustained and ODD-specific performance by an automated driving system of the entire DDT with the expectation that the DDT fall-back-ready user is receptive to automated driving system-issued requests to intervene, as well as to DDT performance-relevant system failures in other vehicle systems, and will respond appropriately;
- **Level 4-High driving automation**: The sustained and ODD-specific performance by an automated driving system of the entire DDT and DDT fall-back without any expectation that a user will need to intervene;
- **Level 5-Full driving automation**: The sustained and unconditional (i.e., not ODD-specific) performance by an automated driving system of the entire DDT and DDT fall-back without any expectation that a user will need to intervene.

In Figure 1.1, the flow diagram for assigning the level of automation is shown.

Nowadays, there are legislative requirements to equip vehicle with some safety control system with certain performances, and the most of the automotive companies invest in the development of the Advanced Driver Assistance Systems (ADAS). These systems control the brake and steering car devices in such situations avoiding crash with the other road actors. Although some attempts have been made trying to overcome the current level of automation, the chance of seeing a reliable car of level 3, 4, or 5 is still far away, because of technological, legislative and infrastructural problems. Indeed, there are no ethical and objective rules to manage autonomous and non autonomous car in the same scenario; and the streets and cities are not provided with the appropriate road signs and technology to interact with vehicle and reduce the faults of camera, radar and lidar sensors. Thus, the perception

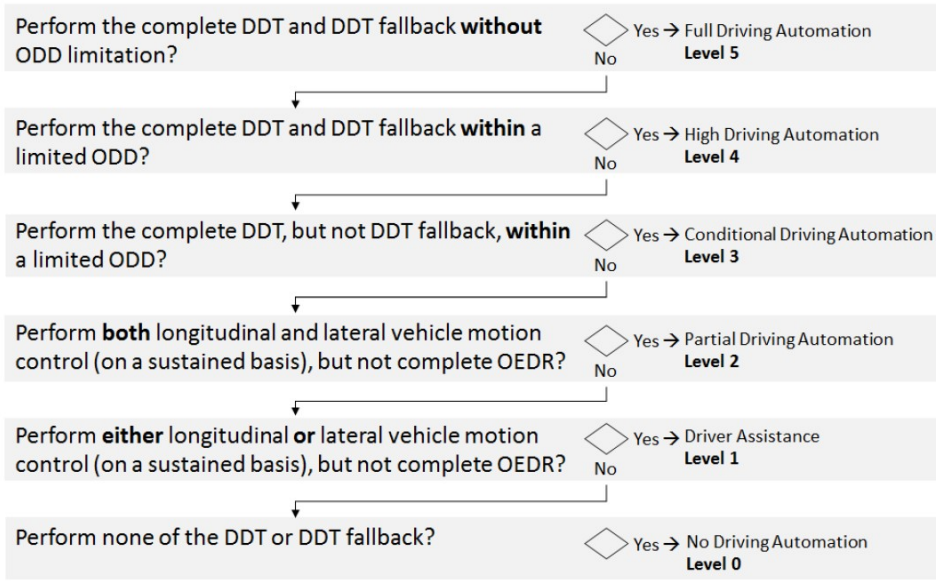

Figure 1.1: Simplified logic flow diagram for assigning driving automation level to a feature.

system is no reliable in a urban area scenario where the environment is dynamic and changes unexpectedly.

In addition, even the control systems doesn't ensure the same performances in all driving conditions: the vehicle dynamics is high non-linear and unpredictable having many unknowns and changes difficult to track and predict. So, both the states estimation, on which the car control system performances depend, and control systems are inefficient under certain dynamic conditions.

1.1 Research question

This PhD thesis was aimed at improving the actual state of the autonomous driving focusing on the development of:

- a state estimator and car localization system;
- a planner and tracker of the performances;
- a controller of the car inputs to ensure stability and improve the dynamic performance.

So, reducing the problem from an urban to a static racing scenario, the goal was to drive the Calabogie race track, shown in Figure 1.2, autonomously in a sports car equipped with Steer-By-Wire (SBW) system and a special Brake-By-Wire (BBW) system developed by Meccanica 42 srl that ensures differentiated and independent braking pressure on the 4 wheels.

Therefore, to achieve the goals, instead of implementing a unique controller with off-line planning, as it is commonly done, it was thought to develop an on-line

Figure 1.2: Calabogie motorsport race track.

hierarchical architecture opening to a possible future implementation on a collision avoiding scenario thanks to the computing of a suitable reference manoeuvre. Starting from common sensors input signals, the work has involved the development of:

1. **State Estimator**, to improve the current estimation potentiality and ensure the correct working of the other control systems;
2. **Trajectory Tracking**, composed of planning and tracking part, with the focus of ensuring a real-time optimization of the trajectory, adapting the performance to the actual states of the car to try to minimize the lap time;
3. **Stability Control Systems**, with longitudinal and lateral part, to achieve an improvement of current performances by increasing passengers safety and vehicle dynamics behaviour.

The entire architecture has been implemented in Matlab-Simulink with the logic flow shown in Figure 1.3, where the Path Planning and Path Tracking layer compose what can be defined as driver model, providing the steering, accelerating and braking car input; while the Stability Control layer, composed by a lateral and longitudinal controller, defines which are the braking corrections that must be given to the predefined inputs to follow the dynamic behaviour of a reference dynamic model.

The continuous and differentiating wheels braking is allowed by a particular BBW system developed by Meccanica 42 srl, and whose braking unit per wheel is shown in Figure 1.4.

In detail, the brake actuators are four electro-hydraulic units interposed between the main pump and the calliper of the common brake system. A control logic and an electric motor compose each unit and command the hydraulic line in order to

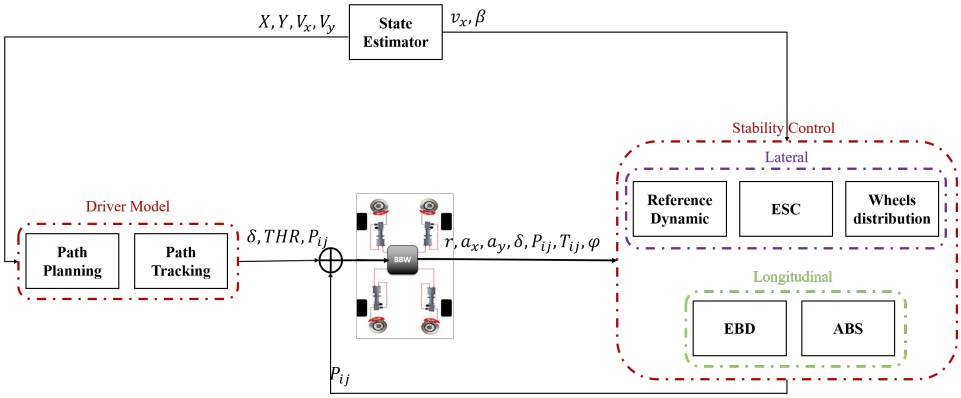

Figure 1.3: Mtlab-Simulink implementation and logical flow of the control architecture.

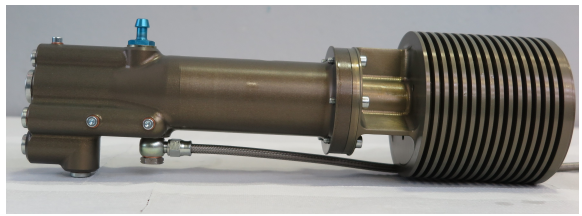

Figure 1.4: Cornering Braking Actuation Unit by Meccanica 42 srl.

deliver the target braking pressure to the wheel's calliper. They can be considered as a CAN controlled device and can track a target pressure imposed by higher-level control systems, simplifying the integration of the whole loop. They can produce a maximum pressure of 100 bar in 0.10 s.

Each layer was developed and tested independently by off-line tests campaign that involved co-simulation environment between Matlab-Simulink and Vi-Grade CarRealTime (CRT), a multi body software that ensures to consider in the simulations the dynamic response of a 14-Degrees of Freedom (DoF) vehicle model.

Then the entire architecture was integrated and tested in a real-time static simulator set in Meccanica 42 srl and shown in Figure 1.5.

Using a Hardware in the Loop (HiL) test rig allows to understand which impact these solutions introduce on vehicle behaviour. It is composed by three main parts:

- **The Real-Time simulator**: consisting in a concurrent-real-time machine, which manages the simulation environment along with the vehicle model. For non-disclosure reasons, the detailed specifications of the benchmark use case cannot be described. However, it is assumed that vehicle rear wheel driving powertrain is actuated to active differential transmission system;

- **The EPSiL steering bench**: reproducing the real behaviour of the steering system, including Electric Power Steering (EPS) system and a steering wheel;

- **Human Interface**: steering wheel, brake pedal and throttle pedal as human-interface devices.

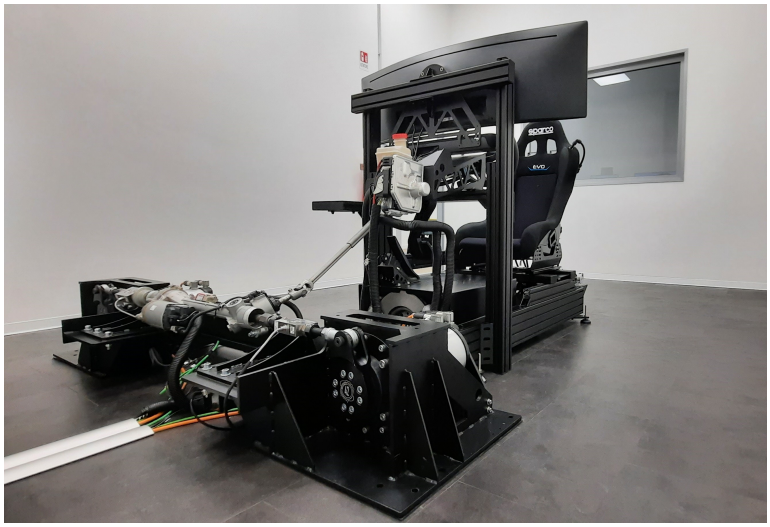

Figure 1.5: Real-time static Hardware-in-the-Loop simulator by Meccanica 42 srl.

In this way, the system integration capabilities were evaluated and the performances compared with the one obtained by a professional driver.

The off-line simulation windows lap top and simulator characteristics are shown in Table 1.1.

Table 1.1: Hardware specifications of the tests campaign.

Tests Campaign	Off-line	Real-time
System	Windows	Linux
RAM	16 GB	32 GB
Core	1 @ 2.6-3.5 GHz	8 @ 3.2 GHz

1.2 Thesis outline

Chapter 2 - Autonomous Race-Car

In this Chapter each field faced in this research are introduced. Especially, their framing with the state of the art by investigating the technologies currently used and the solutions proposed in this study. In the last Section, the models used to represent as faithfully as possible the architecture inputs and outputs are explained and shown in order to realistically represent integration with the vehicle system.

Chapter 3 - Vehicle localization and dynamic states estimation

The estimation of the car global positions and local speeds is discussed in this Chapter. In particular is shown the study done to reduce the absolute error and improved the robustness in the speed estimation. In fact, to overcome the problems encountered with the current technologies performances, a mix approach composed of a state observer, in particular the Unscented Kalman Filter (UKF) one, and

Artificial Neural Network (ANN) was developed and a statistical test was made to validate the hypothesis done. The Chapter is composed of a first part in which both the current technologies are explained and its independent results are shown; then the mix approach used and the testing methodology are presented concluding with the analysis of the results obtained. In the last Section, the application of the State Estimator and Dynamic Localization System to the case of study is given.

Chapter 4 - Trajectory planning and tracking

In this Chapter, the solutions used to optimize the trajectory in real-time of the use of case car model and establish the inputs to control the car to follow that trajectory are shown. In the first Section, an in-depth presentation of the Path Planning algorithm used with its pro and cons is done passing to the description of the Path Tracking choices. Then, the combination of the two layer is validated comparing its performances with the ones of an off-line motion planning optimization process and with the human driver ones.

Chapter 5 - Stability System

Here, the algorithms developed to ensure a longitudinal and lateral stability to the car are shown aiming at a passengers safety increase and car dynamics improvement. All the solutions found were focused on exploiting the potential of the Cornering Braking Actuation (CBA) system developed by Meccanica 42 srl.

The first Section involves the explanation and comparison of three longitudinal control systems developed, showing the results obtained by off-line simulation tests campaign and justifying the final choice done.

In the following Section, the lateral stability system developed is explained showing all the validation and evaluation tests campaign made to prove the stability capability given by tracking the yaw rate and side slip angle provided by reference dynamic model instead of predefined threshold values.

The third Section allows to show the chosen low-level control to actuate the stability systems commands. Two methodologies were explained and tested in a standard manoeuvre used to evaluate the lateral stability control system. By the results obtained the strategy developed by a Colleague PhD student, Tommaso Favilli, seems to increase the potential of the car to perform the manoeuvre and remain more consistent with driver input.

In the last Section, the performance improvement of the entire stability system (longitudinal, lateral and torque allocation control) on the case study compared to using Trajectory Tracking alone is shown. Especially are highlight the benefits given by dynamics stability response to the driver model inputs.

Chapter 6 - Integration results

In this Chapter, the integration of all previous systems presented is shown. In the first Section, the additional logics developed to ensure a better interface between the layers are explained in more detailed underlined the advantages provided. Then the performances achieved by the architecture in a flying lap of the Calabogie race track are shown and compared with the ones obtained by the only Trajectory Tracking implementation and by a professional driver.

Chapter 7 - Conclusion

The conclusions drawn from the studies undertaken are reported, highlighting the achievements and possible developments that can be made to improve the system and verify its use in a real implementation.

Chapter 2

Autonomous Race-Car

The autonomous car field applied to a sportive one that drives in a race track scenario, ensures to develop in a static and safer environment the needed softwares that in a urban scenario should depend on the perception system, not robust enough for the actual cities conditions, and sensor reliability, of which improvement was not the focus of this thesis.

In this Chapter an introduction, a state of the art situation, and the proposed solutions found of each layer developed are shown.

The thesis work was divided into the macro-areas introduced in the previous Chapter and a publication was made for each of the achievements. For this reason, this and the following Chapters will be set up according to the papers submitted.

2.1 State estimation and vehicle localization

The need to reduce situations that endanger people's health and safeguard their wellbeing encourage the automotive sector to develop control system that prevent human faults. But to allow these control systems to improve their performance a proper estimation system is needed to know as accurate as possible the actual states of the vehicle, especially the current global positions and local speeds of the car.

In fact, about the trajectory planning and tracking, they need to have a localization in the world map of the car, and so its lateral and longitudinal global position and speeds, making necessary to develop a system for locating the vehicle within a known track. Instead, about the stability control systems, it needs to know the current value of yaw rate and side slip angle, i.e. the arctangent of the lateral divided by the longitudinal local vehicle speed, making necessary to develop a vehicle speeds estimator.

Following the most used current technology based on the state observer algorithm a non-linear one was developed. However, the errors made on the speed estimation in some dynamic conditions result not appropriate. So, another newer technology already frequently investigated for this field, the ANN, was trained to estimate lateral and longitudinal car speeds. But, even in this case, the errors made in some situations result to be too high.

For these reasons, a mixed approach was developed and a state estimation comparison between a no-linear state observer with and without a measure of the car speeds given by the ANN was made trying to reduce the side slip angle

estimation errors in limit of adherence manoeuvres.

The methodologies and results obtained was submitted in an article and showed in the AIAS2021 conference.

2.1.1 Literature review

The side slip angle estimation involved many research projects because of its important in the vehicle dynamics stability controls developed in the last years [3, 4]; as well as its importance in the development of autonomous driving systems [5]. The problem is that a direct measurement of the car's speeds implies the use of expensive sensors not usable in commercial car. So, in the state of the art, it is possible to find different methodologies to overcome this problem and implement a system that doesn't involve the use of direct measurement [6, 7].

The most commonly strategies consist of: a model based approach with state observers; and a black box approach using the AI capability of approximate any functions. The first strategy cited has been widely investigated by researchers. Some authors implemented a closed-loop state feedback observer [8], others a non-linear observer based on Lypunov asymptotic stabilization function [9], and others a sliding mode observers [10, 11]. However, with all these methods, the estimation is strongly influenced by the uncertainties of the vehicle dynamics. To reduce the errors made, adaptive methods are developed [12, 13], even if the most common method to estimate side slip angle was the Kalman Filter (KF). It was used in many different ways: linear KF [14], and non-linear such as Extended Kalman Filter (EKF) [15–17] and UKF [18–20]. However, the UKF is preferred over the linear KF because it reduces modelling error by representing non-linear dynamics, and over the EKF because it is only reliable for systems which are almost linear within the operating frequency range, and become unstable due to the need to calculate the Jacobians at every time step. Anyway, modelling errors cannot be completely eliminated with model-based observers.

A completely different approach is the one based on machine learning techniques and, specifically, supervised learning. The main algorithm used in the literature is ANN which have been demonstrated to be capable of approximating any function [21]. For this methodology, too, different approaches were employed with regard to both the architecture of the layers and the input quantities. Some authors preferred to use only the inherit platform sensor measures, vehicle accelerations and yaw rate [22]; and others that increase the number of input considering also the Steering Wheel Angle(SWA) and the wheels speed improving the network capability to extrapolate the vehicle model [23]. If these examples implement a deep feed-forward neural network, better results are obtained with Recurrent Neural Network (RNN) layer, being able to learn the temporal links of the various signals [24].

However, even this strategy have issues because it needs to have a big data train to cover all the car's working range.

2.1.2 Proposed solutions

To overcome the problems caused by a model based and a black box approach, a mixed one was chosen [25]. It can ensure to have the advantages of both the strategies: training the ANN to predict the car speeds on a set of manoeuvres with different combinations of lateral and longitudinal vehicle dynamics, and using the

network output as additional input measures of the UKF, that can consider the vehicle dynamic and correct the lack in generalization of the network.

To evaluate the beneficial that the ANN bring to the UKF developed to an autonomous car as side slip angle estimator and car locator, an in-depth statistical analysis was done through the Montecarlo analysis.

2.2 Trajectory Tracking

In recent years, research on the automotive field has focused on making cars more and more able to make decisions autonomously due to the growth of electric and electronic technologies on modern road cars and to the possibility of providing increased safety and improved performance.

In the racing world, where the scenario is static and known, the perception system has a simple implementation, and good results have already been achieved, as shown, for example, in [26].

The main challenge is to improve performance through the use of models that represent the dynamics of the vehicle as faithfully as possible while ensuring an acceptable computational effort for real-time implementation.

The aim of this layer was to develop a Trajectory Planner able to update the trajectory on-line with the car progress on the track, trying to replicate the capabilities of a human driver. Then, the Path Planning was embedded with a Path Tracking consisting of a Linear Quadratic Regulator (LQR) that provides the car's input signals: SWA, accelerator and brake pedals signals.

In this way, even if in a racing world scenario, real-time trajectory optimization can ensure a possible future implementation in emergency situation where avoiding collision could be faced.

The results obtained with the Trajectory Tracking developed was published in a journal paper [27].

2.2.1 Literature review

To ensure a trajectory tracking able to reduce the lap time, the state of the art offers different approaches both from the architecture and methodology point of view. From the architecture point of view, the research is divided between the ones that used a real-time single algorithm to plan and track the trajectory [28, 29], others that preferred to separate the planner from the tracker by having the first off-line and the second work in real-time [30], and others that divided trajectory planning and tracking but implemented them both in real-time [31–33]. The first architecture type, as said in [34], gives the advantage of incorporating tire force constraints in a straight-forward way. However, the integration of trajectory planning and tracking approaches can work for autonomous RC-cars but is difficult to scale to complex scenarios due to the non-convex nature of the constraints imposed by multiple vehicles. In addition, it implies a more complex tuning. Instead, there are many studies about the off-line trajectory planner with good performances in terms of lap time reduction and car set-up, allowing to implement a vehicle model with more DoF [35], adding also a friction coefficient mapping [30] and involving different methodologies. Some authors preferred to develop a geometrical solution by minimizing the curvature [34] or generating a racing line using professional driving techniques [36]. However, these techniques do not provide information about

vehicle dynamics, despite the fact that the trajectory of least curvature ensures lap time similar to the trajectory optimization techniques [34]. Therefore, other researchers preferred to face the problem as a kinodynamic problem by finding the optimal trajectory, minimizing the lap time and considering both the kinematic constraints of the track and the dynamic constraints of the vehicle [30, 37]. Facing the problem from the kinodynamic point of view considers that the non-convexity of the trajectory does not allow a global solution [34, 36] but a local one [38–40] using Sequential Convex Programming (SCP) methodology [33].

2.2.2 Path Planning-Proposed solutions

This study has involved the development of a Trajectory Planner that every 0.1 s provides the speed and trajectory that the car has to follow to minimize the time lap. The real-time implementation of the Trajectory Planning is advantageous in terms of performance and safety. In fact, during the race, a professional driver is able to feel the car conditions and choose the trajectory that ensures the best performance. In the same way, a Trajectory Planner must provide the fastest trajectory for the dynamic and scenario conditions in which the vehicle is located. In [33], it was decided to use a point mass vehicle model and implement a Model Predictive Control (MPC) with the SCP approach. To simplify the algorithm without incurring in infeasibility and further reduce the computational time, it was chosen to solve the Linear Programming (LP) problem instead of the Quadratic Programming (QP) problem and to reduce the losses due to linearisation, it was chosen to represent the car's GG-V with conical constraint equations. Furthermore, the weights and variables of optimization change with the track sequences, allowing the designer to change the constraints with changes in scenario and vehicle dynamics.

2.2.3 Path Tracking-Proposed solutions

To ensure that the car follows the performance requested by the Path Planning it was implemented a Path Tracking control. Defining the SWA, accelerator and brake pedal input through the LQR optimization, it allows to control the car motion every 0.001 s, achieving to represent the vehicle dynamic more accurately than the planner where to limit computational time the vehicle model was simplified.

However, the input delays given by the feed-back control implemented didn't allow to have the proper integration between the planner and the tracker not ensuring to the car to reach the Path Planning acceleration outputs. Thus, a feed-forward control was developed allowing to track the longitudinal and lateral acceleration performances defined by the planner optimization. Ensuring that the vehicle follows the outputs required by the planner is important because allows the car at the next step to achieve optimised performances.

2.3 Vehicle dynamics control

The heart of the following study was not only to develop a system that allows a car equipped with BW actuation systems to drive a lap of a track while optimising its speed, but also to ensure its stability and improved dynamics. For this reason, much of the work involved the development of lateral and longitudinal dynamics control systems, commonly known as the Electronic Stability System (ESC) and

Anti-Lock Brake System (ABS). In order to allow all the control layers to operate in real-time, the stability systems were decoupled from the trajectory optimiser and added as separate layers. Them block diagram is shown in Figure 2.1 where the flow logic and signals exchanged with the vehicle system are made explicit.

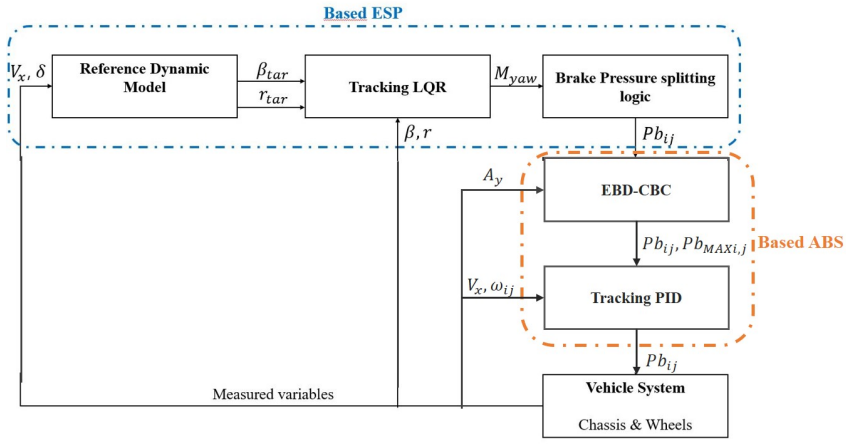

Figure 2.1: Block diagram of the Stability Systems Control.

By the Figure 2.1 it possible to see that the lateral stability control logic, named Electronic Stability Program (ESP), or ESC, needs to have as inputs the current vehicle longitudinal speed, steering road angle, yaw rate and side slip angle, and it is composed by: a Reference Dynamic Model, that defines the target values of yaw rate and side slip angle that the control has to track; a Tracking LQR that reduces the error between the actual and target control states defining the total yaw moment that must be provided to the car; and a Brake Pressure splitting logic that allows to allocate the brake pressure that each wheel has to have to ensure the total yaw moment requested by the control. Once defined the brake pressures necessary on the wheels, to ensure that they would not face themselves with its saturation limits and so lock themselves, an ABS is implemented after being compared with other standard solution studied. This ABS is composed of a first part where the maximum saturation limits of each wheel defined by: the actual lateral acceleration engagement, Cornering Brake Control (CBC); the longitudinal brake distribution, Electronic Brakeforce Distribution (EBD); and actuator constraint limits. Then, after three different methodologies performance comparison, it was chosen to implement a discrete Proportional-Integral-Derivative (PID) that allows to the wheels to reduce the errors between the speeds and a target value defined as the 90% of the actual longitudinal vehicle speed. In this way, a longitudinal slip of the wheels of the 10% is ensured.

In the following Subsection the state of the art and the aims of the stability controls developed are showed.

2.3.1 Longitudinal dynamic control-ABS

Car longitudinal braking control is a research topic that emerged during the last century to avoid skidding-related accidents. During severe braking or braking on a

slippery road surface, the wheels can lock, preventing steering and making the car unstable.

For this reason, the need arose to develop a longitudinal dynamics control, capable of preventing wheel locking and thus ensuring driver control of the vehicle. Different strategies were tested and the results obtained are published in a journal paper [41].

Literature review

In the 1980s, the adoption of the Bosch ABS system [42] led to the rise of longitudinal controllers in cars, improving braking distance and car handling during intense or slippery braking events [43]. Furthermore, the growth of electric and electronic components inside modern road vehicles offered more opportunities for the enhancement of control systems, both longitudinal and lateral. In effect, Electro-Hydraulic-Braking units allow researchers to diversify the target pressure of each wheel, dividing their behaviour and making hydraulic implementation more reliable and faster than mechanical brakes [44]. Moreover, in recent years, automotive industries have been focusing on the development of Electric Vehicle (EV) with In-Wheel Motor(IWM) that independently actuate wheels [45]. This has improved research on longitudinal control systems and detailed the control architecture [46, 47].

In the last two years, some authors have developed ABS systems that try to use these new technologies to improve performance. Researchers devised enhancements by increasing the architecture's complexity and applying a model-based approach. Someone used a Fuzzy Logic to control the longitudinal slip ratio, emphasising the benefit of not using an estimate of the longitudinal speed [48]. Instead, others developed a Modified Optimal Sliding Mode Control trying to ensure that the Sliding Mode Control (SMC) is optimal as well as robust [49]. In [50] was said that the most promising ABS architecture is the one composed of Fuzzy Logic and SMC. The SMC can adapt the ABS control to the vehicle model, and two levels of Fuzzy Logic avoid SMC's chattering problem. Instead, in [51] was used an MPC. This control can consider the car's dynamics model, including all the states and inputs constraints, and predict the vehicle's future behaviour. MPC will probably be the future step in market cars' control implementation, but for now, like all model-based controls, it implies a deep knowledge of vehicle parameters and tire models that is not available in standard vehicles, and is also computationally demanding.

A detailed review of the ABS algorithms used by researchers from simple no-model-based controllers, such as Fuzzy Logic or PID, to sophisticated adaptive-model-based controllers, such as Non-Linear Model Predictive Control(NMPC) is provided in [52]. The authors highlighted that vehicles are highly non-linear systems, and their controls, such as the ABS, must face highly non-linear control problems due to the complicated relationship between their components and parameters. However, they noticed that researchers who used the model-based approach have not achieved satisfactory performance under the changes of various road conditions and need an increase of computation time. For these reasons, in this study, it is suggested to use methods that do not require a model-based approach.

Proposed solutions

To find the better ABS solution, three architectures were developed as result of evolution steps of longitudinal control. At the beginning it was tried to develop an ABS algorithm similar to the one shown in [3]. The controller is no-model-based and uses parameters estimated by standard automotive sensors: wheels' speed. Although it showed good performance by avoiding wheel locking and reducing braking distance, it uses the derivative of the wheels' speed as inputs. The wheels' speeds are sensor quantities, so they have some noises that must be filtered to be derived. The signal filtering can cause a delay and does not always ensure good control actions. Furthermore, even with filtering, the chattering problems remain the same, especially when asphalt is wet, because of the bang-bang logic in the architecture control.

For this reason, it was decided to improve ABS performance by exploiting the BBW system developed by Meccanica 42 srl. Johansen et al.[53] showed a linear model-based controller that allows each wheel to follow a certain slip target, adapting to the vehicle dynamics. It was tried to replicate the control structure thanks of the BBW system, which allows wheels to have a different target of pressure. Because of the impossibility of knowing the tires' properties, the solution that Johansen proposed could not be used. Thus, a discrete PID control was developed with the task of minimising errors between the wheel's actual and desired slip. However, the control requires the expression of the desired longitudinal slip as a function of longitudinal force, and a precise estimation of the vehicle's speed to calculate the actual slip value.

Then, a novel type of ABS was implemented, linking the advantages of both algorithms. This longitudinal control is always a discrete PID control but with the task of reducing the errors between the wheel's actual and desired speed, where the desired speed depends on the car's deceleration requested by the driver. Therefore, it was possible to smooth out the controlled pressure action by using the continuous and differentiating BBWs' work. At the same time, the control logic did not imply the use of estimated quantities.

2.3.2 Lateral dynamic control-ESC

In the last fifty years with the increase of the electronic components on vehicles, the automotive industries have invested in development of stability control systems to ensure passenger safety. Consequently, all the commercial vehicles are equipped by now well-known ABS stability systems which can prevent wheels lock during full braking and preserve handling; since 2011, the EU decided that all new vehicles have to be equipped with a functional ESP, too. The ESP has improved the active safety system passing from a wheel behaviour control to a vehicle behaviour control; in fact, it can keep the vehicle dynamic close to an expected nominal one, managing the torques on wheels to produce a correction yaw moment on the car [3]. However, the ESP acts only in emergency situations, while driving at limit of adhesion.

The developed and tested of this lateral stability control system led to several validation studies with related presentation at conferences and published in journals [54, 55], and one journal paper under submission.

Literature review

Ensuring the lateral stability of road vehicles is a fundamental task, respect both to passenger safety and driving comfort [56]. Also, the recent proliferation of BW and mechatronics systems in the automotive sector [57, 58], as well as autonomous drive applications [59, 60], are incentivating researchers and designers in the development of innovative active safety controllers,e.g. EBD, ABS, Traction Control System (TCS), ESP. Indeed, these systems exhibit an higher level of robustness respect conventional mechanical ones, due to the reduced number of components and required maintenance, as well as improved reliability and fault-tolerance [44].

Recently, academic and industrial interest in the field of Torque Vectoring (TV) techniques is becoming more and more important in the automotive sector, since allows to explore new opportunities concerning the lateral stability control strategies [61]. Also, availability of IWM traction systems and BW technologies consent the implementation of non-conventional control methodology [62, 63], which appear extremely costly or even not feasible without the adoption of Electric/Electronic devices.

In the state of the art different typologies of vehicle stability control can be found. Because of the great non-linearity of dynamic vehicle many authors chose to implement a NMPC, that is able to take into account the non-linearities, the mutual interaction of each dynamic states and the possibility of using constraints for both the states and the inputs [64–68]. The main problem of this type of control is the computational cost that precludes real-time usage. For this reason, other papers proposed to use ANN, capable of reproducing the vehicle dynamics and acts in real-time reducing computational cost [69–71]. However, this type of control based on an end-to-end approach, without any analytic correlation with the dynamics of the system: this is critical for the safety assessment of the control system, not allowing to ensure the robustness of control under any condition. Then, a LQR, lean and easy to implement, was chosen. It permits an optimal control of the dynamic model and a robust control thanks to a representation of the vehicle dynamics. Compared to the few papers found in the state of the art [72–75] that acts leading the side-slip angle and the yaw rate under a saturation limit, not having a continuous control on their values, we implemented a reference model that continuously provides the target values and therefore the errors to be nullified, exploiting the possibilities of the brake actuators. In this way, the onset of instability is prevented and a control delay between the upper controller and the pressure controllers is not leaded.

Proposed solutions

The goal of this study is to build an advanced control that is able to increase the dynamics, ensuring stability and better continuous performance during vehicle motion through the adoption of 4 single wheel braking actuators, each one with its own low actuation logic. The use of this architecture allows to increase the responsiveness of the system, its accuracy, due to the reduction of the inertia related to each calliper and to the possibility of continuously tracking four different pressure targets, and its reliability: being inherently redundant, if one actuator goes to fault conditions, the others can ensure the safety of the brake plant. This has allowed to develop a high-level control system ensuring stability and safety at any time and condition. To achieve this aim, it has been built a reference model that provides the values of the yaw rate and side slip angle that the vehicle has to have to

ensure stability. To make the vehicle following the targets and remaining in safety conditions in any driving scenario, an optimal controller is implemented to actuate the single brake wheel actuators. Because of their capability to detect the vehicle instability the yaw rate and side slip angle are chosen as states of control. The yaw rate is the angular velocity with which the vehicle moves around yaw axis. Its value is given by a standard Inertial Measurement Unit(IMU) sensor already available in all commercial vehicles. The side slip angle, instead, is the angle between the direction of the vehicle velocity and the longitudinal barycentric axis of the car. For this application a new architecture was developed and explained in Chapter 3.

2.3.3 Control Command Actuation

Challenging well-known and widely diffused control algorithms is intent of this Section, aiming at the development of effective low level control strategies which can fully exploit the electronic actuation features. Since the electronic actuation systems are object of reliability constrains, its integration with different control structures need to consider its operational limits. Thus, the consequent increased complexity in the system architectures requires the development of control strategies which combines the contribution of all the involved stability controllers: ESC, EBD and ABS [62, 63, 76].

So, two different torque allocation methodologies are compared, one developed in this work that splits the ESC control output based on the estimated wheel conditions; and another developed by the PhD student colleague Tommaso Favilli that splits the ESC control torque by an optimization process. The results obtained were published ad presented at the EEEIC2020 international conference [77].

On the basis of the results obtained from the comparison, it was decided to implement for the case study the torque distribution logic that uses the More-Penrose pseudoinverse developed by Tommaso Favilli.

Literature review

The availability of more and more sophisticated mechatronics and BW systems [44] in modern road vehicles offers to designers a wide range of innovative opportunities to improve stability performances [55, 78]. Also, vehicle electrification is a fast-growing technology [79] which could lead to dynamical behaviour enhancement due to their promising characteristics [80]. However, the availability of a Regenerative Braking System (RBS) makes appear the EV an over-actuated system [81] which require a synergetic integration between available braking actuators and stability controllers [82]. In fact, coordinate RBS and disc brake effort applications, so called Brake Blending, is fundamental to ensure minimum required braking performances in every operative condition [83, 84]. Respect to previously proposed work in literature, in this paper authors develop a newly ESC strategy using a More-Penrose pseudoinverse based TV technique [78, 85], which aim at minimizing the difference between the driving performances requested by the driver and the controllers, ensuring enhanced stable behaviour by fully exploiting IWM traction and braking characteristic.

Proposed solutions

The output defined by the stability control is the total yaw moment that the car has to have to follow the ideal behaviour. To ensure that the vehicle has this yaw moment, a torque allocation strategy is necessary. As mentioned, two torque allocation methodologies will be compared:

1. Brake Pressure splitting logic;
2. More-Penrose pseudoinverse.

At the beginning, the first logic splits the yaw moment between the two car side depending on the moment sign. Then, according to the wheel adhesion condition, a percentage of braking torque is delivered to the front or rear wheel of that side.

The Second strategy is based on Moore-Penrose Pseudoinverse innovative criteria, to solve a multi-DoF problem for over-actuated systems. This allows to achieve both vehicle stabilization and a driving path which is in accordance with the driver intentions.

2.4 Inputs-Outputs characterization

To ensure developed layers as well as the entire architecture possible functioning, a characterization that considers the inputs and outputs delays and noises is necessary. In this way, the reliability and possible real interface between the control and vehicle system is taken into account.

The control architecture needs to know some inputs signals to work in the proper way; some of these inputs can be given by vehicle common sensors and others need to be estimated. About the estimated one, they can be provided by the state estimator developed and shown in Chapter 3, and are the longitudinal and lateral vehicle speed; instead, about the inputs provided by the sensors these are:

- **Longitudinal and lateral acceleration**: provided by IMU sensor;
- **Yaw rate**: provided by IMU sensor;
- **SWA**: provided by steering sensor;
- **Wheels speed**: provided by phonic wheels;
- **Callipers brake pressure**: provided by pressure sensors;
- **Longitudinal and lateral global position**: provided by standard Global Positioning System (GPS);
- **Global yaw angle**: measured by the yaw rate integral, reset to the camera heading angle measurement and global orientation of the road lines every time that the car is straight and the side slip angle is approximately zero

The sensors shown are the one that are commonly found in the current cars.

Thus, to ensure a characterization of these sensors signals an analysis of their noises and sample time was done based on existing experimental data. Taking the measures in steady state conditions for the signals, their mean values was considered as the ground truths and thus, the deviations and the amplitudes out of them were

considered as the signal noises. The results obtained are visualized in the summary statistics of Figure 2.2, where the mean value is set to 1 and will be replaced during simulation by the actual value given by the CRT vehicle model; the dispersion measure is given by the box-plot in which: the bottom and top edges of the box indicate the 25th and 75th percentiles, respectively; the whiskers are extend to the most extreme data points not considering outliers; and the outliers are plotted individually using the '+' marker symbol.

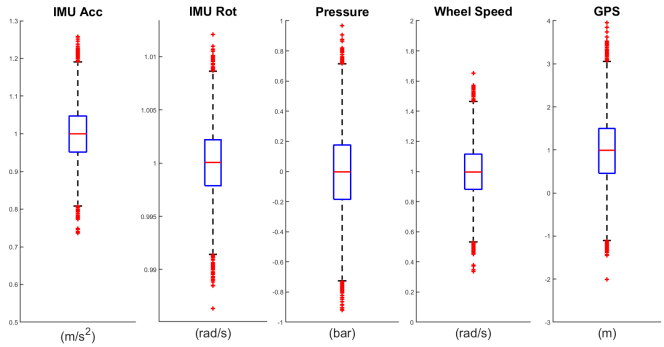

Figure 2.2: Summary Statistics of the sensors data used as control architecture inputs.

These noise distributions are randomly initialized every simulation start.

About the control architecture outputs, and so the vehicle system inputs, they are:

- **SWA**;
- **Pedal accelerator**;
- **Callipers brake pressure**.

If for the first two input itemized a modelling is already ensure by the CRT vehicle model used, the pressure inputs are provided by the CBA system developed by Meccanica 42 srl and explained in Chapter 1.

Thus, to represent the dynamic behaviour of this BBW actuators, thanks to experimental data it was possible to implement a transfer function that gives the time step response as shown in the Figure 2.3.

For confidentiality reasons the graph shown has been normalised to the maximum values.

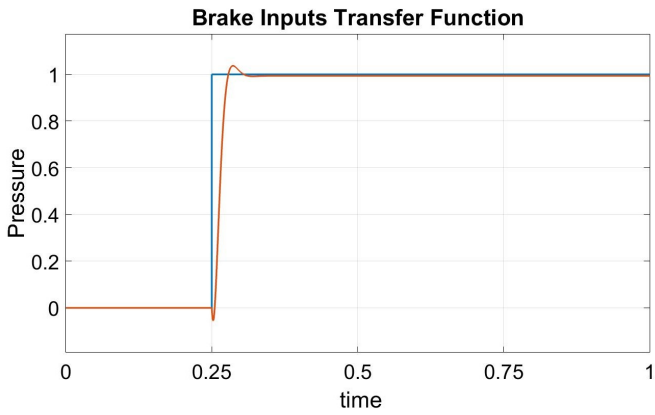

Figure 2.3: Cornering Braking Actuation mathematical model.

Chapter 3

Vehicle localization and dynamic states estimation

The development of autonomous drive is needed to make people life more comfortable and safer, and one of the important skills to make possible the reliability of the all control system is a good localization of the vehicle. For this reason, a non-linear state observer was developed using the UKF algorithm, to estimate the global position, global orientation, and local speeds of a car inside a known path. A characterization of the sensors input measures was made and the measures of longitudinal and lateral vehicle speed were added using an ANN trained in simulated manoeuvres. In this way, it was possible to reduce the error that the observer make on the estimation of the lateral vehicle speed, and so of the side slip angle, making possible an improvement of the control activity. To assess this increase in performance, a Montecarlo analysis was made comparing the architecture proposed, ANN+UKF, with state observed, UKF, with no input measure of lateral speed. The tests were done in co-simulation environment of Vi-Grade's CRT software and Matlab-Simulink.

3.1 State observer

The state observer developed is composed of an UKF [86] able to estimate the actual global position and orientation, and local longitudinal and lateral speed of a car inside a known path. The UKF is a non-linear state observer that uses the unscented transform to propagate the so-called 'sigma points', a group of symmetrically distributed points around the previous estimated system states which contain the information of the expected mean value and variance of the system. Representing the non-linear system in discrete time form with noise as follow:

$$x_{k+1} = f(x_k, u_k, t_k) + v_k \tag{3.1a}$$

$$y_k = g(x_k, t_k) + w_k \tag{3.1b}$$

where $x_k \in \mathbb{R}^n$ represents the state vector, $u_k \in \mathbb{R}^m$ is the input vector, $y_k \in \mathbb{R}^q$ the measurement vector, and the process noise v_k and measurement noise w_k are zero mean white Gaussian noises, and R_k^v, R_k^w as process and measurement covariance

matrices, the UKF algorithm can be presented considering the state vector x_k with mean value $\tilde{x}_k$ and covariance Q_k, and the following steps:

1. initialise mean value and variance matrix:

$$\tilde{x}_0 = \mathbb{E}[x_0] \tag{3.2a}$$
$$Q_0 = \mathbb{E}[(x_0 - \tilde{x}_0)(x_0 - \tilde{x}_0)^T] \tag{3.2b}$$

   where $\tilde{x}_0$ is the a posteriori estimation of the expected mean value for k = 0 and Q_0 is the a posteriori estimation of the variance matrix for k = 0.

2. Calculate sigma points χ_{k-1}:

$$\chi_{k-1} = [\tilde{x}_{k-1} \quad \tilde{x}_{k-1} + A_{k-1} \quad \tilde{x}_{k-1} - A_{k-1}] \tag{3.3a}$$
$$A_{k-1} = \sqrt{(n+\lambda)Q_{k-1}} \tag{3.3b}$$
$$\lambda = \alpha^2(n+k) - n \tag{3.3c}$$

   where λ is a scaling parameter, the constant α determines the spread of the sigma points around x_{k-1} and is usually set to a small positive value. The constant k is a secondary scaling parameter. To calculate the square root of covariance matrix Q_{k-1}, the Cholesky factorization was used for which a Hermitian positive-definite matrix B can be decomposed as $B = LL^+$ with L being a lower triangular matrix with real and positive diagonal terms.

3. Time update by transforming the sigma points with the non-linear functions:

$$\chi_{k|k-1} = f(\chi_{k-1}, u_{k-1}, t_k) \tag{3.4a}$$
$$\Upsilon_{k|k-1} = f(\chi_{k-1}, t_k) \tag{3.4b}$$

   and computing the a priori estimation of the expected mean value $\tilde{x}_{\bar{k}}$, variance matrix $Q_{\bar{k}}$ and measurement estimation $\tilde{y}_{\bar{k}}$:

$$\tilde{x}_{\bar{k}} = \sum_{i=0}^{2n} W_i^{(m)} \chi_{i,k|k-1} \tag{3.5a}$$
$$Q_{\bar{k}} = \sum_{i=0}^{2n} W_i^{(c)} [\chi_{i,k|k-1} - \tilde{x}_{\bar{k}}][\chi_{i,k|k-1} - \tilde{x}_{\bar{k}}]^T + R_k^v \tag{3.5b}$$
$$\tilde{y}_{\bar{k}} = \sum_{i=0}^{2n} W_i^{(m)} \Upsilon_{i,k|k-1} \tag{3.5c}$$

   where the W_i weights are:

$$W_0^{(m)} = \lambda/(n+\lambda) \tag{3.6a}$$
$$W_0^{(c)} = \lambda/(n+\lambda) + (1 - \alpha^2 + \gamma) \tag{3.6b}$$
$$W_i^{(m)} = W_i^{(c)} = 1/\{2(n+\lambda)\} \tag{3.6c}$$

   where γ is used to incorporate prior knowledge of the distribution of the state vector (for Gaussian distributions,$\gamma = 2$ is optimal).

4. Measurement update by computing the measurement estimation variance Q_{ykyk} and covariance matrix Q_{xkyk} between $\tilde{x}_{\bar{k}}$ and $\tilde{y}_{\bar{k}}$:

$$Q_{ykyk} = \sum_{i=0}^{2n} W_i^{(c)} [\Upsilon_{i,k|k-1} - \hat{y}_{\bar{k}}][\Upsilon_{i,k|k-1} - \hat{y}_{\bar{k}}]^T + R_k^w \tag{3.7a}$$

$$Q_{xkyk} = \sum_{i=0}^{2n} W_i^{(c)} [\chi_{i,k|k-1} - \hat{x}_{\bar{k}}][\Upsilon_{i,k|k-1} - \hat{y}_{\bar{k}}]^T \tag{3.7b}$$

and finally, calculating the Kalman gain K_k, a posteriori estimation of expected mean value $\tilde{x}_k$ and variance matrix Q_k:

$$K_k = Q_{xkyk} Q_{ykyk}^{-1} \tag{3.8a}$$

$$\tilde{x}_k = \tilde{x}_{\bar{k}} + K_k(y_k - \tilde{y}_{\bar{k}}) \tag{3.8b}$$

$$Q_k = Q_{\bar{k}} - K_k Q_{ykyk} K_k^T \tag{3.8c}$$

3.1.1 Vehicle model

The model used by the state observer is a double-track vehicle model [87] shown in Figure 3.1.

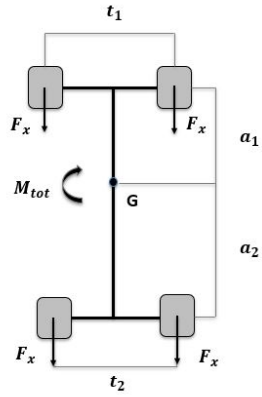

Figure 3.1: Double-Track vehicle model.

The state vector used is:

$$x = [X, Y, \theta, v_x, v_y, r, \alpha_{ij}] \tag{3.9}$$

where X,Y are global car position on the track; θ is orientation of the car, i.e. yaw angle; vx, vy are local vehicle longitudinal and lateral speed; r is yaw rate; and α_{ij} are lateral slips of the four wheels, where ij stands for front-left, front-right, rear-left, rear-right. The evolution of these states from the previous step to the actual one is described by the following time-discrete equations:

$$X_{(k+1)} = X_k + dt\left(v_{x(k)}\cos\theta + v_{y(k)}\sin\theta\right) \tag{3.10a}$$

$$Y_{(k+1)} = Y_k + dt\left(v_{x(k)}\sin\theta + v_{y(k)}\cos\theta\right) \tag{3.10b}$$

$$\theta_{(k+1)} = \theta(k) + dt\left(r_{(k)}\right) \tag{3.10c}$$

$$v_{x(k+1)} = v_{x(k)} + dt\left(\frac{(F_{xfl}+F_{xfr})\cos\delta_f + (F_{xrl}+F_{xrr}) - (F_{yfl}+F_{yfr})\sin\delta_f}{m} + r_{(k)}v_{y(k)}\right) \tag{3.10d}$$

$$v_{y(k+1)} = v_{y(k)} + dt\left(\frac{(F_{xfl}+F_{xfr})\sin\delta_f + (F_{yfl}+F_{yfr})\cos\delta_f - (F_{yrl}+F_{yrr})}{m} - r_{(k)}v_{x(k)}\right) \tag{3.10e}$$

$$r_{k+1} = r_k + dt\left(a\left((F_{yfl}+F_{yfr})\cos\delta_f + (F_{xfl}+F_{xfr})\sin\delta_f\right) - b\left(F_{yrl}+F_{yrr}\right) - \frac{t}{2}\left((F_{xfl}-F_{xfr})\cos\delta_f + (F_{yfl}-F_{yfr})\sin\delta_f\right) - \frac{t}{2}\left(F_{xrl}-F_{xrr}\right)\right)/I_z \tag{3.10f}$$

$$\alpha_{ij(k+1)} = \alpha_{ij(k)} + dt\left(\frac{v_{y(k)}}{rel} - \frac{v_{x(k)}}{rel}\tan\alpha_{ij(k)}\right) \tag{3.10g}$$

where $F_{x/yfl}, F_{x/yfr}, F_{x/yrl}, F_{x/yrr}$ are the longitudinal and lateral wheel forces, a, b the front and rear semi-wheelbase, t the car track, rel the lateral wheels relaxation length, δ_f the front wheel steering angle, and dt the sample time choosing to be 0.001 s.

Thanks to this model, the state observer is able to reduce the error made in the estimation of the unknown variables combining the measured signals and their noise dispersions with the model signals and their dispersions. The dispersion of the model and of the measure is found by a tuning process in co-simulations between CRT dynamic vehicle model and Matlab-Simulink implementation of the state observer.

The measurement vector used by the state observer is:

$$y = [X, Y, \theta, v_x, v_y, r, a_x, a_y] \tag{3.11}$$

where X,Y are global position of the car inside the path measured by the GPS sensor; θ is the orientation of the car relative to the global reference frame of the circuit, measured by the yaw rate integral, reset to the difference between the global orientation of the road lines and the camera heading angle measurement every time that the car is straight and the side slip angle is approximately zero (described in more detail in the Chapter 6); r, ax, ay are vehicle yaw rate, longitudinal and lateral acceleration, measured by the IMU sensor; vx, vy are longitudinal and lateral local vehicle speed, measured by two strategies that are compared in this paper, showed in Figure 3.2.

The first one doesn't have the lateral speed as measure signal but as a state of the filter, and measures the longitudinal speed by the longitudinal acceleration integral,

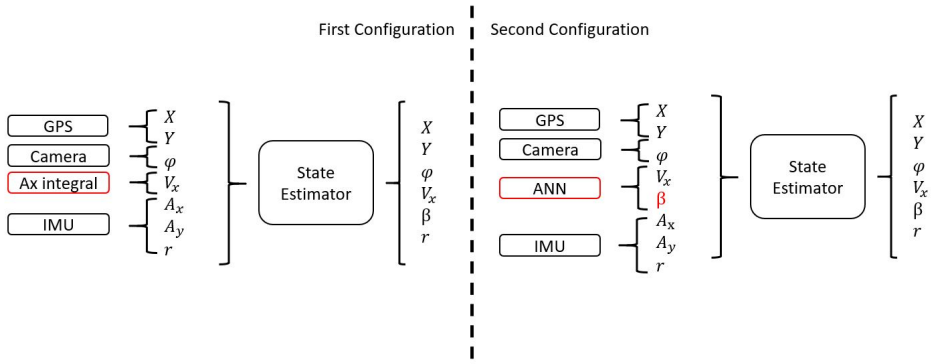

Figure 3.2: Block diagram of the two State Estimators tested.

reset on the mean wheels speed at a specfic time interval during acceleration or uniform drive, as shown in the equation below:

$$Vx = \begin{cases} \int axdt & if \quad StatusBrake = 1 \\ \int axdt \quad reset \quad max(\frac{\omega_{fl}+\omega_{rr}}{2}, \frac{\omega_{fr}+\omega_{rl}}{2}) & if \quad StatusBrake = 0 \end{cases} \tag{3.12}$$

The second strategy involved the use of an ANN able to estimate the actual value of the longitudinal and lateral speed knowing the car acceleration ax, ay, the yaw rate, r, the SWA, δ, and the wheel speeds, ω_{ij}. The ANN developed will be explain in the next Section.

3.1.2 Unscented Kalman Filter Estimation Results

The side slip angle estimation performances obtained by the UKF with the first input measures strategy in a 40 second co-simulated manoeuvres between Matlab-Simulink and CRT are shown in Figure 3.3. The performed manoeuvres covered the steady state and frequency dynamic behaviour of the car model at high and low lateral dynamic engagement.

The estimation data obtained are the result of the dynamic model of the UKF prediction steps where the parameters used are of two types. The first type includes the geometric and inertial parameters of the vehicle such as mass, wheelbase, track width etc. and are taken from the vehicle model given by CRT. Their values are sufficiently accurate and do not have a great influence on the estimation process. On the other hand, as regards the lateral cornering stiffness of the tires, these present a greater uncertainty and have a great weight in the side slip angle estimation. In fact, they represent the dynamic uncertainty that makes the state observer unreliable. As a first step for the determination of these parameters, low lateral engagement step manoeuvres were made in co-simulation environment between Simulink and CRT in order to be in stationary and linear dynamics conditions. In this way, the stiffness values were defined by matching the yaw rate and side slip angle values given by the steady-state single-track vehicle model (defined in Equation 5.18) with those given by the CRT model. Subsequently, these values were corrected by tuning the UKF.

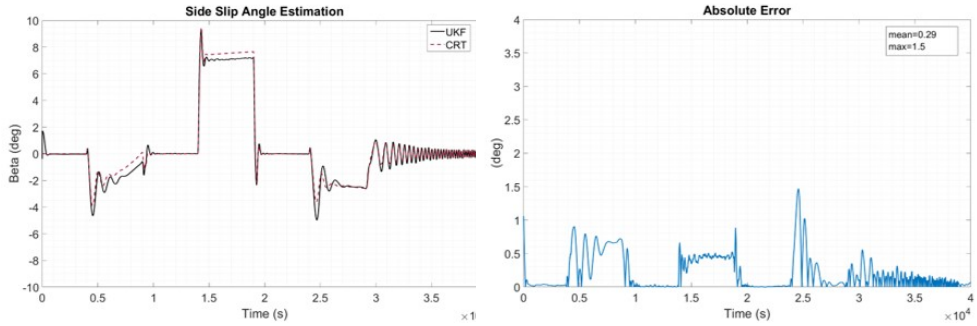

(a) Target and estimated side slip angle of the car.

(b) Absolute error made in the side slip angle estimation.

Figure 3.3: Side slip angle of the car given by CarRealTime multi degree model and by the Unscented Kalman Filter developed, together with the absolute error made in the estimation process, in a set of different manoeuvres.

In the Sub-Figure 3.3b the absolute error made resulted in a mean value of 0.23 degree and in a maximum value of 1.7 degree. Considering that for stability the side slip angle needs to have a maximum value of around 6 degrees, this maximum error represents the 28% of relative error. By the Sub-Figure 3.3a where the actual and estimated value of beta is shown, one can see that the higher errors are obtained in conditions in which the lateral engagement is high and the tires are near to their saturation limits. This highlight the disadvantage of this technology, that depending on dynamic modelling, when the dynamics is not correctly modelled, makes too high errors.

3.2 Artificial Neural Network to side-slip angle estimation

By the tests made a not acceptable error on the lateral speed estimation has been seen in the filter working at limit of adhesion situations using the first strategy as shown in the previous Section. For this reason, it was thought to develop and use as signal measure inputs an ANN [24], that trained in a varied set the car dynamics conditions can estimate the longitudinal and lateral vehicle speed reproducing the non-linearities that a simplify mathematical car model can't represent. The ANN implemented is composed by 8 input, I, and 2 output, O, that are:

$$\begin{aligned} I &= [a_x, a_y, r, \delta, \omega_{ij}]; \\ O &= [v_x, v_y]; \end{aligned} \tag{3.13}$$

where ax, ay and r are the signal measured by the inertial platform, δ is the steering angle at the front wheels, and ω_{ij} are the four wheels speed.

The structure of the ANN is shown on Figure 3.4, where:

- **Sequence layer**: is the Input-Layer and is responsible for feeding inputs into the network in the form of a sequence;

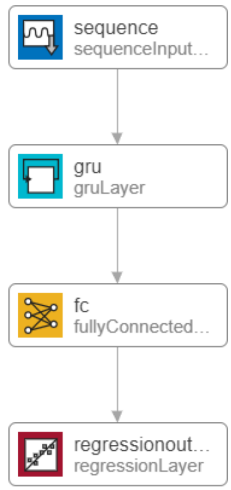

Figure 3.4: Developed Artificial Neural Network layout.

- **GRU layer**: is the first Hidden-Layer and is a RNN able to link signals in time by remembering past instants;
- **Fully Connected layer**: is the second Hidden-Layer and can speed up the training phase and make the network recognise similar sequences by compacting the data;
- **Regression layer**: is the Output-Layer and for typical regression problems, a regression layer must follow the final fully connected layer computing the half-mean-squared-error loss.

Then, the ANN, structured as described, was trained using a set of manoeuvres representative of steady-state and frequency vehicle dynamics, on low and high friction condition, carried out using software simulations and simulations at a static driving simulator. The Data-Set used to train (70% of the data), validate (15% of the data) and test (15% of the data) the ANN is listed in the Table 3.1 and the ANN parameters are shown in Table 3.2.

Table 3.1: Data-Set to train, validate and test the Neural Network.

Friction	Type	Amount time (s)	Vx range (km/h)	Ay range (g)
1	Race-Track	250	10:200	0:1
	Sinus Steer	1200	5:150	0.2:0.8
	Sine Sweep	190	30:80	0.4 @1to4Hz
	Step Steer	1360	5:150	0.2:1
0.7	Step Steer	140	30:150	0.2:0.7
	Sine Sweep	160	30:80	0.4 @1to4Hz
0.5	Step Steer	100	30:150	0.2:0.5
	Sine Sweep	120	30:80	0.4 @1to4Hz

Table 3.2: Artificial Neural Network parameters used.

Layer	Neurons	Activation function	Loss function
sequence	8	-	-
GRU	64	State: tanh Gate: sigmoid	-
FullyConnected	2	-	-
Regression	2	-	Mean Squared Error

3.2.1 Artificial Neural Network Estimation Results

The results obtained by testing the ANN in a Step Steer manoeuvre with high lateral load, and in a Sine Sweep manoeuvre are shown in Figure 3.5, where acceptable errors are achieved, summarized in Table 3.3.

Table 3.3: Root Mean Square Errors estimation obtained by the Artificial Neural Network in a steady state and frequency vehicle response manoeuvres.

	Step Steer	Sweep Steer
RMSE Vx	0.092 km/h	0.137 km/h
RMSE Vy	0.082 km/h	0.133 km/h

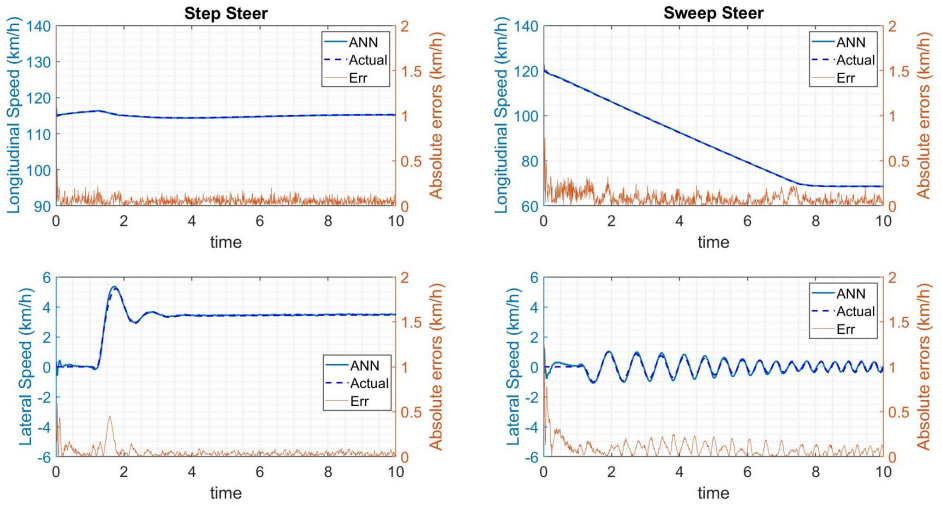

Figure 3.5: Results in terms of longitudinal and lateral speed estimation obtained by the Artificial Neural Network in Step Steer manoeuvre on the left and Sine Sweep one on the right taken from the data-set.

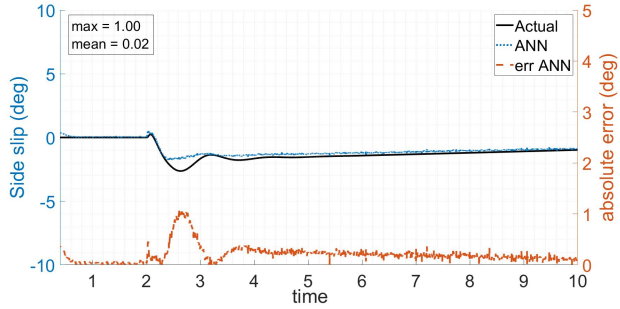

Figure 3.6: Results in terms of side slip angle estimation obtained by the Artificial Neural Network in Step Steer manoeuvre poorly represented in the dataset.

However, these results were obtained by tested the ANN in manoeuvres representative of the data-set used to train, validate and test the network, showing a mean absolute error of the side slip angle of 0.02 deg and a maximum error of 0.29 deg.

Indeed, testing the ANN in simulated manoeuvre poorly represented in the data-set the estimation errors increase, as shown in Figure 3.6. In this case the maximum error resulted higher, about the three times, showing the disadvantages of this technology. Although various ANN architectures have been tried always using recurrent networks, according to the articles found, and tried to change the number of neurons, it turned out that to obtain the same estimation error in the various dynamic conditions, the solution was to increase the data-set or make it more representative. In this way, the search time for the 'optimal' solution increased and the definition of the training data-set became more complicated. Then, was tried to train the network on a simple but fairly representative data-set, based on the acquired knowledge, and to couple the network with a state observer.

3.3 Results

In this Section, the testing methodology used to validate the robustness and accuracy of the algorithm will be shown. The benefits of the proposed algorithm for both the longitudinal velocity and side slip angle estimation will be described. The simulation environment used was the off-line one described in Chapter 1.

In the results shown, the two strategies compared will be named as:

- UKF: localization algorithm composed by only the state observer without the ANN;
- UKF-ANN: localization algorithm composed by the mix between the state observer and the ANN.

3.3.1 Testing methodology

Since the main problem of the neural networks is to guarantee that the ANN provides an acceptable estimation error also outside the testing manoeuvres used during the training phase, and the problem of the UKF is to be able to describe the dynamic uncertainties linked to the tyres, it was thought to join the two systems to

compensate the respective lacks of precision. In order to validate and verify the potential of this architecture under varying initial conditions and vehicle dynamics, a statistical analysis was carried out using the Montecarlo method [88]. This analysis is a statistical one and involves running the estimation system many times for the same manoeuvre by initializing the noise of the input variables in a random and always different way and maintaining the ANN and UKF parameters constant during the test. During the state observer development phase, it was concluded that side slip angle estimation was most affected by variations in longitudinal speed, lateral acceleration and grip conditions. Therefore, it was decided to compare the robustness and accuracy of the UKF-ANN architecture with the UKF by performing a series of step manoeuvres where vehicle speed, steering angle and grip were varied. The manoeuvres repeated 50 times, to reach the RMSE value settled, for the Montacarlo analysis are shown in Table 3.4 and a description of the results is shown in the next Subsection.

Table 3.4: List of the manoeuvres used to assess the influence of different dynamic parameters in the estimators performance through the MonteCarlo analysis.

Influence parameters	Step Steer Manoeuvres			
	SWA (deg)	Vx (km/h)	Ay (g)	Friction
Speed	40	50	0.25	1
	40	80	0.4	1
	40	100	0.6	1
	80	50	0.5	1
	80	80	0.9	1
	80	100	0.95	1
Friction	40	80	0.4	1
	40	80	0.45	0.7
	40	80	0.45	0.5
Lateral acceleration	40	80	0.4	1
	60	80	0.7	1
	80	80	0.9	1

3.3.2 Estimation results

For each type of manoeuvre repeated by randomly initialising the noise present in the input signals, the Root Mean Squared Error (RMSE) performed in the 50 tests was calculated, thus ensuring the reliability of the estimate. The RMSE obtained from the two configurations was then compared as the influence parameters varied (Figure 3.7). About longitudinal speed estimation, as shown in Figure 3.7a, the use of the neural network as input to the UKF reduces the error especially in conditions of high lateral engagement (lateral acceleration at $0.9g$) and low adhesion conditions (friction coefficient at 0.5) reducing the RMSE by about 0.05 km/h. Only in one case a worsening of the estimate is noted (SWA at $80deg$ and vehicle speed at $100km/h$), but one can see that the difference is only $0.001km/h$. Instead, about the side slip angle estimation, the advantages of this mix architecture are more visible. In fact, as shown in Figure 3.7b, the UKF-ANN combination ensures in all the tests

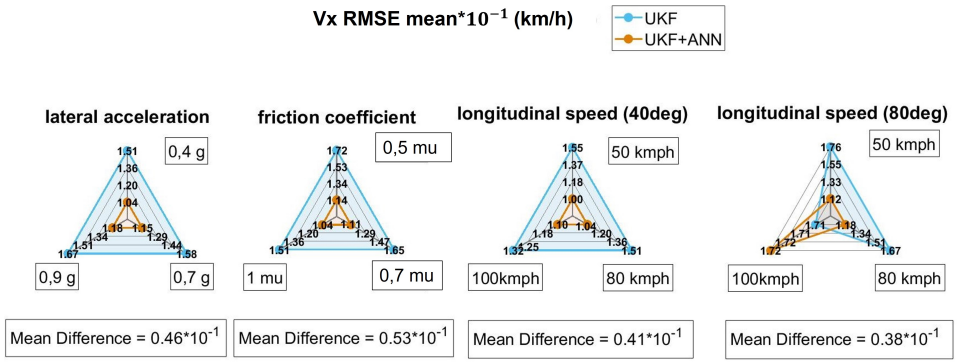

(a) Longitudinal speed.

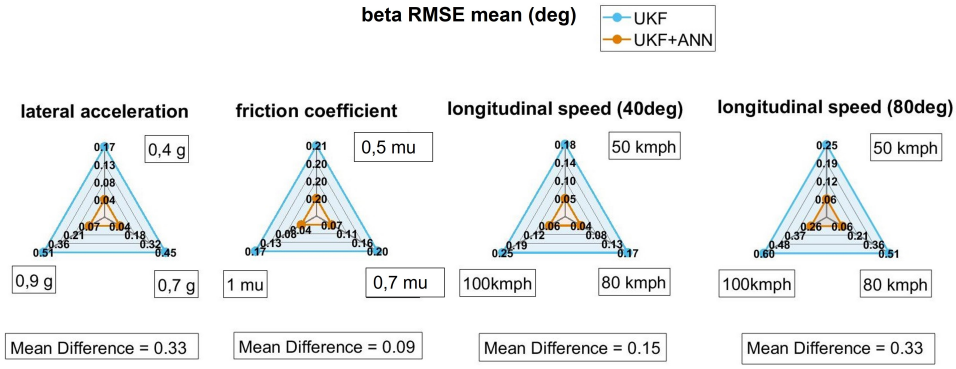

(b) Side slip angle.

Figure 3.7: Comparison of Root Mean Square Errors made in the longitudinal speed multiplied by 0.1 and side slip angle estimation by the two State Estimator configurations with the change of influence parameters.

performed a RMSE reduction of almost 0.33 deg, achieving benefit especially in high lateral engagement and in high longitudinal vehicle speed. Moreover, from the results shown, it possible to see that the RMSE remains almost the same value changing the influence parameters, confirming the greater robustness achieved by UKF-ANN compared to UKF, which instead presents RMSE values varying with the dynamic conditions tested.

A confirmation of these results is shown in Figures 3.8 and 3.9, where the results obtained in the longitudinal speed and side slip angle estimations by changing the steering angle between 40 deg, Figure 3.8a, 60 deg, Figure 3.8b, and 80 deg Figure 3.8c, and by changing the friction coefficient between 1, Figure 3.9a and 0.7 Figure 3.9b are presented. In these figures, it possible to see how the absolute error made by the UKF configuration grows with the time and with increasing steering angle and thus, keeping the longitudinal speed constant, with increasing lateral acceleration. Instead, the absolute error made by the UKF-ANN configuration is almost the same in the three dynamic layout. In addition, when changing the road path conditions both the configuration increases a bit the absolute error but the UKF-ANN configuration maintains a lower one than the UKF configuration.

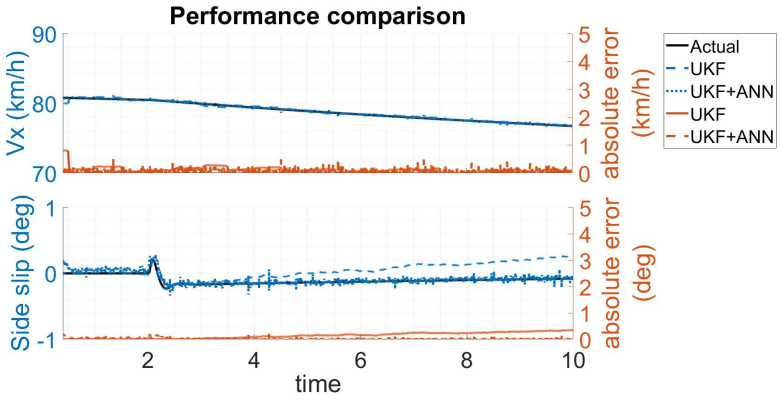

(a) 40 deg.

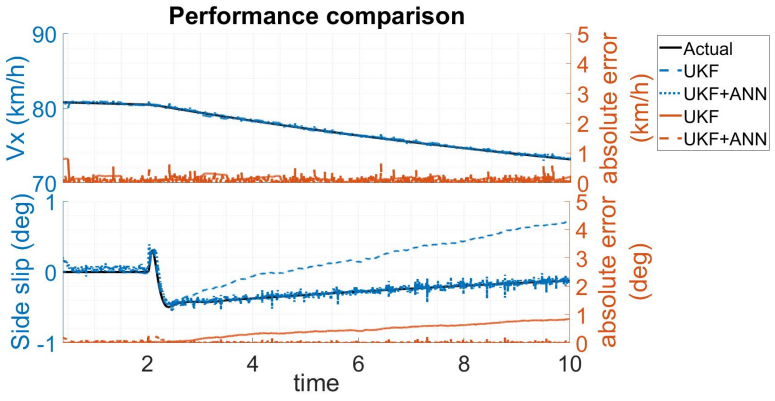

(b) 60 deg.

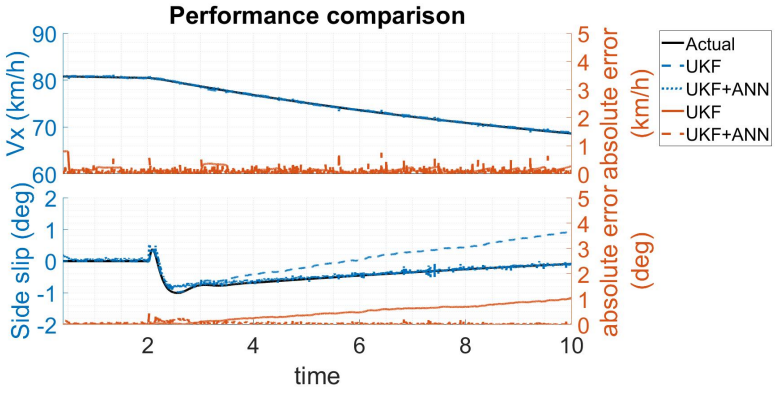

(c) 80 deg.

Figure 3.8: Side slip angle and longitudinal speed estimation results obtained by the two State Estimator configurations in step manoeuvres with different steering angle and a longitudinal speed of 80 km/h.

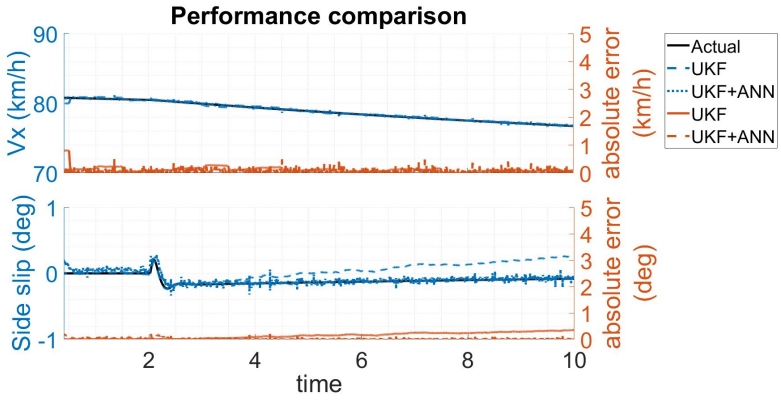

(a) nominal friction.

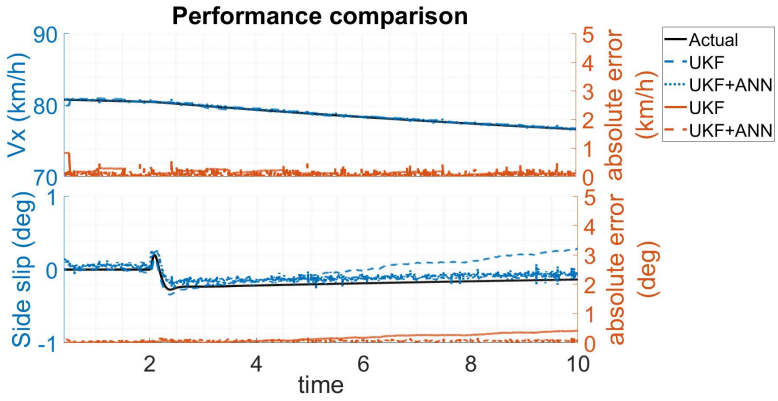

(b) 0.7 friction.

Figure 3.9: Side slip angle and longitudinal speed estimation results obtained by the two State Estimator configurations in step manoeuvres with a steering angle of 40 deg and a longitudinal speed of 80 km/h with nominal and 0.7 friction coefficient.

3.4 Conclusions

In conclusion, the current study was carried out with the intention of reduce the errors made by the state of art systems in the side slip angle estimation. Therefore, a mixed approach was investigated combining the potential of the AI to approximate all the function without knowing a dynamic model, and the state observer capabilities of combining measure signal and dynamic model to reduce the estimation errors.

To test and validate the proposed architecture, a Montecarlo analysis was done by exploring the influence that some dynamic parameters have on the estimation process, such as longitudinal speed, lateral acceleration and friction coefficient.

The results obtained show how the use of a ANN, trained in a data-set of limited and specific manoeuvres, as sensor measure of the vehicle longitudinal and lateral velocities allows a reduction of the estimation errors in all the simulated manoeuvres, ensuring more robust estimation to vehicle dynamic changes allowing better performance of Trajectory planning and Tracking systems, as well as increased reliability of Stability Systems.

3.5 Case study application

The two states estimator configurations developed were tested also to the case of study application: the Localizator and Estimator algorithm provides to the Trajectory Tracking, explained in Chapter 4, the input of global positions and speed. The results in terms of local longitudinal speed and side slip angle estimation during a lap are shown in Figure 3.10. The Mean Absolute Errors (MAE) of both longitudinal and side slip angle is reduced with the combined approach of ANN and UKF. In addition, by the plot one can see that the mix approach is able to converge more quickly to the target values then the solely UKF. However, the side slip angle estimation resulted affected by noise leading to excessively high peak error values in the curves. This most affects the functioning of subsequent layers, as will be seen in the Integration Chapter 6.

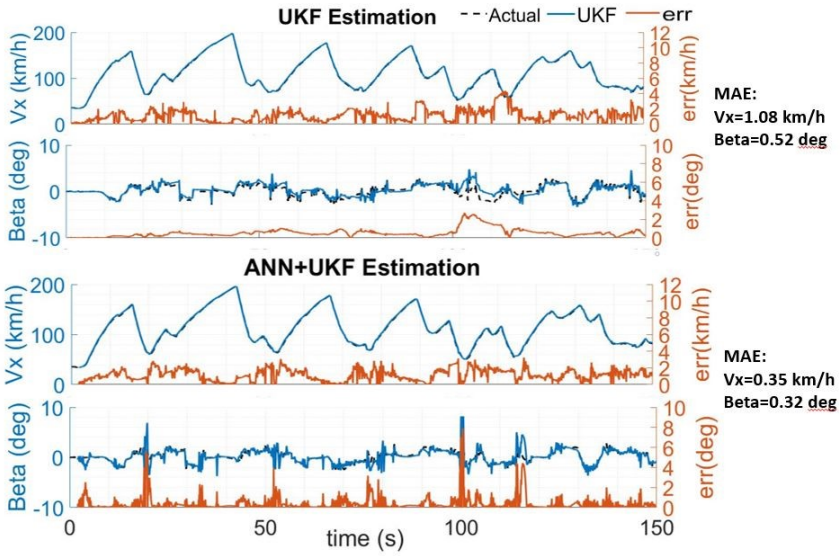

Figure 3.10: Vehicle speed and side slip angle estimation results obtained in the application to the case of study of the two State Estimator configurations developed.

Chapter 4

Trajectory planning and tracking

The aim of the study shown in this Chapter was to develop Trajectory Planning that would allow an autonomous racing car to be driven as close as possible to what a driver would do, defining the most appropriate inputs for the current scenario. The search for the optimal trajectory in terms of lap time reduction involves the modelling of all the non-linearities of the vehicle dynamics with the disadvantage of being a time-consuming problem and not being able to be implemented in real-time. However, to improve the vehicle performances, the trajectory needs to be optimized on-line with the knowledge of the actual vehicle dynamics and path conditions. Therefore, this study involved the development of an architecture that allows an autonomous racing car to have an optimal on-line Trajectory Planning and Path Tracking ensuring professional driver performances. The real-time trajectory optimization can also ensure a possible future implementation in emergency situation where avoiding collision scenarios could be faced. It was chosen to implement a local Trajectory Planning based on the MPC logic and solved as LP by SCP. The idea was to achieve a computational cost, 0.1 s, using a point mass vehicle model constrained by experimental definition and approximation of the car's GG-V, and developing an optimum model-based Path Tracking to define the driver model that allows a car to follow the trajectory defined by the planner ensuring a signal input every 0.001 s.

To validate the algorithm, two types of tests were carried out: a Matlab-Simulink, Vi-Grade co-simulation test, comparing the proposed algorithm with the performance of an off-line motion planning, and a real-time simulator test, comparing the proposed algorithm with the performance of a professional driver. The results obtained showed that the computational cost of the optimization algorithm developed is below the limit of 0.1 s, and the architecture showed a reduction of the lap time of about 1 s compared to the off-line optimizer by updating the trajectory in real-time with vehicle conditions, instead of optimising the car performance on a fixed path of minimum curvature. In addition, it showed reproducibility of the performance obtained by the driver.

4.1 Trajectory Tracking architecture

In Figure 4.1, the architecture developed is shown. The idea is to divide the Trajectory Planning from the Path Tracking instead of implemented a single MPC with a complex and detailed vehicle and tire model by ensuring a real-time implementation of the algorithm that the current technologies do not allow otherwise. Thus, an LP optimizer is implemented as Trajectory Planning, giving the reference position and speed to minimize the lap time every 0.1 s, and an optimum controller is implemented to allow the car to follow reference state values by defining the input SWA, throttle pedal and braking pedal every 0.001 s. These sample time values were necessary because an increase compared to the time of 0.1 s in providing the position and speeds that the vehicle must have is excessive compared to the speed of the vehicle resulting in a delay with respect to its position; from the tests undertaken, an increase in the time of 0.001 s of the controller was found to worsen the performance of the control.

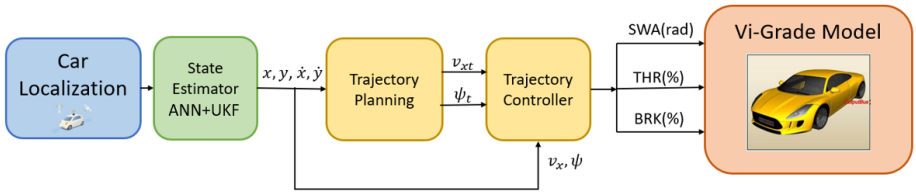

Figure 4.1: Block diagram of the Trajectory Tracking layer.

The Trajectory Planning and Path Tracking use the states of the car in the race track as feed-back. These states are estimated by the Localization Layer described in the above Chapter 3.

All the layers shown in Figure 4.1 were implemented in Matlab-Simulink software and then compiled in C to be used in the real-time car simulator of Vi-Grade. The different control algorithms were integrated into the same Simulink model considering the rate transition between subsystem with different sample time. Since the difference in time step implies that the optimization layer provides the same value for 100 steps of the controller, an integration algorithm between the path planning and trajectory controller is developed (showed in more detailed in Chapter 6). This algorithm ensures that the positions and velocities provided by the optimizer to the controller increase with the constant acceleration optimized, and after 100 steps, the vehicle achieves the position and velocity values expected by the optimizer. In the event that the vehicle fails to be in the expected condition, the change of values given by the change of optimizer steps needs to be compatible with the vehicle's possible acceleration limits based on the state the vehicle is in. The logic is shown in Equation (4.1):

$$V_x = \begin{cases} V_{x0} - (V_{x0} - V_x)0.1 & \text{if } abs(V_{x0} - V_x) > 0.5, \& \Delta t_o \neq 0 \\ V_{x0} + \Delta t_c a_x & \text{if } abs(V_{x0} - V_x) \leq 0.5, \& \Delta t_o = 0 \end{cases}$$

$$V_y = \begin{cases} V_{y0} - (V_{y0} - V_y)0.1 & \text{if } abs(V_{y0} - V_y) > 0.5, \& \Delta t_o \neq 0 \\ V_{y0} + \Delta t_c a_y & \text{if } abs(V_{y0} - V_y) \leq 0.5, \& \Delta t_o = 0 \end{cases}$$

$$X = \begin{cases} X_0 - \Delta t_c V_x & \text{if } abs(V_{x0} - V_x) > 0.5, \& \Delta t_o \neq 0 \\ X_0 - \Delta t_c V_x & \text{if } abs(V_{x0} - V_x) \leq 0.5, \& \Delta t_o t_o = 0 \end{cases}$$
$$Y = \begin{cases} Y_0 - \Delta t_c V_y & \text{if } abs(V_{y0} - V_y) > 0.5, \& \Delta t_o \neq 0 \\ Y_0 - \Delta t_c V_y & \text{if } abs(V_{y0} - V_y) \leq 0.5, \& \Delta t_o = 0 \end{cases} \tag{4.1}$$

where V_x, V_y, X, Y are the speeds and positions that the car has to follow in the current time; V_{x0}, V_{y0}, X_0, Y_0 are the speeds and positions that the car had at the previous time step of the controller; $\Delta t_c, \Delta t_o$ are, respectively, the controller sample time of 0.001 s, and the difference between the actual and previous time of the optimizer in the sample time of the controller; 0.1 is a tuning value that reduced the speed step between the actual and the future value if it is higher than 0.5 m/s.

4.2 Trajectory Planning

To set-up the MPC optimization problems, the Gurobi solver is used, a commercial solver with parallel algorithms for large-scale linear programs, quadratic programs, and mixed integer programs. From the Gurobi optimization reference manual [89], the problem was implemented in the following form:

$$\underset{z}{minimize} \quad -t^T_{j(\tilde{p}^{(Hn)})}\boldsymbol{p}^{(Hn)} + \sum_{i=1}^{Hn}\Big(W_{(j(\tilde{p}^{(i)}))}\eta^{(i)} + R_{\chi F(j(\tilde{p}^{(i)}))}\delta^{(i)} + \cdots \tag{4.2}$$
$$\cdots + R_{\chi R(j(\tilde{p}^{(i)}))}\lambda^{(i)} + R_{\gamma(j(\tilde{p}^{(i)}))}\rho^{(i)}\Big)$$

$$\boldsymbol{x}^{(i)} = A\boldsymbol{x}^{(i-1)} + B\boldsymbol{u}^{(i-1)} \quad \forall i = 1, \cdots, Hn \tag{4.3}$$

$$N_{j(\tilde{p}^{(i)})}\boldsymbol{p}^{(i)} - \eta^{(i)} = diag(N^T_{j(\tilde{p}^{(i)})})T_{(j(\tilde{p}^{(i)})} \quad \forall i = 1, \cdots, Hn \tag{4.4a}$$
$$A_{acc}(\tilde{\boldsymbol{v}}^{(i)}, \boldsymbol{\theta}^{(k)}) \cdot \boldsymbol{u}^{(i)} \leq b_{acc}(\tilde{\boldsymbol{v}}^{(i)})c^2_{(j(\tilde{p}^{(i)})} \quad \forall i = 1, \cdots, Hn \tag{4.4b}$$
$$\forall k = 1, \cdots, tn$$
$$\left[\tilde{Rrot}_{(i-1,i)}\right]\begin{bmatrix}\boldsymbol{u}^{(i-1)} \\ \boldsymbol{u}^{(i)}\end{bmatrix} - \begin{bmatrix}\delta^{(i)} \\ \lambda^{(i)} \\ \rho^{(i)} \\ \rho^{(i)}\end{bmatrix} = 0 \quad \forall i = 1, \cdots, Hn \tag{4.4c}$$

$$\tilde{p}^{(i)}_x - v_{t\,max}\Delta t \leq p^{(i)}_x \leq \tilde{p}^{(i)}_x + v_{t\,max}\Delta t \quad \forall i = 1, \cdots, Hn \tag{4.5a}$$
$$\tilde{p}^{(i)}_y - v_{t\,max}\Delta t \leq p^{(i)}_y \leq \tilde{p}^{(i)}_y + v_{t\,max}\Delta t \quad \forall i = 1, \cdots, Hn \tag{4.5b}$$
$$-v_{t\,max} \leq v^{(i)}_x \leq v_{t\,max} \quad \forall i = 1, \cdots, Hn \tag{4.5c}$$
$$-v_{t\,max} \leq v^{(i)}_y \leq v_{t\,max} \quad \forall i = 1, \cdots, Hn \tag{4.5d}$$
$$-A_{Max}(\tilde{v}_t) \leq a^{(i)}_x \leq A_{Max}(\tilde{v}_t) \quad \forall i = 1, \cdots, Hn \tag{4.5e}$$
$$-A_{Max}(\tilde{v}_t) \leq a^{(i)}_y \leq A_{Max}(\tilde{v}_t) \quad \forall i = 1, \cdots, Hn \tag{4.5f}$$
$$\eta^{(i)}, \delta^{(i)}, \lambda^{(i)}, \rho^{(i)} \geq 0 \quad \forall i = 1, \cdots, Hn \tag{4.5g}$$

where the *Objective Function* (4.2), the *Vehicle Model* (4.3), the constraints used to represent the vehicle dynamic and track limitation (4.4), and the *Bound Constraints* (4.5) are shown and will be explained in the following Subsections.

The problem is faced as an LP optimization, and its solutions are found by iterating the optimization every time step: the positions, $\tilde{p}^{(i)}$, velocities, $\tilde{v}^{(i)}$, and accelerations, $\tilde{u}^{(i)}$, are the state values optimized at the previous step; so the current iteration defines the optimum state, $x = [p_x, p_y, v_x, v_y]$, and input, $u = [a_x, a_y]$ for all the prediction horizon lengths. The variables weights of the *Objective Function*, $W_{(j(\tilde{p}^{(i)}))}$-$R_{\chi F(j(\tilde{p}^{(i)}))}$-$R_{\chi R(j(\tilde{p}^{(i)}))}$-$R_{\gamma(j(\tilde{p}^{(i)}))}$, are defined by a tuning process, and the prediction horizon was chosen to be composed of $120 * 0.1$ time steps to ensure that the optimizer should be able to see the following curve when the longest straight begins, as tests have shown that the performance was satisfactory. Having a velocity dependent event horizon length ensures to have the planner to see far away when it needs allowing the event horizon to be stable at the nodes closest to the car state. In fact, if the optimiser could not see the next curve, it would not be able to establish the best trajectory in the straight by oscillating at each iteration step. From the Figure 4.2 it is possible to see the trajectory predicted along the event horizon in ten successive iteration steps. As one can see, the trajectory has variations at nodes on the end of the event horizon but remains fairly constant at nodes close to the car, not compromising efficiency.

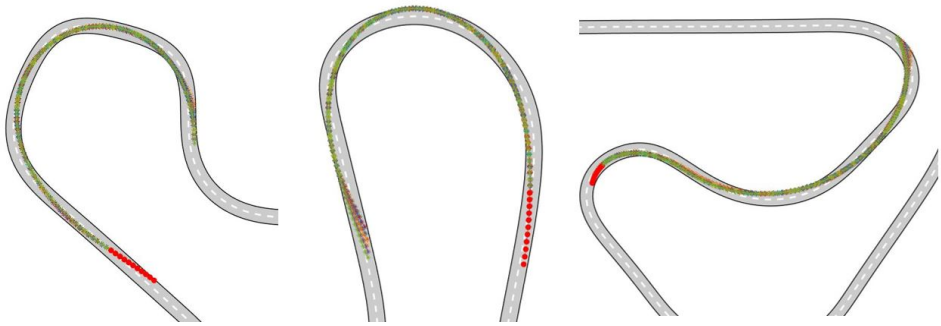

Figure 4.2: Prediction event horizon in ten successive optimisation steps to handle three curves of the race-track.

4.2.1 Models

To ensure a computational cost of 0.1 s, the vehicle was modeled as a point mass model, with the following assumption:

- The vehicle's side-slip and tires' slip angles are negligible. This means that the velocity vector is always tangent to the trajectory and it allows to ignore behavior such as drifting, spinning, or sliding;
- The tires' slippage is negligible;
- The longitudinal and lateral weight transfers are neglected in the vehicle model but will be considered in the constraint formulations;
- The racetrack is flat.

Therefore, referring to the coordinate system shown in Figure 4.3: x,y are the global coordinate system when stationary with respect to the racetrack; χ,γ are the vehicle coordinate system; and ψ is the vehicle yaw angle that indicates the tangent to the trajectory. The dynamic model was implemented in the discrete state space Equation (4.6) and detailed by Equation (4.7).

$$x^{(i)} = Ax^{(i-1)} + Bu^{(i-1)} \tag{4.6}$$

$$\begin{bmatrix} p_x^{(i)} \\ p_y^{(i)} \\ v_x^{(i)} \\ v_y^{(i)} \end{bmatrix} = \begin{bmatrix} 1 & 0 & \Delta t & 0 \\ 0 & 1 & 0 & \Delta t \\ 0 & 0 & 1 & 0 \\ 0 & 0 & 0 & 1 \end{bmatrix} \begin{bmatrix} p_x^{(i-1)} \\ p_y^{(i-1)} \\ v_x^{(i-1)} \\ v_y^{(i-1)} \end{bmatrix} + \begin{bmatrix} \frac{\Delta t^2}{2} & 0 \\ 0 & \frac{\Delta t^2}{2} \\ \Delta t & 0 \\ 0 & \Delta t \end{bmatrix} \begin{bmatrix} a_x^{(i-1)} \\ a_y^{(i-1)} \end{bmatrix} \tag{4.7}$$

where, in this case, i indicates the time-step index; $x^{(i)} \in \mathbb{R}^4$ is the state vector composed by the vehicle position and velocity vector in the global coordinate system, $\boldsymbol{p} = [p_x, p_y]$ and $\boldsymbol{v} = [v_x, v_y]$; $u^{(i)} \in \mathbb{R}^2$ is the input vector composed by the vehicle acceleration vector in global coordinate system, $[a_x, a_y]$; $A \in \mathbb{R}^{4x4}$ is the system matrix and $B \in \mathbb{R}^{4x2}$ is the input matrix made explicit in Equation (4.7). From these equations, it is possible to deduce that to have a linear system, the time-step, Δt, must chose constant. Thus, the prediction horizon is discretized with constant time intervals, and the discrete model, shown in Equation (4.3), is then iterated forward in time from a time-step to the subsequent one.

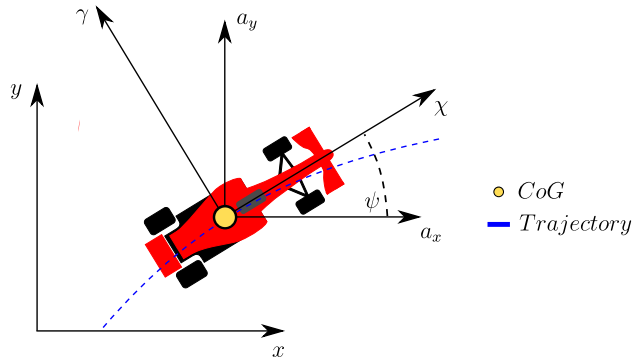

Figure 4.3: Global and vehicle coordinate systems.

At the first iteration step, the points of the event horizon are considered to be known by starting from a known x and y position on the track and null velocities and finding the next 119 nodes of the horizon using the equations of uniformly accelerated motion. Subsequently, the optimiser receives as input the vehicle states at the previous step and the entire predicted event horizon at the previous step minus the first node. From these it calculates the new optimised horizon. In off-line Path Planning where the trajectory is optimized for the entire race-track also the final nodes are constrained. However in this case, no final conditions were set. Actually, these constraints would presuppose that the planner knows in which position and speed conditions the vehicle is in the race-track at the end of the event horizon. But, the planner was designed to work on-line and adapt to the dynamic

conditions of the car as it travels, allowing the last nodes the ability to vary from lap to lap with the states of the vehicle.

4.2.2 Objective Function

The *Objective Function* proposed in this work is purely linear, as shown in Equation (4.2). This is a benefit because it reduces the optimization time and allows one to not worry about defining a positive objective matrix to ensure a feasible solution. It is composed of two strategies:

- Minimizing time strategy;
- Slack variables.

The first strategy aims to minimize the lap time, and the second one allows softening the hard limit of the constraints.

Minimizing Time Strategy

Since a constant discretization time Δt of the prediction horizon is chosen to make Equation (4.7) linear, maximizing the distance traveled in the direction of the tangent vector of the mid-line could be a strategy to cover the largest number of racetrack sectors. This strategy was expressed within the objective function as follows:

$$\underset{z}{minimize} \quad -t^T_{j(\tilde{p}^{(Hn)})} \begin{bmatrix} p_x^{(Hn)} \\ p_y^{(Hn)} \end{bmatrix} = -t^T_{j(\tilde{p}^{(Hn)})} \boldsymbol{p}^{(Hn)} \tag{4.8}$$

where it maximized the longitudinal and lateral distance between the current, $\boldsymbol{p}^{(Hn)}_{x,y}$, and previous, $\tilde{p}^{(Hn)}$, position points projected in the tangent direction, $t_{j(\tilde{p}^{(Hn)})}$, for all the points of the prediction horizon Hn.

Slack Variables

To avoid the infeasible problem, the slack variable strategy is used [90]. This methodology ensures avoiding that the constraints equations are not strictly equal to a constant limit but to an enlarged or reduced one by adding to the constraint a positive variable, weighted in the objective function. In this way, the designer can strengthen or relax the constraints by increasing or decreasing the associated weights.

$$\begin{aligned} \underset{z}{minimize} \ \sum_{i=1}^{Hn} \Big(& W_{(j(\tilde{p}^{(i)}))} \eta^{(i)} + R_{\chi F(j(\tilde{p}^{(i)}))} \delta^{(i)} + \cdots \\ & \cdots + R_{\chi R(j(\tilde{p}^{(i)}))} \lambda^{(i)} + R_{\gamma(j(\tilde{p}^{(i)}))} \rho^{(i)} \Big) \end{aligned} \tag{4.9}$$

In Equation (4.9), $\eta^{(i)}$, $\delta^{(i)}$, $\lambda^{(i)}$ and $\rho^{(i)}$ are the slack variables and $W_{(j(\tilde{p}^{(i)}))}$, $R_{\chi F(j(\tilde{p}^{(i)}))}$, $R_{\chi R(j(\tilde{p}^{(i)}))}$, $R_{\gamma(j(\tilde{p}^{(i)}))}$ are the weights, respectively. In this work, by associating the weights to the nodes of the mid-line, $(j(\tilde{p}^{(i)}))$, it is possible to impose to the solver not only the ability to vary the constraints but also to decide whether one point of the racetrack is more important than another in terms of limit variations available, as a human driver can do.

4.2.3 Linear and Quadratic Constraints

To ensure optimized solutions compatible with vehicle dynamics and track limits, the vehicle accelerations and positions are limited by constraint Equations (4.4), which can be divided into three categories:

- Racetrack limitations, (4.4a);
- g-g limitations, (4.4b);
- jerk limitations, (4.4c).

Racetrack Limitations

In order to constrain the optimizer to provide output car positions within the path area, the optimization was solved by using the SCP approach as [91] suggested. Thus, the constraint is not the entire racetrack area, which involves a non-convex problem, but smaller racetrack sections where the problem is convex and so solvable. Using the curvilinear abscissa to express the position of the material point would probably have allowed for a convex constraint. But at the same time would have made the dynamic system non-linear. In addition, optimising over the entire trajectory at the same time would have increased the calculation time, so a path discretization would have been done anyway. This coupled with the fact that the s-domain formulation cannot be used if the vehicle has to stop or revert the direction of travel on the track has made the curvilinear abscissa not usable for our case. Actually, we want to make the optimisation as general as possible to be applied also in scenarios outside of the race-track one.

Therefore, it was decided to sample the middle line with points 1 m apart, $T_{Mid(j)}$, and to make these correspond to those intercepted on the inner and outer edge by the normal vector to the middle line and named, respectively, with $T_{IN(j)}$ and $T_{OUT(j)}$ in Figure 4.4. Then, it was possible to constrain the output states of the solver, $p^{(i)}$, within the path area, using the following equations:

$$\begin{aligned}
\left(\boldsymbol{p}^{(i)} - \boldsymbol{T}_{Out(j(\tilde{p}^{(i)}))}\right)^T \left(-n_{j(\tilde{p}^{(i)})}\right) - \eta^{(i)} = 0 \quad \forall i \in \{1, \cdots, Hn\} \\
\left(\boldsymbol{p}^{(i)} - \boldsymbol{T}_{In(j(\tilde{p}^{(i)}))}\right)^T \left(n_{j(\tilde{p}^{(i)})}\right) - \eta^{(i)} = 0 \quad \forall i \in \{1, \cdots, Hn\} \\
\eta^{(i)} \geq 0 \quad \forall i \in \{1, \cdots, Hn\}
\end{aligned} \tag{4.10}$$

where $p^{(i)}$ is the position state vector found by the optimization in the current optimization step; $T_{Out(j(\tilde{p}^{(i)})}$ and $T_{In(j(\tilde{p}^{(i)})}$ are the limits given by the outer and inner edge referred to the solution found in the previous iteration step, $\tilde{p}^{(i)}$; $n_{j(\tilde{p}^{(i)})}$ is the normal direction to the mid-line, which allows the distance between the two points to be projected in the normal direction; and $\eta^{(i)}$ is the slack variable, which, being constrained in the *Bound Constraints* Equation (4.5g) as positive, forces the position of the vehicle to be less than zero making the racetrack constraints more or less rigid depending on the weight assigned to it in the *Objective Function* (4.2). Therefore, it is possible to vary the weight of the slack variable in a differentiated way according to the position of the car in the track, being able, for example, to soften it in the presence of a curb by allowing the car to go out of the limits of the track where possible to improve performance.

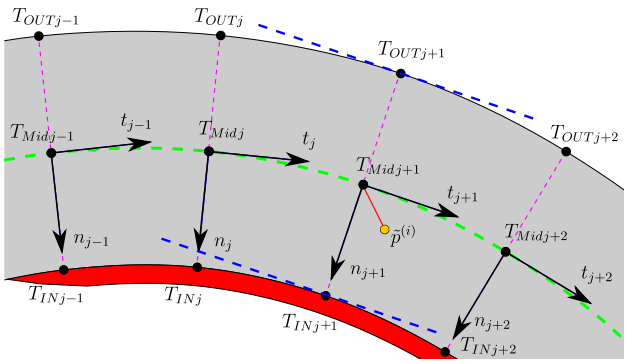

Figure 4.4: Representation of the racetrack linear approximation.

GG Limitations

In order to represent the exchange of forces occurring at the point of contact between wheel and road, it was decided to not implement a tire model but to bound the car's acceleration inside the GG diagram, measured at the center of gravity under steady-state conditions, such as [33, 87, 92].

The papers [93–95] show that the acceleration constraints area has the shape of two semi-ellipses: one stands for the forward acceleration, shown by the blue line in Figure 4.5a, and the other stands for backward acceleration, shown by the red line in Figure 4.5a.

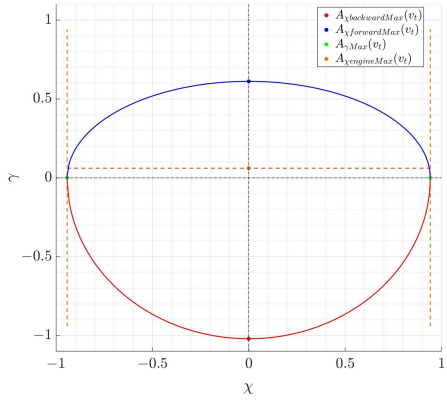

(a) Approximation method for the g-g diagram: two half ellipses for tire limits and a line for engine limit.

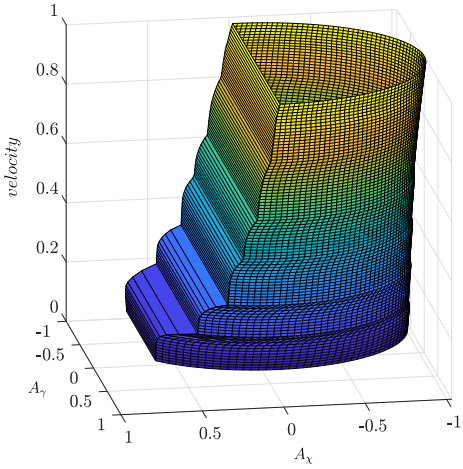

(b) Autonomous driving car GG-V diagram, evaluated through simulation tests.

Figure 4.5: Single GG constrain diagram of the vehicle model and its change as function of the vehicle speed.

Empirically defining the maximum acceleration values, $A_{\gamma Max(v_t)}$, $A_{\chi backwardMax(v_t)}$ and $A_{\chi forwardMax(v_t)}$, the semi-axes of the ellipses are defined and so, the tire, aerodynamic and vehicle system limits are taken into account. Therefore, if the blue

and red lines in Figure 4.5a show the limits just mentioned, the horizontal orange line shows the maximum performance that the car's engine can achieve in forward acceleration. In addition, these limits change with the vehicle speed because of the drag and engine influence [96, 97]; thus, in Figure 4.5b, different GG diagrams were implemented in the function of the car speed obtaining the car GG-V diagram.

However, to better represent the vehicle dynamic and improve the performance, the idea was to implement the GG-V as quadratic constrains and not linearize its curves as is usually done, while maintaining the sample time under the specification of 0.1 s. However, due to the ability of the LP to handle only one convex quadratic constraint for each variable, a mixed approach was implemented: a conical constraint to reproduce the bigger, lower region associated with the vehicle braking capabilities exactly, and linear constraints to approximate the upper region, which is associated with the vehicle forward acceleration capabilities, being tested empirically, resulting in this region being well-described by the three orange dotted lines shown in Figure 4.5a. Therefore, the lower GG constraints are implemented as a negative semi-ellipse with the semi-axes values equal to the car's maximum deceleration. This inequality constraint is shown in the vehicle coordinate system by Equation (4.11) and in the global coordinate system by Equation (4.12).

$$(\frac{A_{\chi backward}}{A_{\chi backwardMax}(v_t)})^2 + (\frac{A_{\gamma}}{A_{\gamma Max}(v_t)})^2 - c^2 \leq 0 \tag{4.11}$$

$$\begin{aligned} a_x^2(\frac{v_x^2}{v_t^2}A_{\gamma Max}^2 + \frac{v_y^2}{v_t^2}A_{\chi backwardMax}^2) + a_y^2(\frac{v_y^2}{v_t^2}A_{\gamma Max}^2 + \frac{v_x^2}{v_t^2}A_{\chi backwardMax}^2) + \\ + a_x a_y(\frac{v_x v_y}{v_t^2}(A_{\gamma Max}^2 - A_{\chi backwardMax}^2)) - A_{\chi backwardMax}^2 A_{\gamma Max}^2 c^2 \leq 0 \end{aligned} \tag{4.12}$$

Instead, the upper GG constraints are represented as a set of lines tangent at the positive semi-ellipse. These lines are calculated by finding the tangents at the ellipse in points described by different angles, θ, thanks to Equation (4.13) in the coordinate vehicle system and Equation (4.14) in the global coordinates system.

$$(\frac{A_{\chi forward}}{A_{\chi forwardMax}(v_t)})cos\theta + (\frac{A_{\gamma}}{A_{\gamma Max}(v_t)})sin\theta - c \leq 0 \tag{4.13}$$

$$\begin{aligned} a_x(\frac{v_x}{v_t}A_{\gamma Max}cos\theta - \frac{v_y}{v_t}A_{\chi forwardMax}sin\theta) + a_y(\frac{v_y}{v_t}A_{\gamma Max}cos\theta + \\ + \frac{v_x}{v_t}A_{\chi forwardMax}sin\theta) - A_{\chi forwardMax}A_{\gamma Max}c \leq 0 \end{aligned} \tag{4.14}$$

In all the equations shown, the ratio between the longitudinal speed component, v_x, and speed vector, $v_t = \sqrt{v_x^2 + v_y^2}$, is the cosine of the yaw angle ψ; and the ratio between the lateral speed component, v_y, and speed vector, $v_t = \sqrt{v_x^2 + v_y^2}$, is the sine of the yaw angle ψ. Both of these ratios are used to rotate the input vector $u = [a_x, a_y]$ in the global coordinate system and group the constraints in Equation (4.4b).

The variable c is a scalar coefficient that can expand or narrow the boundary of the GG diagram and change the tire performances representing degraded contact conditions due, for example, to rain or tire wear. c could be scaled in a global manner for all of the track or could be varied online in local sections being related to the position of the vehicle on the racetrack.

Jerk Limitations

Since the vehicle is modeled as a point mass, sudden variations in acceleration, $\boldsymbol{u} = [a_x, a_y]$, can lead to the generation of an angular trajectory that does not represent a real trajectory of a racing car, which actually tends to be smooth. Usually, to avoid this problem, the quadratic variation of the accelerations is implemented as a term of the *Objective Function* to minimize it. In this study, to maintain the *Objective Function* as linear, the *Jerk Limitations* are implemented as constraint equations that require the jerks to be equal to positive slack variables. Therefore, the slack variables are inserted in the cost function as a linear term and a certain weight is assigned to them according to the point on the track where the car is located. In this way, the optimizer is able to determine the accelerations variation necessary to increase performance and maintain a smooth trajectory, and the designer can choose which direction of acceleration to favor in relation to where the car is located on the track, e.g., in a straight line the lateral acceleration can be forced to vary more slowly, favoring a faster variation of the longitudinal accelerations.

In Equation (4.4c), the strategy is shown, where $\left[\delta^{(i)}, \lambda^{(i)}, \rho^{(i)}, \rho^{(i)}\right]$, are the slack variables used to soften the zero hard limit given to the input vector variation, $\left[\boldsymbol{u}^{(i-1)}, \boldsymbol{u}^{(i)}\right]$, rotated in the global coordinate system by $\left[\tilde{Rrot}_{(i-1,i)}\right]$. In addition, it was chosen to implement different slack variables for different acceleration vectors diversifying the jerk of the various dynamic system: δ for forward longitudinal acceleration, λ for backward longitudinal acceleration, and ρ for lateral acceleration.

4.2.4 Bound Constraints

As usual, the optimization variables must be limited to effectively guide the solver in the optimization phases. This allows a faster search for the correct solution and reduces the possibility of facing the infeasible problem that results in a reduction in the optimization time. For this reason, the following trust regions were added to the solver: Equations (4.5a) and (4.5b), which limit the positions; Equations (4.5c) and (4.5d), which limit the speeds; Equations (4.5e) and (4.5f), which limit the accelerations; and Equation (4.5g), which imposes a slack variable that is greater than zero.

4.3 Path Tracking

Regarding the Path Tracking, an optimum control was chosen to be implemented by decoupling the longitudinal and lateral vehicle dynamics and ensuring a low computational cost. The developed LQR has a sample time of 0.001 s to define the car input with a certain continuity as a driver will do. In this way, the Path Planning is embedded with a Path Tracking to compose the trajectory Tracking with a dynamic vehicle model and a reduced time step.

4.3.1 Vehicle Model

To ensure a linear model to the LQR, the longitudinal and lateral vehicle dynamic are decoupled and modeled separately, obtaining a model where the longitudinal part defines the inputs pedals throttle and brake percentage, and the lateral part defines the SWA signal input.

Longitudinal Model

About the longitudinal model, it is supposed to have the single track vehicle model, shown in Figure 4.6, in which the longitudinal acceleration of the vehicle is set equal to the sum of the longitudinal tire forces:

$$a_x = \sum_{i=1}^{4} F_{xi} \tag{4.15}$$

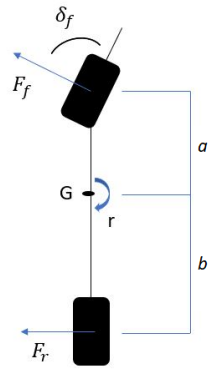

Figure 4.6: Single track vehicle model.

Considering the total longitudinal force that the car has to have as a percentage of the maximum tracking force that the engine and braking system can express, the longitudinal vehicle model could be implemented as:

$$\ddot{x} = \frac{CF_{max}}{m} \tag{4.16}$$

where $\ddot{x}$ is the vehicle longitudinal acceleration; C is the throttle or brake pedal percentage in the range [0–100](%); F_{max} is the maximum force that the engine and brake system can give; and m is the vehicle mass.

Lateral Model

Regarding the lateral model, the single track vehicle model shown in Figure 4.6 was used, considering the lateral and yaw dynamic balance given by [87], as follows:

$$\dot{v} = -\frac{(C_{yf} + C_{yr})}{mu}v + (-u + \frac{C_{yf}a - C_{yr}b}{mu})r + \frac{C_{yf}}{m}\delta_f \tag{4.17}$$

$$\dot{r} = -\frac{(C_{yf}a - C_{yr}b)}{Ju}v + \frac{(C_{yf}a^2 + C_{yr}b^2)}{Ju}r + \frac{C_{yf}a}{J}\delta_f \tag{4.18}$$

where v and r are, respectively, the lateral speed component and yaw rate; C_{yf} and C_{yr} are the cornering stiffness tire parameters; u is the longitudinal speed component; a and b are, respectively, the front and rear wheelbase of the vehicle; m,J and R are the mass, vertical moment of inertia and wheel radius of the car.

4.3.2 Optimum Control of the Inputs

Considering the longitudinal and lateral vehicle dynamics shown in the previous Subsection, a LQR can be implemented by tracking the longitudinal and lateral vehicle speed and position found by the Trajectory Planning. In fact, the optimized longitudinal vehicle speed can be considered as the target speed that the vehicle has to have and subtracted from the actual longitudinal vehicle speed obtaining:

$$\dot{e_x} = \dot{x} - \dot{x_t} = \frac{de_x}{dt} \tag{4.19}$$

$$\ddot{e_x} = \ddot{x} - \ddot{x_t} = \frac{(C - C_t)F_{max}}{m} \tag{4.20}$$

where F_{max} and m are constant variable and $(C-C_t)$ is the throttle pedal percentage if the speed error, $\dot{e}_x$, is positive and the brake pedal percentage if it is negative, saturated from 0 to 100%.

Instead, to follow the lateral dynamics suggested by the Path Planning, the yaw and lateral vehicle position and speed are tracked, considering the errors between the actual vehicle values and the reference values exiting the Trajectory Planning. Thus, replacing the Equations (4.17) and (4.18) in (4.21) and considering the longitudinal vehicle speed, u, as a constant variable, the following was obtained:

$$\dot{e_y} = \dot{y} - \dot{y_t} = v + u\psi - v_t - u\psi_t \qquad \ddot{e_y} = (\dot{v} - \dot{v}_t) + u(r - r_t) \tag{4.21}$$

$$\ddot{e_y} = -\frac{(C_{yf} + C_{yr})}{mu}\dot{e_y} + \frac{(C_{yf} + C_{yr})}{m}e_\psi + \frac{(C_{yf}a - C_{yr}b)}{mu}\dot{e_\psi} + \frac{C_{yf}}{m}(\delta_f - \delta_{ft}) \tag{4.22}$$

$$\dot{e_\psi} = \dot{\psi} - \dot{\psi_t} = r - r_t \tag{4.23}$$

$$\ddot{e_\psi} = -\frac{(C_{yf}a - C_{yr}b)}{Ju}\dot{e_y} + \frac{(C_{yf}a - C_{yr}b)}{J}e_\psi + \frac{(C_{yf}a^2 + C_{yr}b^2)}{Ju}\dot{e_\psi} + \frac{C_{yf}a}{J}(\delta_f - \delta_{ft}) \tag{4.24}$$

therefore, the dynamic state space has the following representation:

$$\begin{Bmatrix} \dot{e_x} \\ \ddot{e_x} \\ \dot{e_y} \\ \ddot{e_y} \\ \dot{e_\psi} \\ \ddot{e_\psi} \end{Bmatrix} = A \begin{Bmatrix} e_x \\ \dot{e_x} \\ e_y \\ \dot{e_y} \\ e_\psi \\ \dot{e_\psi} \end{Bmatrix} + B \begin{bmatrix} (C - C_t) \\ (\delta_f - \delta_f t) \end{bmatrix} \tag{4.25}$$

where the errors of longitudinal, lateral and yaw position and rate are the LQR states, $X = [e_x; \dot{e}_x; e_y; \dot{e}_y; e_\psi; \dot{e}_\psi]$, which must be minimized by defining the car input $U = [(C - C_t); (\delta_f - \delta_{ft})]$ as follows:

$$U = -KX \tag{4.26}$$

here, K is the gains matrix calculated by solving the following off-line optimization:

$$minimize \sum X^T Q X + U^T R U \tag{4.27}$$

where the state and the input vectors are appropriately weighted by the matrices Q and R.

However, the state space formulation shown in Equation (4.25) does not ensure that the tracking errors converge to zero, even though the matrix $(Ax - BK)$ is asymptotically stable [98]. This is due to the omission of the term steady state:

$$B_2\dot{\psi}_{ss} \tag{4.28}$$

to ensure zero steady state errors, a feed-forward term is added to the state feed-back assuming that the steering controller is obtained by state feed-back plus a feed-forward term:

$$\delta = -Kx + \delta_{ff} \tag{4.29}$$

where δ_{ff} is:

$$\delta_{ff} = \frac{mu^2}{RL}[\frac{b}{C_{yf}} - \frac{a}{C_{yr}} + \frac{a}{C_{yr}}k_3] + \frac{L}{R} - \frac{b}{R}k_3 \tag{4.30}$$

where m, L, a, b are, respectively, the mass, the total wheelbase, the front and rear wheelbase of the car; R, C_{yf}, C_{yr} are the radius, the front and rear stiffness of the wheel; and k_3 is the third component of the matrix gain K calculated with Equation (4.27).

In addition, to compensate for the delay that the feed-back control produces in the actuation of the longitudinal input, a feed-forward term is added to the longitudinal feed-back state defining the acceleration and brake pedal control as:

$$C = -Kx + K_{ff}A_{xt} \tag{4.31}$$

where K_{ff} is the feed-forward gain found by a tuning process, and A_{xt} is the longitudinal acceleration target output from the path planning layer.

4.4 Experimental Results and Discussion

Two sessions of tests were carried out to validate the architecture proposed:

- Comparison with an off-line motion planning;
- Comparison with a driver.

The first test session involved the comparison of the developed autonomous control architecture with an off-line optimization algorithm developed by VI-Grade CRT. The intention of this comparison was to validate the optimization algorithm developed with a state of the art algorithm and to show that the on-line optimization of the trajectory improves the performances. The test is composed of two phases: the first one involved co-simulation between the Trajectory Tracking developed in Matlab-Simulink and the car model of the dynamic simulation software CRT; and the second one involved the minimum curvature optimization of Calabogie racetrack, shown in Figure 1.2, and the execution of the max-performance event explained in more detail in the next Subsection.

The simulations were carried out using a laptop PC with the characteristics given in Table 1.1 by setting the optimization as in Table 4.1.

The second test session had the intent of showing the real-time functionality of the entire structure by exploiting the static simulator shown in Figure 1.5a and located

at Meccanica 42 s.r.l. In this way, the model developed in the Matlab-Simulink environment needed to be compiled in C in the simulator's hardware provided by VI-Grade, and a test model has to be built where the systems communication is simulated as would be in the car. The results obtained are then compared with the performance of a driver obtained at the same simulator to verify that the model-simplified but constraint enhancing representation of dynamics achieves performance comparable to that of a professional driver.

The hardware characteristics and computational performance of the simulator are shown in Table 1.1 under the real-time test campaign reference.

In Table 4.2, one can see that the Path Planning computational time that resulted for both the hardware implementations is below the required specification of 0.1 s.

Table 4.1: Optimization algorithm settings.

Parameter	**Value**	**Units**
Prediction horizon length	120	step
n° optimization per step	1	
mid-line discretisation	1	m

Table 4.2: Path Planning computational performances in the two campaign configurations tested.

	Off-line test	**Simulator test**
Max computational time	0.07 s	0.06 s
Mean computational time	0.05 s	0.05 s

4.4.1 Comparison with Off-line Motion Planning

These tests have involved the comparison of the architecture proposed with the max-performance event simulation of CRT suite. The max-performance simulation is used to define the dynamic speed limit profile on a given racetrack [99]. This off-line simulation uses an iterative process where a specific static solver computes a velocity profile and then a dynamic solver verifies if the computed speed profile is feasible. Basically, the vehicle model used for static prediction has no suspensions and inherits all properties from the full CRT model. The effect of aero forces is considered and the effect of suspension jounce is taken into account by the presence of ride height maps, which link the dependency of ride heights to the vehicle velocity. The trajectory chosen to perform the max-performance event is that of minimum curvature of the Calabogie racetrack shown in Figure 1.2. In the literature, this trajectory is often used as a reference, and it has been found that it is a trajectory that allows getting very close to the minimum lap time on a racetrack. For these tests, the simulation road is considered flat, neglecting the dynamics effects that the racetrack slopes and banks have on the performance.

In Figure 4.7, the car's longitudinal and lateral accelerations as a function of speed, GG-V, achieved by the car model controlled by the algorithm proposed and

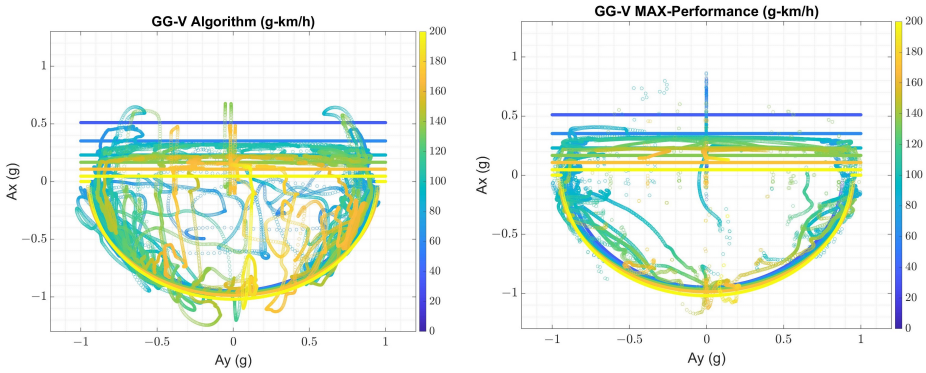

(a) Algorithm GG-V.

(b) Max-performance GG-V.

Figure 4.7: GG-V performances obtained by the Trajectory Tracking and the CarRealTime Max-Performance event.

by the max-performance event are shown. In the same figures, the GG-V constraints implemented in the Path Planning are shown. By Figure 4.7b, it is possible to see that the constraints assumed in the Trajectory Tracking are representative of the car, and by Figure 4.7a, it is possible to see that the car controlled by the algorithm developed is able to keep the car inside the constraints imposed, even if with respect to the max-performance results, it goes through the transients more instead of staying within the limits of grip. This may be due to the inputs given to the vehicle being noisier than those of the off-line control, as shown in Figure 4.9.

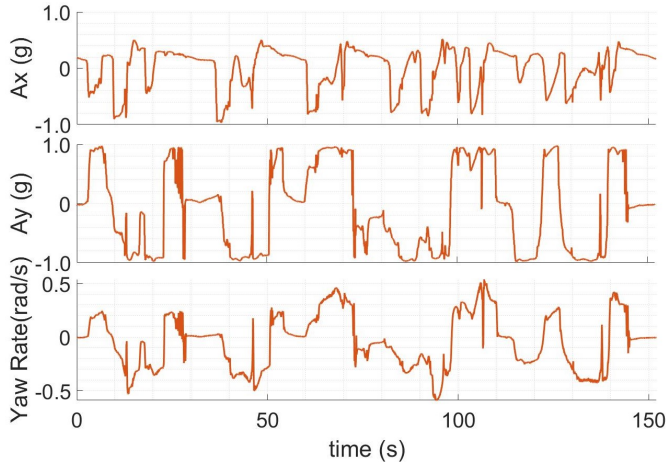

Figure 4.8: Longitudinal and later acceleration and yaw rate planned by the Path Planning compared with the one made by the car.

Looking at Figure 4.8 the estimated longitudinal end lateral acceleration together with the car yaw-rate are shown. This quantities could justify part of the inputs noise shown. This is most visible between the end of a curve and the beginning of the straight and during a curve with high lateral acceleration engagement. Some of this noise was reduced by tuning the jerk in the cost function in different way depends

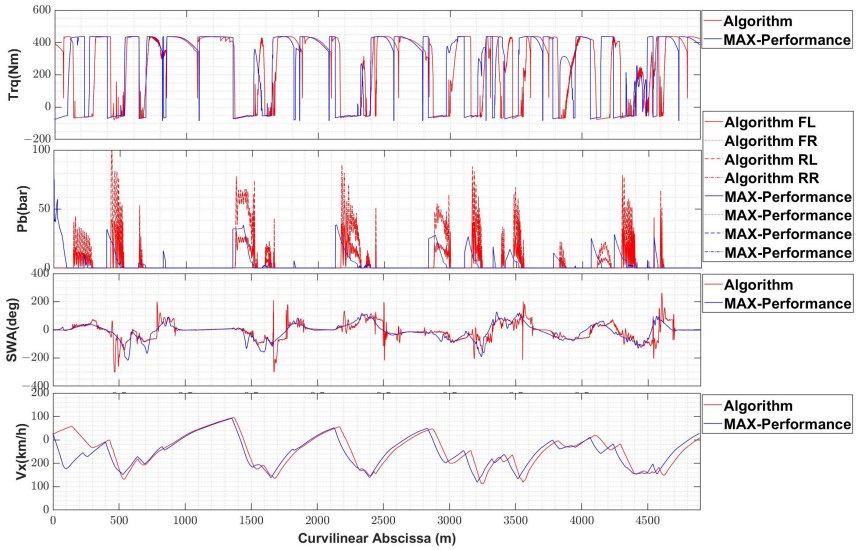

Figure 4.9: Car input commands and longitudinal speed achieved by the Trajectory Tracking proposed and CarRealTime Max-Performance event.

on the track sectors. Having used a steady state model, the acceleration rates, i.e. the jerks, are independent of each other without considering the contribution of the yaw rate. Even if the results obtained despite this simplification are comparable with those of the driver and those of the off-line optimiser with a more complex model, being able to link the acceleration jerks with a linear function could make it possible to reduce the noise where the dynamics are combined. Anyway, an in-depth study in the choice of the jerk weights must be done to reduce this input noises.

The accelerations and yaw rate estimated by the planner are not the only reason why the input values are so noisy. Another cause is due to the trajectory tracking tuning process. In fact, to ensure the right longitudinal acceleration input to the car the weight on the longitudinal speed must have a fairly high value. However, this value leads to noise braking input that is more efficiency. Probably, a weights differentiation between longitudinal acceleration and deceleration could be reduced this input noise, but at a first attempt this seams to be less efficiency.

Anyway, the engine torque, the chamber brake pressures and the SWA shown in Figure 4.9 are almost similar in quantities with differences due to the different trajectory made, even if there is a visible difference in the amplitude and timing between the two configurations, i.e., the algorithm performed higher and delayed brake pressures with respect to the max-performance event. This is reflected in the speeds achieved by the car, which are almost similar, but the algorithm's one brakes later, maintaining the high speed for more time than the max-performance speed, resulting in a reduction of lap time, as shown in Table 4.3.

4.4.2 Comparison with Driver

This second session of tests involved the comparison of the performance achieved by a professional driver and the Trajectory Tracking proposed.

Looking at Figure 4.10, where the GGs obtained by the vehicle driven by the driver and by the algorithm are shown, one can see that the algorithm is able to respect the acceleration constraints imposed, by guaranteeing the limits of the engine and the tires and replicating the results obtained by the driver.

In terms of performance, the results show that the algorithm developed is able to match the ones of the professional driver, although simplifications have been made to the vehicle model to keep the computational cost down, in fact, speed and input curves have the same trend and peak values, as shown in Figure 4.11. The lap times shown in Table 4.3 confirm that the Trajectory Tracking developed is able to replace the results of a human driver, and that the system integration performs well.

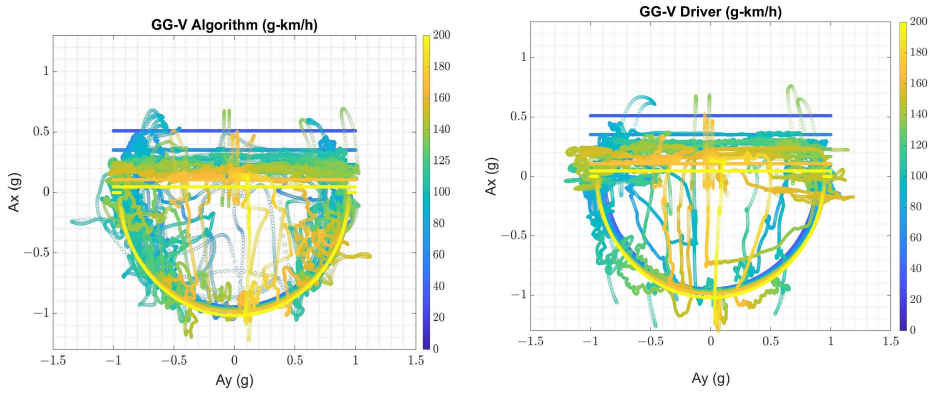

(a) Algorithm GG-V.

(b) Driver GG-V.

Figure 4.10: GG-V performances obtained by the Trajectory Tracking and driver.

Table 4.3: Lap time achieved by the Trajectory Tracking proposed and CarRealTime Max-Performance event.

	Lap time (s)	
Test 1	Algorithm	151.0
	Max-Performance	151.9
Test 2	Algorithm	150.7
	Driver	150.5

The different lap time made by the algorithm in the two test sessions are due to the different conditions of the track, flat in the first case and with the actual slopes in the second. For this reason, during the layers integration work phase a bank angles compensation logic was added to the planner as explained in Chapter 6.

In Figure 4.12 the trajectory made by the algorithm with and without bank angles compensation logic are shown together with the 3D map of the Calabogie race-track. As one can see the trajectories are almost the same, but there are

some discrepancies in the sections marked by numbers that correspond to the road sections where there are slopes, as shown in the 3D map. In the section enumerates as 1, the two trajectories differ throughout all the section and it can be seen that the trajectory that considers the slopes of the road at the section exit kept a closer trajectory with a shorter distance to travel than the other; in section 2 the two trajectories differ at the exit of the curve and the trajectory where the slopes are considered manages to be more internal; the same is true in the following sections 3, 4, 5; in section 6 the two trajectories differ at the section entrance and exit, and the trajectory with the compensation of the slopes also in this case ensures a more internal trajectory.

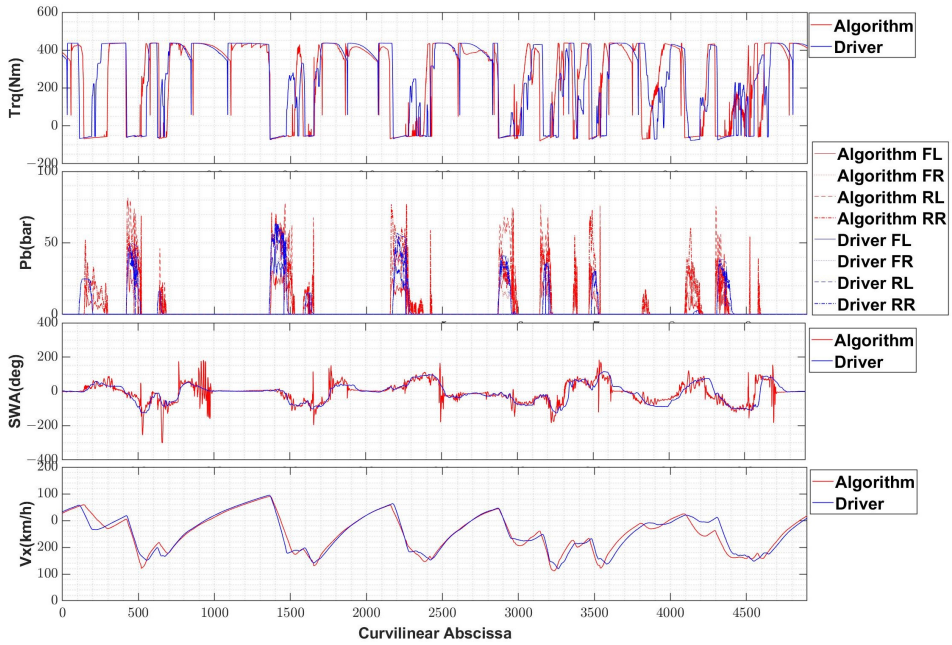

Figure 4.11: Car input commands and longitudinal speed achieved by the Trajectory Tracking proposed and driver.

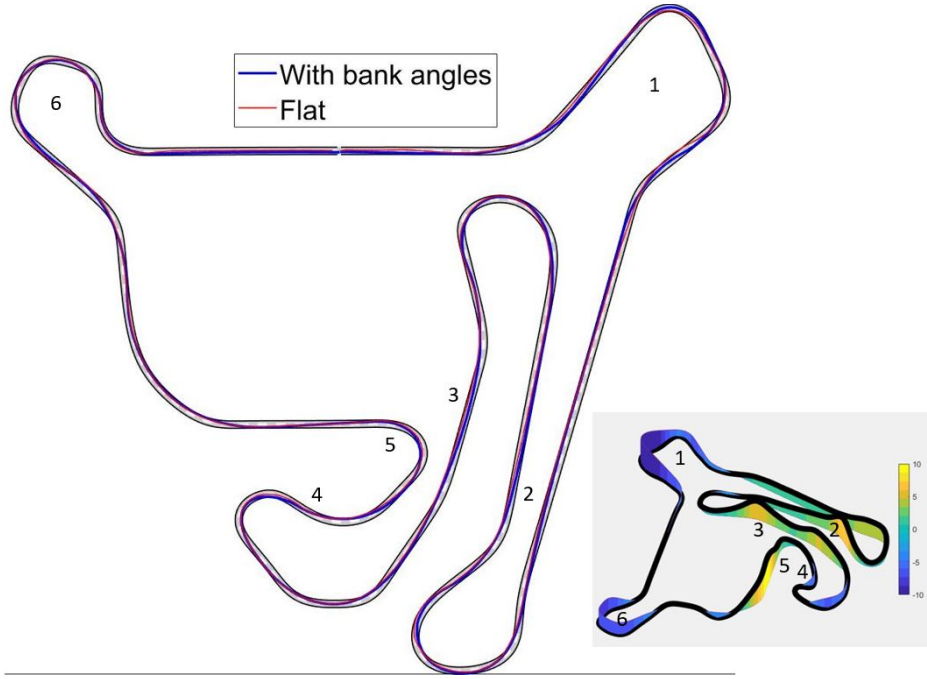

Figure 4.12: Trajectory made by the Trajectory Tracking proposed in the case of flat road and road with bank angles.

4.4.3 Trajectory Comparison

In Figure 4.13, the trajectories made by the algorithm developed, max-performance event and driver are compared, highlighting the curves where the different strategies are more visible and impact the performance. In zoom 1, it is possible to see that the trajectory of least curvature achieved by the off-line optimization exits the curve keeping the car on the outer side of the track, whereas the proposed Path Planning drives the car to the inner side of the track to anticipate and prepare the car for the following curve, as the driver does, too. In this track section, the max normal distance between the trajectory made by the algorithm with respect to the one made by the max-performance event is 5.86 m; whereas, the one made by the driver can be considered equal to the algorithm one. In zoom 2, the different approaches are more visible and impact more on the performance: the trajectory of least curvature maintains the inner side, whereas the algorithm developed goes to the outer side, achieving a max normal distance of 8.00 m; this behaviour was proved by driver tests, which improves the performance of the car and reduces the lap time, even if the driver made a trajectory 3.20 m closer than the algorithm. However, in zoom 3, if at the beginning of the curves, the max-performance optimization maintains the car on the outer side, and the driver and on-line algorithm choose the narrowest trajectory, achieving a max normal distance of 5.60 m, and at the end of the curves, the algorithm follows the max-performance, enlarging the trajectory later of almost 6.00 m with respect to the driver losing longitudinal speed.

In Table 4.3 the lap time differences are shown.

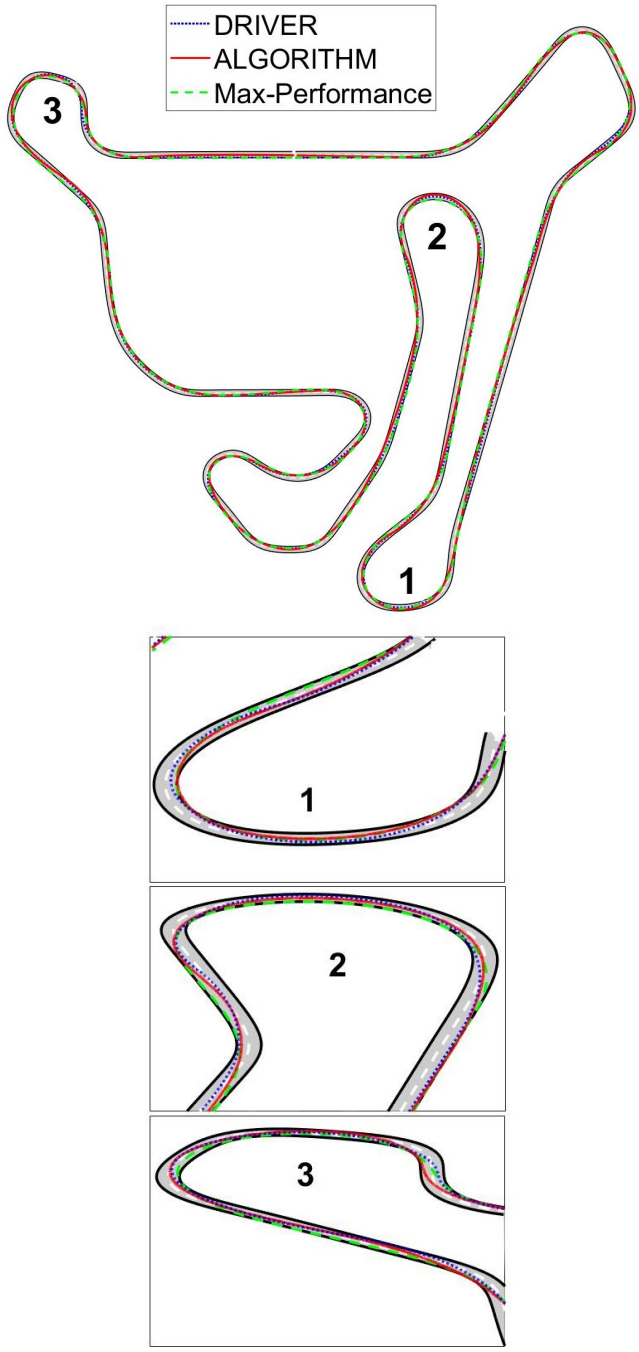

Figure 4.13: Trajectory made by the Trajectory Tracking proposed, CarRealTime Max-Performance event and driver.

4.5 Conclusions

In this Chapter, the development of an autonomous racing car trajectory tracker that was able to update the optimized trajectory on-line to reduce the time lap as well as control the car is shown. It is validated by comparing it with the performance of off-line Path Planning and a human driver.

The intention of the study was to ensure the on-line functionality of an autonomous controller to match the decisions of a human driver instead of optimizing the trajectory off-line considering a possible development for collision avoiding thanks to the computing of a suitable reference manoeuvre.

This aim was achieved by dividing the Path Planning algorithm from the Trajectory control one and building a hierarchical control architecture, where the vehicle model complexity increased and the sample time decreased, i.e., the Path Planning uses a point mass vehicle model with a sample time of 0.1 s, and the Path Tracking uses a single-track vehicle model with a sample time of 0.001 s. To ensure a correct communication between the two systems and the car, the computational time of the trajectory optimization was chosen to be below 0.1 s: the division between the Path Planning and Path Tracking and the implementation of LP instead of QP ensured the respect of these constraints, as shown in Table 4.2. Furthermore, to increase the Path Planning representation of the vehicle dynamic, the GG-V constraints were implemented as a quadratic ellipse, and the weights and the constraints of the optimization could be changed as a function of the track sections, adapting the car to the characteristics and conditions of the track. The comparisons made with a state of the art off-line path planner validated the optimizer developed . Indeed, better performance was achieved in terms of lap time, reducing it by almost a second.

The comparison made with a professional driver can prove that even if the autonomous architecture developed uses a simplified vehicle model to reduce the computational cost, the car is able to replicate its performance, matching the lap time.

Chapter 5

Stability Systems

Usually, in the autonomous driving control logic, the longitudinal and lateral vehicle dynamics are implemented in the NMPC as a non-linear vehicle model, adding constrain equations that limiting some dynamic variables to ensure a certain level of stability performances. Instead, in this study, it was chosen to implement the Stability Control layer independently of the Trajectory Tracking. In this way, the motion planning optimization algorithm can considered a simple point mass vehicle model, without increasing the computational cost and ensuing an on-line implementation; and the stability systems works as in the common car representing a low level control layer. Thus, it was possible to track the stability while the car is running and not in an off-line optimization process, ensuring that dynamic stability is controlled during changes in conditions that may arise and threaten safety.

In this Chapter the solutions found for lateral and longitudinal stability control algorithm are presented and them performances once applied to the case of study application are shown.

5.1 Longitudinal Stability Control

This study made on the longitudinal control system concerned the development and testing of three types of ABS: a standard on-off wheel's acceleration control; a wheel's longitudinal slip controller based on a discrete PID control; and a novel type of ABS that involves controlling the wheel's speed through a discrete PID. The aim of this was to find a more efficient way to ensure longitudinal dynamic stability to the car by exploiting the BBW device seen in Chapter 1 and using the current vehicle sensors and communication protocols. Furthermore, it must be easily integrated with other controls and electronic components in terms of sampling time and values.

The *standard ABS* seems more appropriate than the others two because it uses only parameters defined by sensors and it has a simple architecture that does not have the problem of computational time. However, in recent years, cars have been equipped with Electro Hydraulic Braking units that improve the performance of the system controls. In fact, it is possible to use a control that allows actuators to follow a continuous target and smooth out pressure actions. Even if the longitudinal *Slip Controller* has a simple architecture and uses a PID control, it is limited to using quantities estimated instead of measured: the tires' friction coefficient, the

tires' longitudinal stiffness, and the car's speed. Therefore, the use of a *Wheel Speed Controller* is the right compromise to link the advantages of both controllers by following the braking pressure continuously and not needing to know the condition and properties of the tires. The results of tests carried out in a HiL system are showed and involved a complex vehicle model implemented in real-time.

5.1.1 Vehicle Model

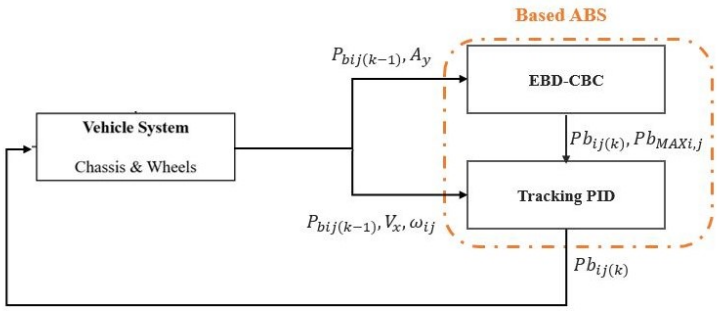

Figure 5.1: Longitudinal stability control system block diagram.

Three types of ABS with different control system was developed and tested implementing them indifferently as one of the parts of the overall vehicle control architecture. A longitudinal control scheme was defined and composed of different sub-models, as shown in Figure 5.1, that considering the measured previous step calliper brake pressures provide to the vehicle the current calliper pressures that ensure stable braking. These sub-models are:

- **Electronic Brake-force Distribution(EBD)**: Longitudinal braking force distribution on the two pairs of wheels to prevent the wheels from locking due to longitudinal weight transfer. For the car model used it was decided that the braking force distribution should be the same on front and rear wheel pairs, leaving the ABS to modulate braking on the individual wheels;
- **Cornering Braking Control(CBC)**: a logic that, as a function of lateral acceleration, defines the maximum value of the pressure that each brake actuator can supply to the wheel to prevent it from reaching the limit of adhesion, which has changed due to lateral weight transfer;
- **ABS**: longitudinal control that aims to avoid wheels locking, reducing braking distance, and ensuring that the car is steerable;
- **CBA**: a BBW system developed by Meccanica 42 srl and described in the Chapter 1;

The car model is a multi-degree vehicle model developed in ADAMS environment and implemented in Vi-Grade CRT to be co-simulated with Matlab-Simulink. The design specification involves to implement the ABS algorithm developed with the following input sensor measures:

- **IMU**: inertial platform that measures the car model's three translation accelerations and three rotation accelerations;
- **Wheel Speed Sensor**: sensor that measures the angular speed of the wheel;
- **Pressure Sensor**: sensor that measures the value of pressure that the CBA provides to the calliper.

To consider the real interface that is created between the ABS, the sensors and the braking system, the sensor characterisation and CBA model described in Chapter 2.4 have been added to define input and output quantities.

5.1.2 Cornering Braking Control logic

As said, this logic was implemented to prevent that the wheels reach its saturation limit during cornering braking manoeuvres due to lateral weight transfer. The logic allows to saturate the maximum brake pressure that the braking actuator must provided to the wheel as a function of the lateral acceleration of the car. An example of the function applied to the left wheel is shown on Figure 5.2 where the maximum possible pressure change with the lateral engagement.

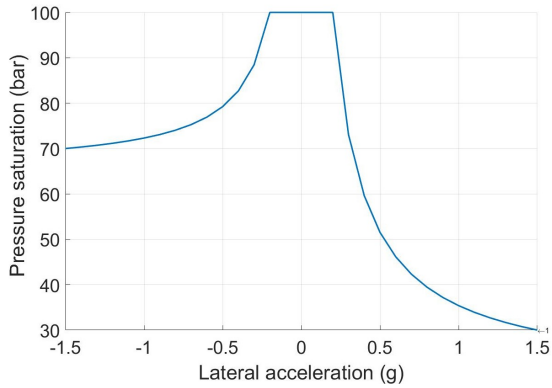

Figure 5.2: Cornering Braking Control logic implemented on left wheels.

The maximum pressure values are established with trial and error procedure and the function is implemented as Look-up table. So, during a right corner, where the lateral acceleration is negative, the left wheels have an increased load and therefore more braking possibilities, with a higher limit. Instead, during a left corner, the left wheels are decreased of the weight and so a reduced saturation limit.

5.1.3 Anti-lock Brake System Controllers

The ABSs are itemized below, and will be explained in detail in the following Subsections:

- **Standard ABS**;
- **Slip Controller**;
- **Wheel Speed Controller**.

The three types of ABS share the same aim and interact with the entire architecture in the same way; the ABS has as inputs the braking pressure required by the driver via the brake pedal, and the braking pressure required by the lateral stability control system, through the wheels longitudinal forces that allow the car to achieve the yaw moment that stabilizes dynamics. Instead, the ABS outputs are the four wheel pressures that CBA units must provide to the callipers to improve performance by ensuring input requirements. Therefore, the ABS input target pressure is defined by: the percentage-to-pressure coefficient that converts driver pedal input, $Pedal$, to requested pressure, P_t (Pa), matching the 100% with the maximum pressure that the actuators can reach, P_{max}, as shown in Equation 5.1; and the force-to-pressure coefficient, c_p, that as a function of the braking piston's area and braking piston's friction, converts longitudinal forces requested by the ESC, F_d, into pressure, P_d (Pa), as shown in Equation 5.2.

$$P_t = P_{max} * Pedal \tag{5.1}$$

$$P_d = \frac{F_d}{c_p}; \qquad c_p = A_p * \mu \tag{5.2}$$

All three ABS logics work with a sample time of 0.001 s, and disable their control when the car speed is under 2 m/s. This switch-off is necessary to improve braking performance without threatening stability. In effect, when vehicle speed is low, the brake actuator can provide its maximum potential without risks.

Since the study involves sensitive data all the tuning parameters and gains used can't be shown and only the formulations and functions implemented will be presented.

Standard ABS

By using the name, *'standard'*, it is highlighted that the longitudinal control includes logic that is already available in all commercial vehicles. This logic works as a bang-bang control, where the braking pressure of the callipers is increased, decreased, or held depending on the wheel acceleration value.

So, a *Standard ABS* was developed trying to obtain the same results as the system developed by Bosch [100]. It is composed of an algorithm that raises, maintains, or reduces pressure (w.r.t. driver pressure demand) as a function of two states: wheel acceleration, $\dot{\omega}$, and measured vehicle longitudinal speed, u. The measured vehicle speed is the vehicle longitudinal speed estimated by integrating the car's longitudinal acceleration. To avoid the drift in estimation due to a little bias of the acceleration, the integration is reset to the mean value of the four wheel speeds thanks of the pulse function $g(t)$ of 0.1 s width and 1 amplitude value, as shown in Equation 5.3.

$$u_i = a_i * dt + c(g(t)) = \begin{cases} c(g(t)) = u_{i-1} & if \quad g(t) = 0 \quad \forall i = 1, 2, ...T \\ c(g(t)) = mean(\omega_{ij} R_j) & if \quad g(t) = 1 \quad \forall i = 1, 2, ...T; \\ & \qquad\qquad\quad \forall j = 1, 2, 3, 4 \end{cases} \tag{5.3}$$

So, two threshold bands are defined, which depend not only on the wheels' acceleration, as usual, but also on the wheels' speed. These thresholds smooth out the controller action, improving the ABS performance respect the one that controls only the wheels acceleration.

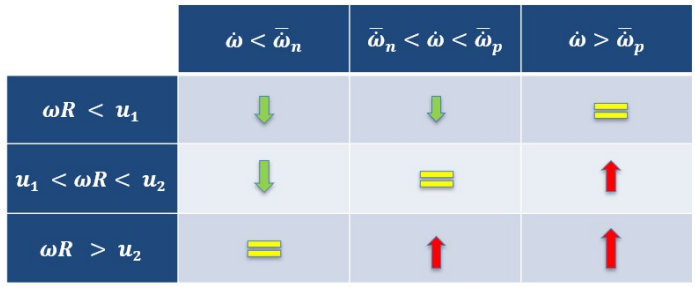

Figure 5.3: Standard Anti-lock Brake System thresholds logic definition.

Figure 5.3 shows the logic used. Nine sectors divide the ABS work, and each sector depicts: a reducing of pressure with the green arrows; a raising of pressure with the red arrows; and a holding of pressure with the equals sign.

The band threshold defined by u_1 and u_2 ensures that the different between the vehicle speed and the wheel speed, i.e. the slip velocity, does not exceed the percentage distance, $u_2 = k_2 * u$, from the saturated value of the tire by reducing pressure. At the same time, the acceleration performances are improved by holding and increasing the pressure if the slip velocity is inside $u_2 = k_2 * u$ and $u_1 = k_1 * u$ or above $u_1 = k_1 * u$. Instead, the threshold band defined by $\overline{\dot{\omega}_p}$ and $\overline{\dot{\omega}_n}$ avoids the risk that longitudinal wheel speed declines quickly to zero controlling that the slip does not reach the saturation limit.

Table 5.1: Anti-lock Brake System thresholds definition.

Variable	Value
u_1	$k_1 * u$
u_2	$k_2 * u$
$\overline{\dot{\omega}_n}$	$\frac{1-\sigma_t}{R} * a_{xm}$
$\overline{\dot{\omega}_p}$	$\frac{1-\sigma_t}{R} * a_{xp}$

The tuning process has involved the definition of the threshold parameters, k_1, k_2, a_{xm} and a_{xp} by physical observation and formulation, shown in Table 5.1, and nine pressure slops by trial and error approach. The speed thresholds were defined trying to maximize the brake pressure capabilities and avoid to lock the wheel. So, it was supposed that if the 90% of the slip velocity ensures a near to maximum longitudinal wheel force, a difference of the wheel speed from the vehicle speed bigger than a 80% could cause a saturation of the tire. Regarding wheel acceleration thresholds, they were established by the physical formulation shown in Equation (5.4) where the slip ratio function is derived by considering a fixed target slip, σ_t and the wheel radius, R. The minimum deceleration value of the wheel was estimated using $a_x = a_{xm}$, that is the maximum absolute longitudinal deceleration that the vehicle can express. Instead, the positive upper acceleration threshold was estimated using $a_x = a_{xp}$, that is a tuning parameter.

$$\sigma_t = \frac{u-\omega*R}{u}; \qquad \omega = \frac{1-\sigma_t}{R} * u; \qquad \dot{\omega} = \frac{1-\sigma_t}{R} * a_x \tag{5.4}$$

The brake pressure slopes were defined by a trial and error process at the simulator with the aim to obtain a robust and repeatable behaviour in term of avoiding wheel locking and maximizing the performances by smoothing out the signals. In fact, a maximization of the performance in high friction condition did not ensure a safety and effective braking in low friction condition, where the signal oscillations prevented to increase the pressure slop. However, depending on the designer's requests, it is possible to adjust the upward and downward pressure rates to obtain higher performance under certain conditions, not ensuring a continuity of performance in all the dynamic or contact condition. The tuning process work is shown in Figure 5.4

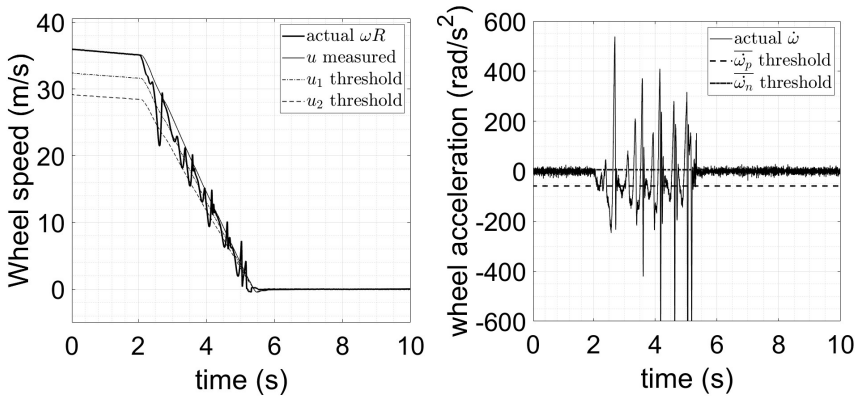

Figure 5.4: Standard Anti-lock Brake System thresholds logic visualization.

It is important to point out that the slopes of decreasing and increasing pressure change depending on the speed of the vehicle: when it is travelling faster than $50km/h$, the slopes have one value; when it is slower than $50km/h$, they have a different value. This schedule was necessary because during the tuning phase on several manoeuvres, the use of unique gradients did not guarantee the correct operation of the vehicle at low speeds.

Slip Controller

However, the *Standard ABS* is a bang-bang control, so it has a noisy behaviour that is not comfortable for passengers and results in lower efficiency, also involving a long tuning process. So, an ABS was developed that could track the longitudinal slip of the tire, as in [53], ensuring a continuous control of the braking pressure. The *Slip Controller* aims to minimize the error between the wheels' actual and target longitudinal slip, and its working structure is shown on Figure 5.5. In this Figure, the *Target Braking Pressure* block provides: the target pressure, P_t, requested by the driver and calculated by Equation 5.1; and the target longitudinal slip, σ_t calculated as function of the target braking pressure as follows:

$$F_{xt} = -c_p * P_t \tag{5.5}$$

$$\sigma_t = f(F_{xt}) \tag{5.6}$$

where c_p is the force-to-pressure coefficient defined in Equation 5.2, and $f(F_{xt})$ is the longitudinal tire characteristic found with the tire testing event of CRT at a normal load of 3000 N. To ensure that the controller works only when the wheel is braking, and not when it is in traction, the σ_t is saturated between 0 and -0.1. This range ensures that the wheel slip is such as to have the greatest longitudinal force, and therefore braking pressure, without reaching the wheel lock, i.e. maintaining a certain margin from the 100% of slip.

About the actual value of the car longitudinal slip, σ, it is estimated by the following formulation:

$$\sigma = -\frac{v_{xij} - \omega_{ij} * R_{ij}}{v_{xij}} \tag{5.7}$$

where i stands for front or rear and j left or right values; the v_{xij} is the longitudinal wheel speed as function of the longitudinal, lateral and rotational vehicle speed; and ω_{ij} and R_{ij} are respectively the angular wheels speed and the wheels radius.

So, as shown in Figure 5.5 the error between the target, σ_t, and actual, σ, longitudinal slip represents the input of the discrete PID which thanks of the tuning three gains, $K_{i,p,d}$, and working at a sample time of 0.001 s, minimize the proportional, derivative and integral errors of the residual of the states, defining the pressure P to be subtracted from the target one P_t.

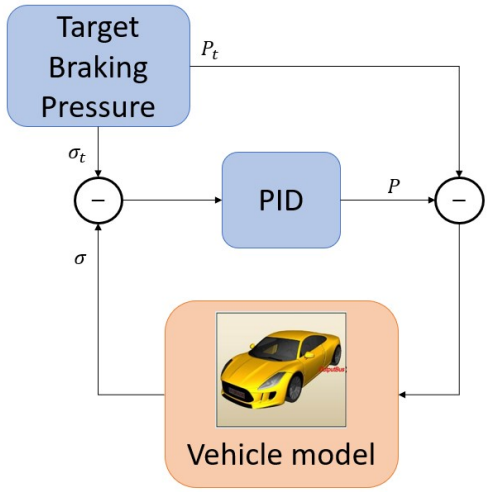

Figure 5.5: Longitudinal slip controller block diagram.

The main problem of this control is the slip estimation. In fact, if for the *Standard ABS* is sufficient a measure of the speed, to have a satisfactory longitudinal slip estimation and so a good performance of the *Slip Controller*, a precise longitudinal vehicle speed relative to the wheel it is necessary. As shown in Figure 5.6, because of the small values that the slip has, a small error on speed estimation, in the order of cm/s, leads to a large error on slip estimation. This error has the same order of magnitude of the quantities in question. If in high friction condition the errors are not relevant, in low friction condition they influence the *Slip Controller* functionality reducing the performance of the braking. For the same reason, i.e.

because it is a small size compared to the longitudinal speed, the noise in the wheel sensors has a significant influence on the slip estimation and therefore also on the operation of the *Slip Controller*.

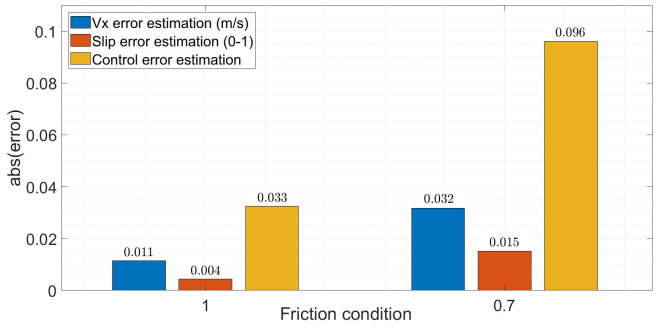

Figure 5.6: Influence on Slip Control of the error on speed estimation during full brake manoeuvre in high and low friction conditions.

As for the *Standard ABS*, to ensure the correct operation of the controller at low speed, the discrete PID was scheduled with the longitudinal speed of the vehicle(e.g. when u is less than $36km/h$, the gain values are significantly reduced).

Wheel Speed Controller

If the *Slip Controller* ensure a smoother behaviour than *Standard ABS*, maintaining a certain level of performance in nominal contact path, involves estimating the longitudinal slip and therefore the longitudinal and lateral speed of the vehicle as accurately as possible to ensure the same performance at degraded contact path. But, with the current sensors and technologies a certain error is achieved in combined slip if the tire is near to the saturation, and when the contact condition are not the nominal one (reduced friction condition). For these reasons, a novel type of ABS was developed linking together the two longitudinal controls showed. So, to guarantee a tracking of the braking pressure, a discrete PID controller with a sample time of 0.001 s was chosen; and to not need of estimated values, the wheel speed was chosen as the state to be controlled by measuring its value with sensors and not with an estimation model.

The architecture of the controller is the same of the *Slip Controller* shown in Figure 5.5, but instead of a target longitudinal slip, the discrete PID controller has to minimize the error between the wheel speed and a reference value, u_2, defined as a percentage of the measured vehicle speed, u, as for the *Standard ABS*:

$$u_2 = k_2 * u \tag{5.8}$$

the u is calculated by Equation 5.3 and k_2 is a tuning parameter that defines the target speed value that the wheel must have to avoid locking and ensure the deceleration required by the driver, as shown on Figure 5.7. In this Figure, the measured speed, u, does not stop at zero m/s due to the car body movements at its stop detected as positive acceleration. However, the algorithm works with a saturated u that must be greater than or equal to zero.

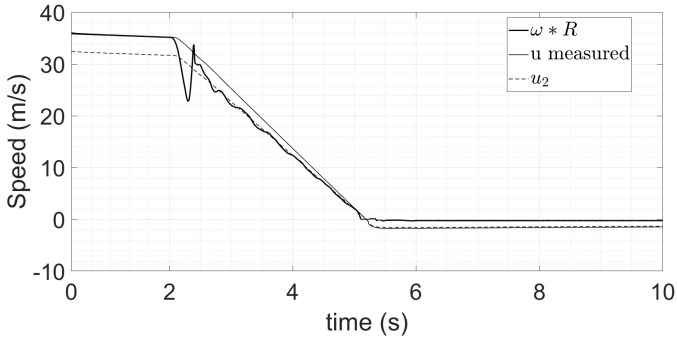

Figure 5.7: Wheel Speed control threshold logic visualization.

The continuous-time PID formulation is the one shown in Equation 5.9 with its Laplace transform shown in Equation 5.10. However, to consider the signals transmitted inside the car the discrete PID formulation, obtained with the backward Euler methods for both the integral and derivative terms and shown in Equation 5.11, was used and implemented.

$$u_{(t)} = K_p e_{(t)} + K_i \int_0^t e_{(\tau)} d\tau + K_d \frac{d}{dt} e_{(t)} \tag{5.9}$$

$$C_{(s)} = K_p + \frac{K_i}{s} + \frac{N K_d}{1 + N/s} \tag{5.10}$$

$$C_{(z)} = K_p + \frac{K_i T z}{z - 1} + \frac{N K_d (z - 1)}{(1 + NT)z - 1} \tag{5.11}$$

So, (z) is the discrete time variable in the Z-Domain and the input of the discrete PID, $I(z)$, is the error e described in Equation 5.12. Its value will be reduced by tuned PID parameters, K_p, K_i and K_d that through the formulations shown in Equations 5.13 define the discrete PID output, $U(z)$: the braking pressure, P_t to be subtracted to the pressure requested by the driver ensuring that the wheel does not lock.

$$e = (u_2 - \omega * R) \tag{5.12}$$

$$\begin{aligned}
C_{(z)} &= \frac{U(z)}{I(z)} = \frac{B_0 + B_1 z^{-1} + B_2 z^{-2}}{A_0 + A_1 z^{-1} + A_2 z^{-2}} \\
B_0 &= K_p * (1 + N * T) + K_i * T * (1 + N * T) + K_d * N \\
B_1 &= -(K_p * (2 + N * T) + Ki * T + 2 * K_d * N) \\
B_2 &= K_p + K_d * N \\
A_0 &= 1 + N * T \\
A_1 &= -(2 + N * T) \\
A_2 &= 1 \\
P_t &= -\frac{A_1}{A_0} * P_1 - \frac{A_2}{A_0} * P_2 + \frac{B_0}{A_0} * e + \frac{B_1}{A_0} * e_1 + \frac{B_2}{A_0} * e_2
\end{aligned} \tag{5.13}$$

In Equations (5.13), the discrete dynamic control system is shown and in addition to the parameters already defined are present: T that represents the sample time of 0.001 s; N is the low-pass filter parameter, to make derivative term less noisy, and usually has the value of 100; B_0, B_1 and B_2 are the numerator coefficients of the discrete transfer function, $\frac{U(z)}{I(z)}$; A_0, A_1 and A_2 are the denominator coefficients of the same transfer function; P_1 and P_2 are the output values at the time $(t-1)$ and $(t-2)$ considering that t is the current time step; and e_1 and e_2 are the input values at the time $(t-1)$ and $(t-2)$. Compared to the other longitudinal controllers presented this one has not been needed of a scheduling with the longitudinal vehicle speed. Thus, its tuning process was quicker and more simple due to the definition of only three parameters, K_p, K_i and K_d.

5.1.4 Tests and Results

As said in Chapter 1, the longitudinal control logic was implemented in Matlab-Simulink and tested in co-simulation environment with Vi-Grade CRT software and the real-time static simulator shown in Figure 1.5.

Two types of manoeuvres under different asphalt surface conditions were carried out to evaluate the ABS response. They are:

- Longitudinal braking;
- Combined braking.

Table 5.2 summarizes their specific characteristics.

Table 5.2: Characteristics of the manoeuvres tested

	Longitudinal braking		Combined braking	
Friction level	1.0	0.7	1.0	0.7
Longitudinal speed	130-80 (km/h)	130-80 (km/h)	80 (km/h)	80 (km/h)
Lateral acceleration	0 (g)	0 (g)	0.9-0.5 (g)	0.5 (g)

From the tests, the results highlighted the capability of all three ABS to avoid wheel locking, reduce braking distance, maintain a stable trajectory, and improve deceleration level.

The results below show sensitive data. For this reason, they are normalized with respect to the values of the model without controls and are shown, for the sake of brevity, only the graphs of longitudinal braking manoeuvres at 130 km/h with friction levels of 1.0 and 0.7, and combined braking manoeuvres at 0.9 g with a friction level of 1.0. However, Tables 5.3 and 5.4 show the results of all the manoeuvres.

Longitudinal Braking

The ISO standard [101] states that the longitudinal braking manoeuvre used to test the ABS control must establish if it is able to prevent the wheels from locking and give more stability to the car. The manoeuvre consists of starting from a certain longitudinal speed and braking sharply until the vehicle comes to a complete standstill. The driver's braking has a pressure increase slope of 1000 bar/s.

The authors tested the same manoeuvres with a friction level of 0.7 to assess its performance in slippery conditions.

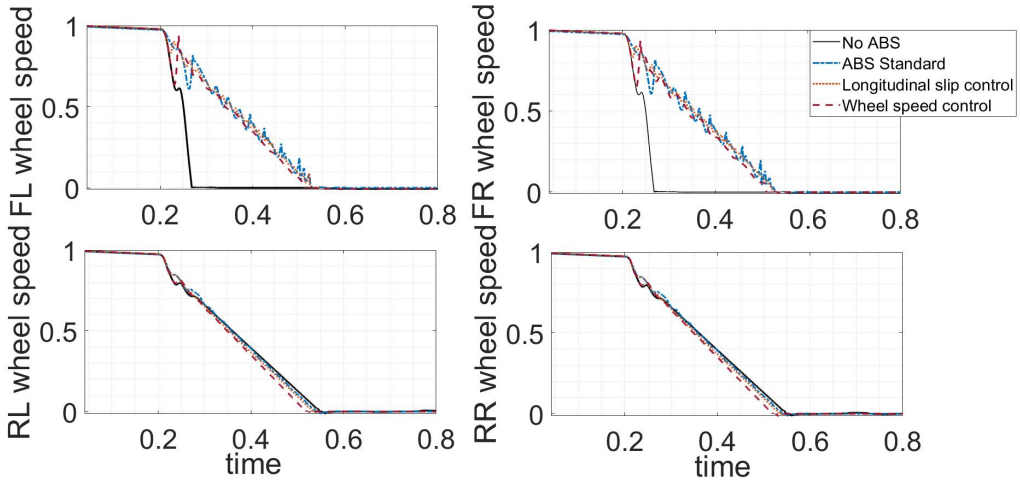

(a) Dry surface of friction level equal to 1.

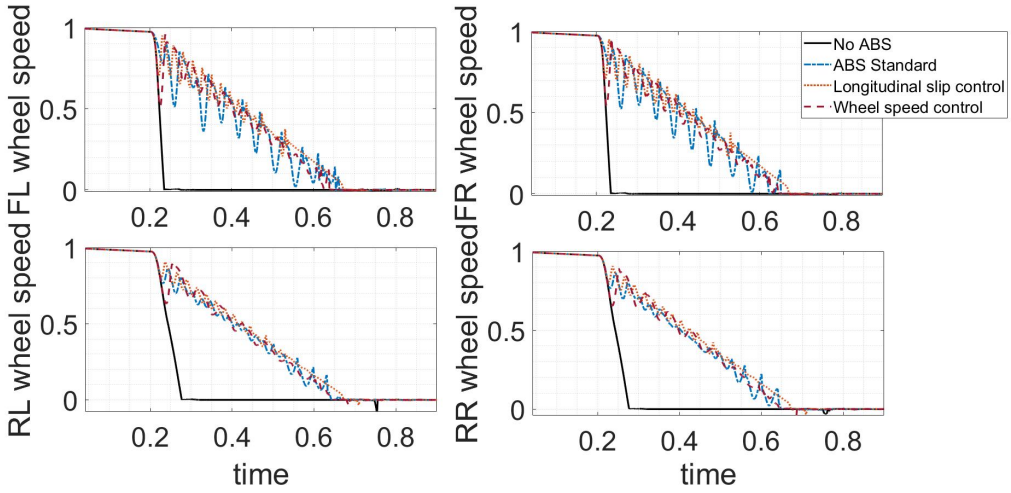

(b) Wet surface of friction level equal to 0.7.

Figure 5.8: Wheel angular speed in longitudinal braking from 130 to 0 km/h with and without Anti-lock Brake System.

Figure 5.8 shows the wheels' speeds from the starting speed to when the vehicle is completely stationary in nominal (a) and reduced (b) friction condition. It shows that the absence of the ABS leads to the locking of the front wheels, or all wheels when friction is 0.7. On the other hand, the presence of any of the three types of ABS makes possible to avoid locking. However, the *Standard ABS* compared with the *Slip Controller* and the *Wheel Speed Controller* has a chattering behaviour, especially in reduce friction condition, reducing the performance and adding noise to the all system.

These results are confirmed in Figure 5.9, that shows in (a.2) and (b.2) the car's trajectory until the vehicle is stationary and in (a.1) and (b.1) the longitudinal

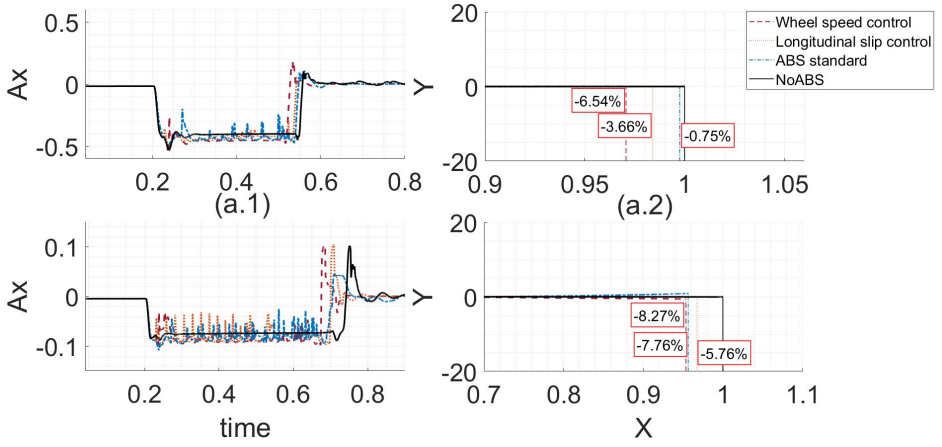

Figure 5.9: Longitudinal vehicle acceleration and car trajectory in a longitudinal braking from 130 to 0 km/h with and without Anti-lock Brake System. (**a**) Dry surface of friction level equal to 1. (**b**) Wet surface of friction level equal to 0.7. X and Y stand for longitudinal and lateral vehicle displacement and figures (a) have the same horizontal axis, time, as well as figures (b), X.

deceleration of the car in nominal, (a), and reduced, (b), friction condition. The values shown are normalized with respect to the maximum longitudinal distance, and longitudinal deceleration achieved by the car without controls. The numbers inside the red rectangles represent the percentage of reduction in braking distance compared to the vehicle without controls and underlined that the *Wheel Speed Controller* is able to achieve a shorter braking distance of the others reaching almost double the reduction of the other controls under nominal friction conditions. It is also interesting to note that if in nominal friction condition the *Slip Controller* has better performance than the *Standard ABS*, thanks of its smoother behaviour, in reduced friction condition its performance go worse in terms of braking distance because of the multiple estimated values involved (longitudinal speed, longitudinal force and longitudinal slip). So, the *Wheel Speed Controller* has less braking distance than other controllers, even if it shows a small right side-shift in the case of the slippery surface. However, this shift still allows the car to stay inside the roadway without risk of danger. Furthermore, about the car's longitudinal acceleration the three longitudinal controllers tested allow the car to reach higher decelerations than the case without ABS and in both contact conditions, the smoother behaviour of the *Wheel Speed Controller* ensures to maintain higher longitudinal deceleration and for this reason the braking distance is reduced. This behaviour is useful especially when the friction is 0.7, whereas *Standard ABS* and *Slip Controller* act in a very noisy way because of quick on-off switches, and a poor estimate of the tire contact conditions respectively.

Combined Braking

This manoeuvre underlines the ability of the ABS to ensure that the vehicle follows the driver's inputs as neutrally as possible, avoiding a loss of control from over-

steering or under-steering and the wheels locking. It starts with a steering ramp up to the desired lateral acceleration and then a sharp braking from the start speed to when the vehicle is completely standstill.

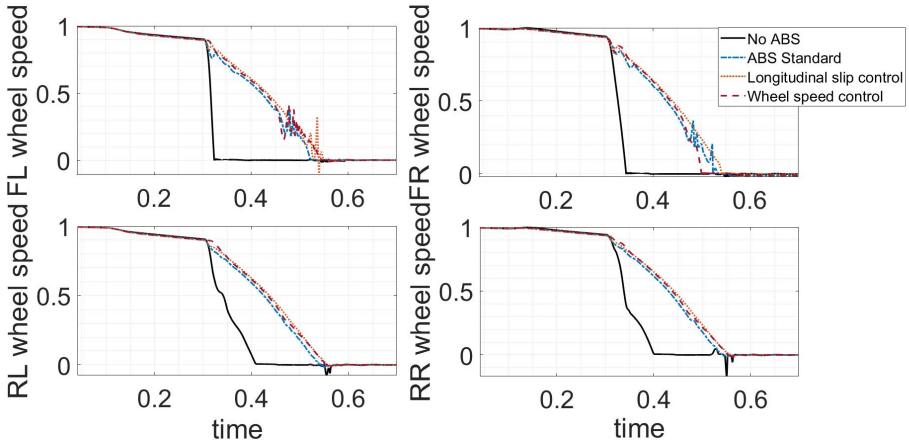

Figure 5.10: Wheel angular speed in combined braking from 80 to 0 km/h at lateral acceleration of 0.9 g with and without Anti-lock Brake System.

Figure 5.10 shows that the wheels do not lock only with the action of three ABS controls. Moreover, all three longitudinal controls can provide linear lateral deceleration in front of an increase in longitudinal acceleration, instead, the absence of ABS leads to a sudden loss of lateral acceleration with the following loss of stability as is shown in Figure 5.11.

In Figure 5.12, the trajectory of the car during the manoeuvre,(a), and its zoom from when braking starts until the end of the manoeuvre, (b), are shown comparing the radial distance achieved by the three controllers from reference trajectory. The reference trajectory represents the constant radius path, which allows the car to maintain the target lateral acceleration at the target speed, and for this manoeuvre is $\frac{[22{,}2(m/s)]^2}{9(m/s^2)}$. The graph shows this trajectory as a series of consecutive points. So, it shows that the *Standard ABS* achieves better performance than the others because it ensures the shortest radial distance, even if the performance of the three ABSs are very close and satisfactory allowing the vehicle to maintain the trajectory sets. In fact, the vehicle without control loses its stability by spinning out.

Complete Results

In Tables 5.3 and 5.4 can be determined which type of ABS ensures the best performance in a wider range of manoeuvres.

In the columns, the characteristics of the manoeuvres are defined as: the type, longitudinal or combined; the friction level, 1 or 0.7; the car's speed, 130 km/h or 80 km/h; and the car's lateral acceleration, 0.9 g or 0.5 g. As a friction level of 0.7 limits vehicle dynamics, only combined braking manoeuvres with a car's lateral acceleration less than 0.5 g was done.

Instead, in the rows, are indicate the type of ABS algorithm that equips the car (*Standard ABS*, *Slip controller*, and *Wheel Speed controller*) and the performance considered (longitudinal braking distance = L and radial distance = D).

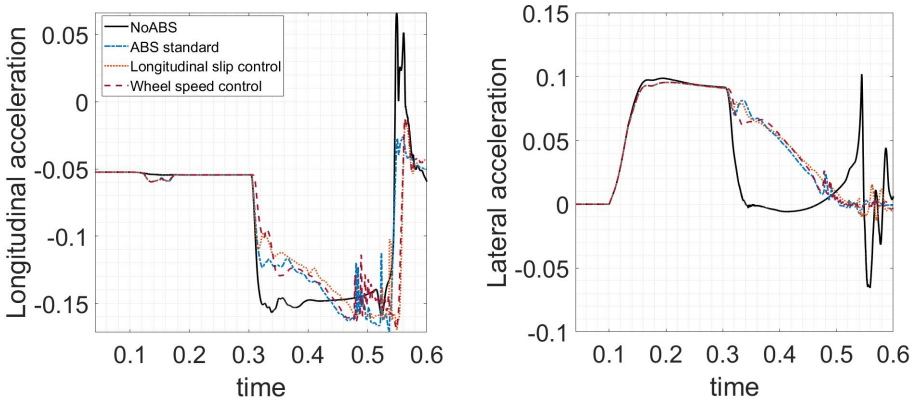

(a) Car longitudinal acceleration.

(b) Car lateral acceleration.

Figure 5.11: Vehicle accelerations in combined braking from 80 to 0 km/h at lateral acceleration of 0.9 g with and without Anti-lock Brake System.

Table 5.3: Test results about braking distance performance

		Longitudinal braking				**Combined braking**		
		Friction				*Friction*		
		1		*0.7*		*1*		*0.7*
		Speed (km/h)				*Lateral acceleration (g)*		
		130	*80*	*130*	*80*	*0.9*	*0.5*	*0.5*
Standard ABS	*L*	-0.75%	2.25%	-7.76%	-2.03%	0%	0%	0%
Slip control	*L*	-3.66%	-0.41%	-5.76%	1.78%	0.3%	-0.9%	0.01%
Wheel control	*L*	-6.54%	-3.90%	-8.27%	-3.9%	-0.4%	-1.5%	-0.7%

The negative values shown in the table are the percentage reductions of the braking distance and radial distance respect the vehicle without longitudinal control, instead the positive ones are the percentage increases. The red values specify when the car had the lowest braking distance in longitudinal braking, and the lowest radial distance from the constant radius reference trajectory in combined braking. Thus, as it possible to see in Table 5.3, the results obtained by the controllers in the longitudinal braking manoeuvres show that in high friction conditions the *Standard ABS* has a little percentage improvement at 130 (km/h) and even an increase in braking distance at a speed of 80 (km/h) due to an increase in the oscillating behaviour of the controller, instead in low friction conditions the brake distance is ensured in both 130 and 80 (km/h); regarding *Slip Control ABS*, it allows a greater reduction in braking distance compared to the *Standard ABS* in high friction conditions. Instead, in low friction conditions its performance gets worse because of the estimation errors seen in Section 5.1.3. At the speed of 80 (km/h), these estimation errors increase the braking distance compared to the vehicle without controller; the performances of the *Wheel Speed Control* are the most effective in terms of reducing the braking distance, ensuring continuity of

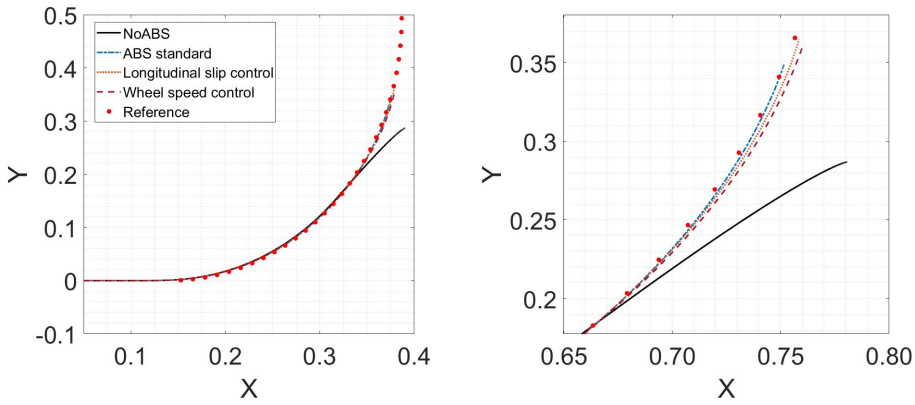

(a) Entire trajectory.

(b) Zoom of the trajectory.

Figure 5.12: Vehicle Trajectory in combined braking from 80 to 0 km/h at lateral acceleration of 0.9 g with and without Anti-lock Brake System; X and Y stand for longitudinal and lateral vehicle displacement.

Table 5.4: Test results about radial distance performance

		Longitudinal braking				**Combined braking**		
		Friction				*Friction*		
		1		*0.7*		*1*		*0.7*
		Speed (km/h)				*Lateral acceleration (g)*		
		130	*80*	*130*	*80*	*0.9*	*0.5*	*0.5*
Standard ABS	*D*	90%	9.2%	9%	50%	-99.3%	-70.2%	-69.2%
Slip control	*D*	58%	8.6%	0.7%	80%	-96.3%	-69.8%	-73%
Wheel control	*D*	99%	3.2%	5.5%	85%	-91.7%	-60.3%	-62%

behaviour when subjected to different speeds and different road contact conditions.

In Table 5.4, the radial distance of the longitudinal braking manoeuvres represents the lateral deviation of the vehicle at the time of stopping. The three controls show a high percentage value of increase in lateral distance compared to the vehicle not equipped with ABS. This is because, since all the actuators have the same pressure target, the car without longitudinal control reaches lateral displacements of the order of a millimetre in high friction or centimetre in low friction, so even if in the other controls the car moves sideways by a few centimetres or tens of centimetres the percentage increase is very large. However, all three controls in the different types of manoeuvres have a lateral displacement due to a different pressure distribution on the right and left wheels of less than 20 cm.

Whereas, the results obtained by the longitudinal controllers and presented in Table 5.4 for the combined braking manoeuvres show a decisive percentage reduction in the radial distance from the reference trajectory. It happened because during braking the car without controls saturates the wheels and turns. In this case, the ABS developed ensure that the vehicle maintains the set trajectory by increasing

the stability of the vehicle both on dry and wet surface.

The braking distance performance in combined braking manoeuvres, shown in Table 5.3, is calculated as reduction or improvement percentage respect the *Standard ABS*, because the car without control spins out and so its trajectory is not a good comparison metric. In this case, the difference between the three controllers is in the order of a few centimetres.

5.1.5 Conclusion

In this work, the different behaviour of three types of a car's longitudinal stability control are developed in order to choose which should allow best performance for the control architecture implemented and improved the current braking performance. The tests done have been involved the use of a co-simulation environment between CRT and Matlab-Simulink, where the three types of controllers have been incorporated with: an EBD, a CBC, and a CBA model. The aim of the activities carried out was to ensure safety, improve the performances of the braking system during full braking manoeuvres by ensuring the driver a vehicle response as close as possible to his requirements with an integration that allows all the systems involved to work at their best and with a sampling time of 0.001 s.

The figures shown and Tables 5.3-5.4 allow to say that all the types of longitudinal controller developed avoid wheel locking and ensure less braking distance compared to the car operating without ABS. In addition, the combined braking tests show that the vehicle remains stable and steerable in wheel saturation limit conditions thanks to the longitudinal control actions.

However, the *Wheel Speed controller* is preferred for the following reasons: it exhibits a continuity of performance in all conditions under which it has been tested; compared to the *Standard ABS* it allows CBA to track the braking pressure in continuous and have a smoother behaviour both in dry and wet surface, ensuring a less disturbing intervention and, therefore, more comfort for passengers; compared to the *Slip Control* it does not have necessary of estimated tire longitudinal slip that are functions of the tire conditions and run into errors in low friction conditions that compromise the ABS operation; and having only three parameters, K_p K_i K_d, that define its functionality it allows a simpler and faster tuning process compared to both the other controllers providing easy integration and implementation of the system in current cars. Probably, if longitudinal slip were known, the *Slip Control* should have a feasible equilibrium set point under any friction condition. But due to its values between 0 and 1, errors in speed estimation, even if low, lead to a high error in longitudinal slip estimation, resulting in loss of ABS performance, especially in low friction conditions. Therefore, the *Wheel Speed controller* ensures better ABS performance in all road conditions, while still allowing the desired slip to be followed, even if in friction changes the speed estimation has errors and the slip followed is not the optimal one.

5.2 Lateral Stability Control

This Section presents the development of a vehicle stability control system that is able to operate in real-time, ensuring to enhance vehicle dynamics and safety. The commercial cars have an ESC that acts actuating the brakes autonomously to correct the vehicle dynamics at limit of adhesion conditions. In this study it

will be shown how the stability control system proposed can operate autonomously and constantly during vehicle motion, thanks to a controller based on a simplified vehicle model and a brake unit that operates in continuous.

The control system consists of an advanced lateral stability automotive controller and four BBW actuators. The control is an LQR that ensures to stabilize the yaw rate and the side slip angle minimizing the errors between the actual car values and the values given by a steady state dynamic reference model. To reach this aim the LQR gives the values of total yaw moment that the vehicle has to achieve. This value is split in the wheel braking pressure by the torque allocator logic shown in Section 5.3, Control Command Actuation, and sent to the CBA models that with their own logic and proximity to the wheels ensure a vary fast actuation, stabilizing the vehicle and providing safety.

The control system has been design to be used as a stability system on commercial cars, requiring of common vehicle sensors, ensuring better performances and stability even in driving at limit of adhesion conditions, but also to be installed in an autonomous vehicle being able to act independently from the driver.

To calibrate and develop the control system different manoeuvres were performed in off-line co-simulation between Matlab-Simulink and CRT. Instead, to validate the control system a set of test campaigns were carried out:

- **Subjective evaluation**: professional driver evaluation on the real-time dynamic simulator placed at Danisi Engineering srl comparing its performance with a standard torque vectoring algorithm;

- **Performance evaluation**: a comparative investigation with the lateral stability automotive controllers developed by the colleague PhD student Tommaso Favilli, and a commercial solution, on the real-time static simulator placed at Meccanica 42 srl.

These comparisons has the aim of improving the stability performances achieved by a combined tracking of yaw rate and side-slip angle through the application of optimal efforts.

About the Tommaso Favilli's SMC solution, it relies on the same approach developed by me for the control objectives definition, but differ from the action perspective. In fact, if the solution developed in this thesis involves the adoption of differential braking actuation technique to deliver a desired yaw moment to the car body to track controlled states, the sliding controller can also track torques of hub-motor configurations as well as steering corrections, achieving vehicle stability and a driving response in accordance with the pilot intentions. Results show that both solutions ensure higher handling performances, if compared to Non-controlled or Commercial-controlled vehicle scenarios.

5.2.1 Lateral Controller Structure

The considered BBW architecture is able to continuously track four different target pressures, to be assigned to each wheel. This allows the development of a tracking control system which ensures stability and safety, using an optimum control approach by implementing an LQR. To achieve this, the controller aims at the direct regulations of actual yaw rate and side-slip angle of the vehicle expressed by the single-track dynamic vehicle model, while the reference states rely on ideal kinematic model. Therefore, the outputs of the optimal control are the errors

between the actual and reference states, which are minimized by delivering to the vehicle body a desired yaw moment. This is applied through a continuous and independent braking actuation actions on the wheels.

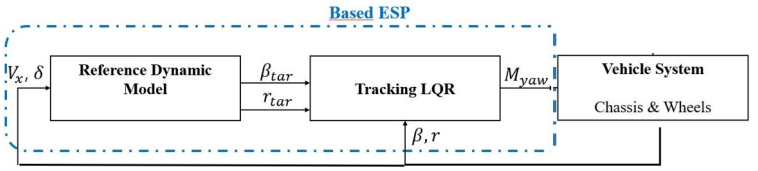

Figure 5.13: Lateral stability control system block diagram.

The controller architecture, shown in Figure 5.13, is composed by a reference model and LQR tracking controller. According to the real-time conditions, the control quantities have been discretized with a sample time of 0.001 seconds. The reference model has the task of providing the desired values of the side-slip angle and yaw rate. It receives, as inputs, the same driver demand steering and the same longitudinal velocity of the car and thanks to the formulations shown in the following model explanation Subsection, it reproduces the vehicle behaviour and allows side slip angle and yaw rate to remain under low values and ensures stability. The LQR controller works in real-time, providing, at each time step, the correction gains to compensate the errors of the vehicle compared to the reference model.

The solution of the control problem is the total barycentric yaw moment that the vehicle must follow to reach the dynamic of the reference model.

Reference Dynamic Model

The core aim of this study is to ensure that our vehicle follows at any time an ideal behaviour and achieves stability and optimal performances. During a manoeuvre, lateral and yawing dynamics of the vehicle change over time according to initial condition, SWA and longitudinal velocity imposed by the driver. To extrapolate the inner characteristics of the vehicle and be able to act the brakes to compensate the understeering, or the oversteering behaviour of the vehicle, the steady state values of the yaw rate and side-slip angle are calculated. The understeering gradient, Δ, is the difference between actual and kinematic steering. Taken difference between front and rear slip angles, α_i, it's the gradient to lateral acceleration that represents Δ. In this way, the yaw rate of the vehicle can be expressed as a function of the vehicle parameters (front and rear wheelbase, a_1, a_2, and mass, m), of the cornering stiffness, $C_{yf/r}$, and of the driver's inputs, steering, δ, and speed, u, (5.14, 5.15 and 5.16).

The steady-sate values of the side-slip angle can be estimated by the understeering gradient too, using the linearized congruence equations (5.17).

$$\alpha_f = \frac{m}{L}\frac{a_2}{C_{yf}} ru; \alpha_r = \frac{m}{L}\frac{a_1}{C_{yr}} ru \tag{5.14}$$

$$\delta - \frac{L}{R} = \alpha_f - \alpha_r = \frac{m}{L}(\frac{a_2}{C_{yf}} - \frac{a_1}{C_{yr}}) ru \tag{5.15}$$

$$\Delta = \frac{m}{L}(\frac{a_2}{C_{yf}} - \frac{a_1}{C_{yr}}) \tag{5.16}$$

$$\alpha_r = -\beta + \frac{(ra_2)}{u} \tag{5.17}$$

$$r_{des} = \frac{u}{(L + u^2\Delta)}\delta; \beta_{des} = \frac{(a_2 - \frac{(ma_1u^2)}{(LC_{yr})})}{(L + u^2\Delta)}\delta \tag{5.18}$$

These values of the yaw rate and of the side-slip angle (5.18) are the values that the vehicle has to follow in order to ensure a linear steady-state behaviour having assumed constant understeering gradient and steady-state load transfer, $\sum F_{yf} = ma_{yf} = mru\frac{a_2}{L}$. This behaviour is the one that allows to maintain low values of side-slip angle and so ensuring stability.

On the other hand, these expressions do not ensure to consider the limit of adhesion of the wheels. Considering a safety factor of 0.85, target yaw rate can be bounded by (5.19), as described in (5.20).

$$|r_{bound}| \leq 0.85\frac{\mu g}{u} \tag{5.19}$$

$$\begin{cases} r_{tar} = r_{des} & if|r_{des}| \leq r_{bound} \\ r_{tar} = r_{bound} \cdot sign(r_{des}) & if|r_{des}| > r_{bound} \end{cases} \tag{5.20}$$

Limiting the target side-slip angle is also very important, because higher values of β lead the tires lose their linear behaviour, approaching the limit of adhesion. Thus, is upper bounded by the empirical relation (5.21), as visible in (5.22).

$$|\beta_{bound}| \leq r_{tar}\left(\frac{b}{V_x} - \frac{m \cdot a \cdot V_x}{C_{yr} \cdot (a + b)}\right) \tag{5.21}$$

$$\begin{cases} \beta_{tar} = \beta_{des} & if|\beta_{des}| \leq \beta_{bound} \\ \beta_{tar} = \beta_{bound} \cdot sign(\beta_{des}) & if|\beta_{des}| > \beta_{bound} \end{cases} \tag{5.22}$$

In this way, our reference model is implemented to provide the yaw rate and the side-slip angle knowing the steering angle and the longitudinal velocity, ensuring that the vehicle remains in conditions of grip and handling.

Since these reference values change while the vehicle is in motion, to be able to implement them in the control, we have to represent them in a state-space form. We can do this defining the gradients of r_{tar} and β_{tar} in the Laplace transform derivative, where s is the Laplace variable and $\tau_i = 0.1$ is the time constant:

$$\dot{\beta}_{tar} = \frac{s\beta_{tar}}{(1 + \tau_\beta s)}; \dot{r}_{tar} = \frac{sr_{tar}}{(1 + \tau_r s)} \tag{5.23}$$

so, the state-space of these transfer functions is composed by side-slip angle and yaw rate as states. This represent the reference that the vehicle must follow.

Vehicle Optimal Control Mode

Because we decide to use an optimal controller we must defined a vehicle dynamic model where the correlation between sates and inputs are linearized at each time step (5.24-5.25).

$$\dot{X} = AX + Bu \tag{5.24}$$

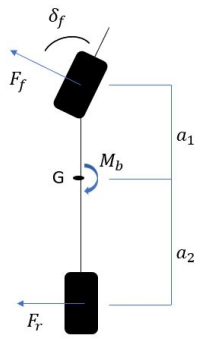

Figure 5.14: Single Track Vehicle Model.

$$Y = CX + Du \tag{5.25}$$

To ensure this aim, a single-track model of vehicle with 2 degree of freedom, lateral and yaw, was implemented (Figure 5.14). The dynamic is expressed by the equations shown in (5.26-5.27), where the brake forces, that has to control the vehicle, are defined as a total yaw moment added in the yaw moment balance equation.

$$m(\beta\dot{u} + ru) = F_{yf} + F_{yr} + F_{xf} \tag{5.26}$$

$$I\dot{r} = (F_{yf} + F_{xf})a_1 - F_{yr}a_2 + M \tag{5.27}$$

Every time step the following hypothesis are assumed:

- constant longitudinal velocities;
- lateral forces are in linear proportional relation with the lateral slips

so, taken congruence equations, it is possible to define the lateral forces as dependent to side-slip angle and yaw rate. Tanks to this, a State-Space of the vehicle was implemented, where the states (5.28) are the side-slip angle and the yaw rate, and the input (5.29) is the total yaw moment given by the brake forces on the wheels that the actuators can ensure.

$$X = [\beta, r] \tag{5.28}$$

$$u = [M_{tot}] \tag{5.29}$$

$$A_r = -\begin{bmatrix} \left(\frac{(2C_{yf}+2C_{yr})}{mu}\right) & 1 + \frac{(2C_{yf}a_1 - 2C_{yr}a_2)}{(mu^2)} \\ \frac{(2C_{yf}a_1+2C_{yr}a_2)}{I} & \frac{(2C_{yf}a_1^2+2C_{yr}a_2^2)}{Iu} \end{bmatrix} \tag{5.30}$$

$$B_r = -\begin{bmatrix} 0 \\ \frac{-1}{I} \end{bmatrix} \tag{5.31}$$

Linear Quadratic Regulator Controller Design

Our problem is composed by a given system $\dot{x} = f(x, u)$ and a feasible target (x_{tar}), and we wish to design a compensator of the form $u = \alpha(x, x_{tar})$ such that $\lim t \rightarrow \inf((x - x_{tar}) = 0)$. This is known as Tracking Problem. To design a controller capable of solving this type of problem, the vehicle model State-Space was concatenated with the reference model State-Space achieving a new dynamic model (5.32, 5.33, 5.34 and 5.35). In this way, it was possible to define the outputs as the errors between the actual and the target values of the states. So, the goal of the control becomes find the right input to minimize these errors.

$$X = [\beta, r, \beta_{tar}, r_{tar}] \tag{5.32}$$

$$Y = [\beta - \beta_{tar}, r - r_{tar}] = [e_\beta, e_r] \tag{5.33}$$

$$A = \begin{bmatrix} A_r & 0 \\ 0 & A_{tar} \end{bmatrix}; B = \begin{bmatrix} B_r \\ B_{tar} \end{bmatrix}; \tag{5.34}$$

$$C = \begin{bmatrix} 1 & 0 & -1 & 0 \\ 0 & 1 & 0 & -1 \end{bmatrix}; D = \begin{bmatrix} 0 \\ 0 \end{bmatrix}; \tag{5.35}$$

Once specified the dynamic model, the control is ensured by the LQR that is an optimal linear control. This type of control uses the minimization of a quadratic cost function (5.36) producing the necessary gains to each state to define the value of the input (5.37).

$$J = \int_0^\infty (y^T Q y + u^T R u) dt \tag{5.36}$$

$$u = -K_r x - K_{tar} x_{tar} \tag{5.37}$$

In these equations x and x_{tar} represents respectively the model states and the reference states; u is the input, namely a total brake yaw moment; Q and R are the weight matrixes respectively for the outputs and the inputs and $K = [K_r, K_{tar}]^T$ is the gain matrix given by the minimization of the cost function, J, solving the Riccati equations:

$$P_k = Q + A' P_{(k+1)} A - A' P_{(k+1)} B (R + B' P_{(k+1)} B)^(- 1) B' P_{(k+1)} A \tag{5.38}$$

$$K = (R + B' P B)^{-1} B' P A \tag{5.39}$$

The LQR control is, as already mentioned, an optimal control, i.e. it is optimal compared to an appropriate performance index. This performance index is the cost function, defined in (5.36), whose minimization allows to solve the problem, in this case of reference model tracking, finding the law of control in state feedback (5.37).

At this point the control is applied in real time.

5.2.2 Test and Results

Different test campaigns are done to calibrate, evaluate and validate the lateral stability control developed. These tests are itemized below and its description and results are shown in the following Subsections.

- **Off-line simulation tests**: the calibration and validation of the lateral stability performance was done carrying out a series of manoeuvres through co-simulation environment of Matlab-Simulink and Vi-Grade CRT. Here the comparison with the uncontrolled vehicle allows to verify the dynamic stability improvement achieved with the controller;

- **Subjective tests**: the evaluation of the tracking control logic implemented was done comparing the performances obtained having an on-line definition of the target states by a model based approach, with the ones obtained by a standard torque vectoring where the target control states are given by look-up table saturation limits. The tests were performed in a real-time dynamic simulator by a professional test driver with open-loop manoeuvres;

- **On-line performance evaluation**: the evaluation of the performances obtained by two advance lateral stability control systems (tracking LQR and SMC) compared with a non-controlled and a commercial controlled vehicle is done in a real-time static simulator with Human in the Loop interface.

Off-line simulation tests

To calibrate and test the control, a series of manoeuvres were carried out through the co-simulation environment of Matlab-Simulink and Vi-Grade CRT. These manoeuvres were made to bring the vehicle at limit of handling and in steady-state conditions:

- Steering pad;

- Sine with Dwell (SWD), given by the ESC test procedure of the ECE-R 13-H European normative [102].

These are close-loop manoeuvres with a sample time of 0,001 second. The characteristics of every manoeuvre are shown in the Table 5.5:

Table 5.5: Manoeuvres definition used in the off-line simulation tests.

MANEUVERS	Longitudinal velocity	Steering amplitude	Steering frequency
SWD	80 (km/h)	270 (deg)	0.7 (Hz)
Steering Pad	100-150 (km/h)	200 (deg)	1 (deg/s)

Thanks of this tests, a tuning of the control and of the reference dynamic model were possible, changing respectively the controller weights and the target understeering parameters. In addition, a validation of the improve of dynamic stability respect the uncontrolled vehicle was proved.

Steering Pad This test is intended to assess the maximum lateral acceleration under quasi-stationary conditions that the vehicle can maintain. It involves bringing the vehicle to a certain longitudinal speed and then applying a steering rotation with constant angular velocities. In the graphs below, the manoeuvres done with different velocities, 100 km/h and 150 km/h, are shown

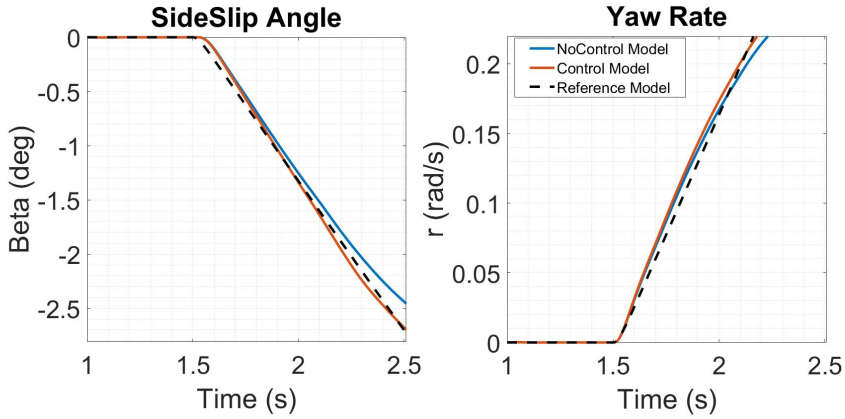

Figure 5.15: Side slip angle and yaw rate achieved by the no-controlled vehicle, controlled vehicle and reference model during a Steering Pad manoeuvre at 100 km/h.

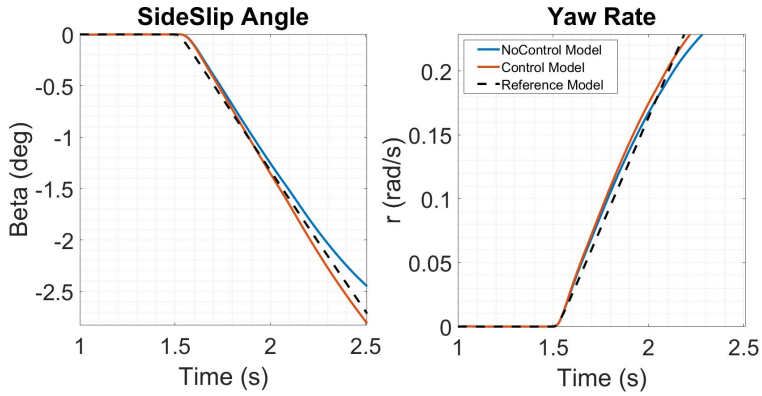

Figure 5.16: Side slip angle and yaw rate achieved by the no-controlled vehicle, controlled vehicle and reference model during a Steering Pad manoeuvre at 150 km/h.

Figures 5.15, 5.16 show the trends of side-slip angle and yaw rate over time at various speed, in case of uncontrolled vehicle, controlled vehicle and reference model. It's possible to see that the reference model, that represent a quasi-stationary state, has a linear trend, in which the vehicle responds to the driver's inputs in a smooth manner, ensuring good handling and stability. The controlled vehicle follows the trend of the reference model ensuring better performance than an uncontrolled vehicle.

Being the vehicle is in understeering condition, the controller actuates the inner rear wheel ensuring a closer trajectory than the vehicle without the controller (Figure 5.17). As the speed increases, the brake pressure also increases to counteract the additional lateral force generated.

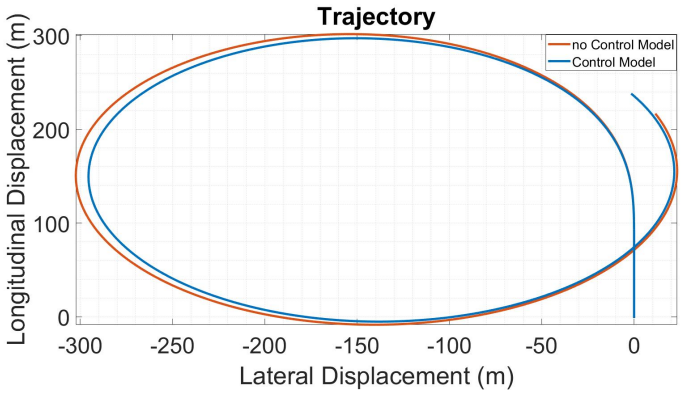

Figure 5.17: Trajectory made by the no-controlled vehicle, controlled vehicle and reference model during a Steering Pad manoeuvre at 100 km/h.

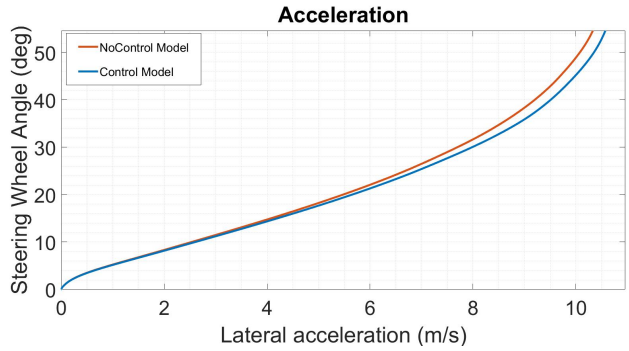

(a) 100 km/h.

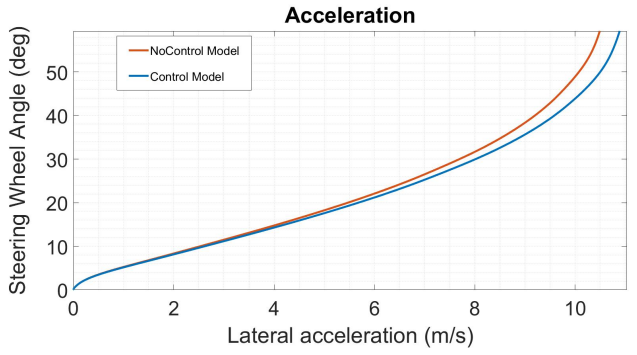

(b) 150 km/h.

Figure 5.18: SWA as function of lateral acceleration made by the no-controlled vehicle and controlled vehicle during a Steering Pad manoeuvres.

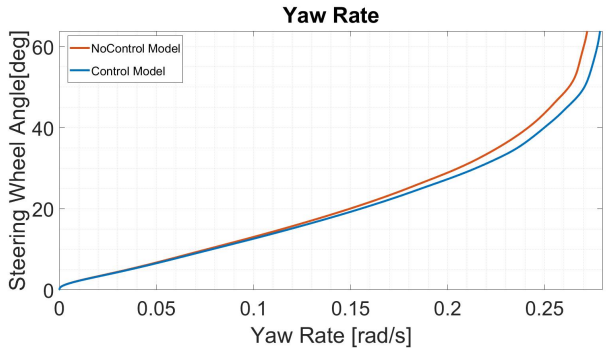

(a) 100 km/h.

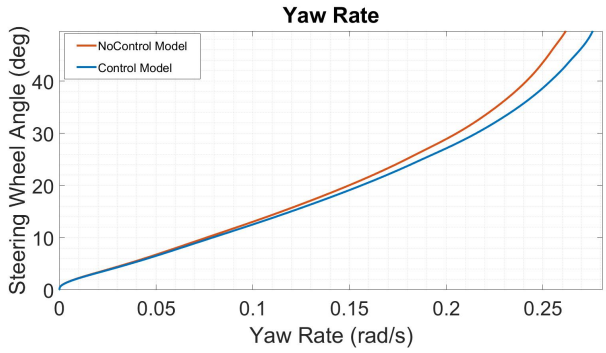

(b) 150 km/h.

Figure 5.19: SWA as function of yaw rate made by the no-controlled vehicle and controlled vehicle during a Steering Pad manoeuvres.

Figures 5.18a, 5.18b, 5.19a and 5.19b, instead, shows the improvement of the vehicle performances. The trend of the understeering curve (Figures 5.18a, 5.18b), where the steering is given as function of lateral acceleration, illustrates that the vehicle equipped with the control in both situations can reach higher lateral acceleration and the slope of the curve is lower. This means an improvement of the performances, because the vehicle is able to maintain stability at higher accelerations and an improvement of vehicle handling, because it replies at the driver steer in more neutral way. In the end, in Figures 5.19a and 5.19b it's shown the trend of the steering as function of the yaw rate. We can see that the steer remains linear for higher values of the yaw rate. This is another index of the better levels of the car and results in the achievement of closer trajectory (Figure 5.17).

Steering With Dwell This manoeuvre allows to verify the stability of the vehicle as it is very demanding and brings the vehicle to the limit of handling. The type of test, required by the normative, involves identifying the steering angle, δ_0,at which the car achieves lateral acceleration of 0.3 g with a longitudinal speed of 80 Km/h. Then, another series of tests involve the SWD steering input with an increasing amplitude of $\delta = k\delta_0$, from k=1.5 to k=6,5. In this study the maximum value of the steering amplitude is 270 deg, and only the results achieved with this steering angle are shown below, as they represent the most critical driving condition.

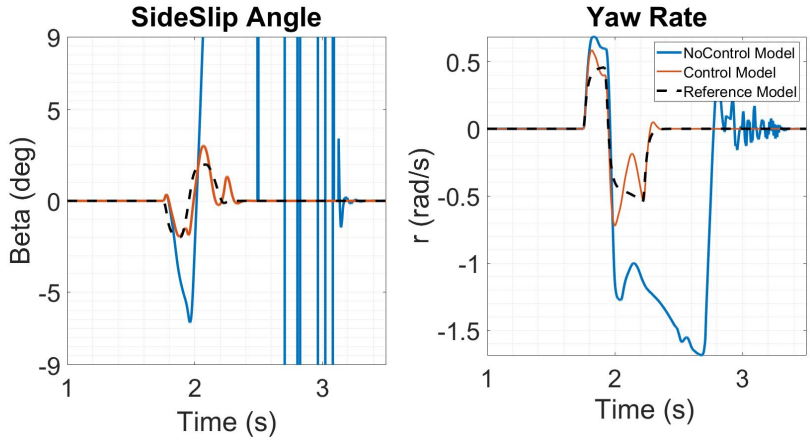

Figure 5.20: Side slip angle and yaw rate achieved by the no-controlled vehicle, controlled vehicle and reference model during a Sine With Dwell manoeuvre.

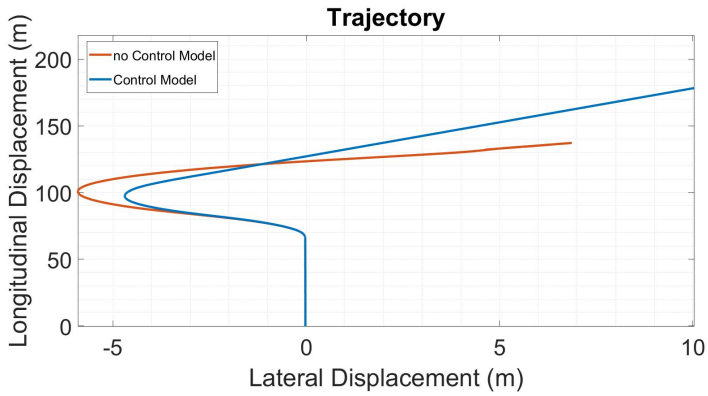

Figure 5.21: Trajectory made by the no-controlled vehicle, controlled vehicle and reference model during a Sine With Dwell manoeuvre.

The plots show how the vehicle without the controller loses its stability and starts to spin. In the Figures 5.20 the reference, the controlled and the no-controlled model are shown. It is clearly visible that the controlled vehicle is able to follow the side-slip angle and yaw rate values given by the reference and is able to maintain stability. The wheels braked are the outer front ones. In fact, the uncontrolled vehicle shows an oversteering behaviour that ends with its spin. Figure 5.21 shows the trajectory of the vehicle with the controller and without the controller. It is possible to see how the uncontrolled vehicle can't finish the manoeuvre and loses its stability. Instead, the controller ensures stability and control also at limit of handling condition.

Subjective tests

To validate the stability control system developed a comparison with a standard torque vectoring was done, testing both on a real-time dynamic simulator and collecting the subjective impressions had by a professional test driver. The results

are shown in Table 5.6, and the evaluation was done in different driving manoeuvres on a Proving Ground (PG) scenario at high and low friction conditions, in addition to obstacle avoidance and longitudinal braking where right and left wheels side have different friction conditions (Mu-split).

Table 5.6: Subjective evaluation of lateral stability systems

	Proposed ESC	Standard Torque Vectoring
High-mu PG	-Efficacious control -Faster in interventions -Overall higher performances	-Efficacious control -Slower in intervantions -Less performances
Low-mu PG	-Efficacious control -Stability is not guaranteed in Cornering Braking -Overall higher performances	-Efficacious control -Stability is not always guaranteed -Less effective
Obstacle avoidance	-Efficacious control -More SWA needed -Max speed: 110 km/h	-Efficacious control -Max speed: 120 km/h
Mu-split	-Efficacious control -Less SWA correction -Easy to control -Better performance	-Efficacious control -Presence of steering torque in high mu direction -Less effective

By the results shown, can be said that the proposed lateral stability system, which can rely on a continuous definition of the targets given by a dynamic model, respect to the standard torque vectoring ensures an overall higher performances in almost all the scenario tested with faster and less invasive interventions. However, during obstacle avoidance tests, even if both the controller are resulted efficacious, the standard torque vectoring ensures to perform the test with higher longitudinal speed resulting more effective.

On-line performance evaluation

Then, the performances were evaluated through the comparison with another advance lateral stability system and a commercial one installed on the real-time static simulator shown in Figure 1.5 both of which are described below.

Sliding Mode Lateral Stability Control This lateral stability solution is based on Sliding Mode methodology and was developed by the PhD student Tommaso Favilli [77]. The objective is the direct control of vehicle side-slip angle β and yaw rate r by the application of corrective steering and TV efforts. The SMC-based ESP algorithm, whose simplified block diagram is visible in Figure 5.22, is developed on three different layers, depending on the task the sub-controller must accomplish:

- **High-level layer**: which defines the control objective according to driver intention and vehicle states, e.g. longitudinal speed, side-slip angle, yaw rate;
- **Intermediate-level layer**: consisting in a first order SMC;
- **Low-level layer**: devoted to the generation of the control references for the actuators, i.e. SBW, BBW and traction motors.

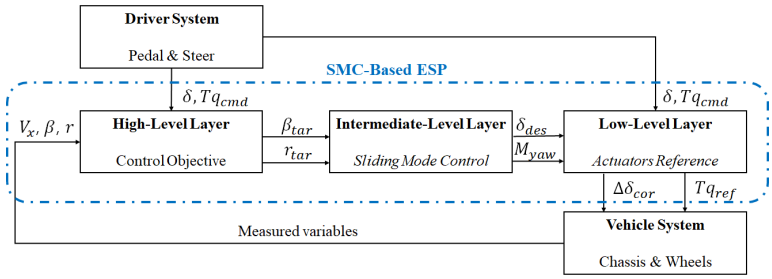

Figure 5.22: Block diagram of the Sliding Mode Control developed by Tommaso Favilli.

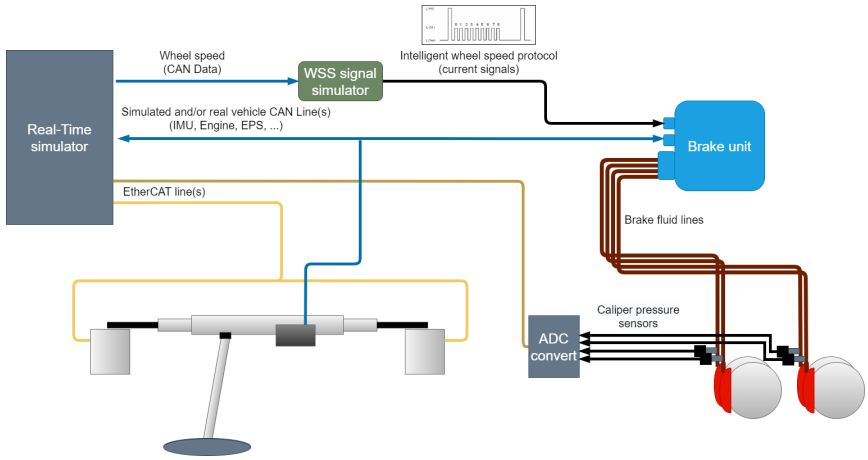

Figure 5.23: Static simulator setup.

Braking Unit A commercially available BBW system, known as **MKC1** produced by Continental GmbH, has been implemented on the simulation rig by the PhD student Federico Alfatti [103]. The installation layout is described in Figure 5.23. The stock brake plant is mounted on the simulator. It includes the brake tubes (with the correct diameter and length), which are connected to the electromechanical units of 4 independent stock brake callipers, acting on the original brake discs. The brake pedal is directly integrated on the unit, and it constitute the main braking unit driver-machine interface device.

The brake unit communicates through the communication lines using a CAN protocol, receiving all the signals that are usually exchanged on real vehicles (e.g. from IMU), simulated by the model on the real-time computer. In addiction, this unit needs the intelligent wheel speed signals via a direct communication line. For this reason, virtual wheel speed sensors has been implemented, which converts the the wheel speeds (received via CAN from the real-time machine) to the typical signal type provided by intelligent wheel speed sensors [104].

Finally, 4 pressure sensors have been installed on the callipers, and their signals are sent back to the vehicle model via an EtherCAT measurement line, closing the loop, controlling the vehicle deceleration after a brake demand from the driver.

The unit functionalities have been tested in [103], comparing the responses and

behaviours on the static simulator respect to a real vehicle, proving its effectiveness on a previously validated vehicle model.

Test Campaigns In this phase, a driver replicates some reference cornering test with the real-time driving simulator through the Human in the Loop interface system. To assure reliable comparative metrics, reference closed-loop manoeuvres are repeated supposing four scenarios, in which the vehicle model is alternatively implemented with different controlling techniques:

- **Non-Controlled Scenario**: in this case the vehicle is driven without the assistance of any kind of lateral stability controller. Thus, it was possible to establish inner vehicle manoeuvrability and test the driver capabilities. Many free driving tests are conducted in order to identify the limit of controllability;
- **Commercial-Controlled Scenario**: tests are conducted with the *Continental GmbH* proprietary ESP controller. The strategy, from our side, is completely unknown. However, we can make some assumptions, supposing the control technique is advanced and represent the state of the art of the industrial ESP solutions, which is actually implemented on different vehicles in the market.
- **LQR-Controlled Scenario**: the LQR Tracking Control is tested, thanks to the real-time co-simulation capabilities of the virtual environment, between *MATLAB Simulink* and *VI-Grade*;
- **SMC-Controlled Scenario**: here the SMC is investigated, exploiting the same control rig of the previous scenario (ESP in *MATLAB Simulink* and vehicle model in the *VI-Grade*).

The investigated reference manoeuvres are repeated many times, selecting as results the ones which appear more comparable. Indeed, to ensure reliable comparative metrics its fundamental to reproduce the close-loop test as similar as possible. Selected cornering tests are summarized in Table 5.7.

Table 5.7: Investigated reference manoeuvres.

Name	**Standard**
Step Steer	ISO 7401:2003
Sine Steer	ISO 7401:2003
Lane-Change	ISO 3888-1:2018

However, boundary conditions specified by the related standards are modified to guarantee more severe conditions, in terms of stability performances. This is useful to highlight the results [105]. Indeed, due to the excellent handling capabilities of the vehicle model, using the reference operative scenario produce no unstable behaviour, making difficult to assess the improvements related to the investigated controllers. Main contributions of ESP systems concern the stabilization of vehicle trajectory and desired driving path, when unstable non-linear behaviour onset.

To ensure easy understanding of the results, output plots are presented for LQR and SMC, compared with Non-controlled and Commercial-controlled scenarios.

Step Steer Inspired by the ISO 7401:2003 standard, a *Step Input* test is performed in both directions: left and right turning. Respect to the reference manoeuvres, this one is carried out in closed-loop conditions with initial longitudinal speed of $150km/h$ and wheel steering angle of $90deg$. It worth nothing to say that this lateral test actually exhibits a ramp steering command. Indeed, human driver can't apply an instantaneous angle to the steering wheel [106]. However, the steering rate is high enough to produce a rapid cornering manoeuvre, letting us to investigate vehicle fast transient behaviour.

Results of Figure 5.24 clearly show that both controllers succeed in tracking yaw rate and side-slip angle, if compared to Non-controlled and Commercial-controlled scenario. Controlled states errors are reduced for LQR and SMC solutions thanks to the application of optimal control efforts, visible in Figure 5.25 and Figure 5.26.

It is inserting to highlight that both proposed controllers apply different torque vectoring efforts respect to the benchmark ESC. In the first stage (at about $1.5s$) all the stability systems perform quite similar, despite the fact that SMC and LQR solutions show higher control actions. In the steady-state phase of the manoeuvre, indeed, controllers actuate the wheels on the opposite side respect to Commercial-controlled scenario. This is due to the fact that the developed solutions aim at the control of side-slip angle, in addition to yaw rate, which typically is the solely control objective of wide diffused ESC in the market.

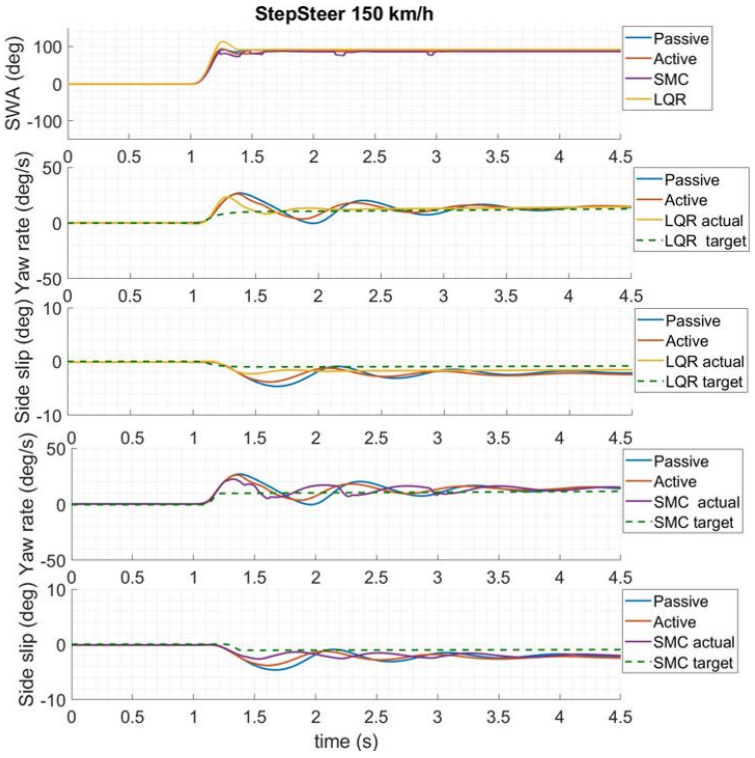

Figure 5.24: Evaluation of the states tracking performances in case of Non-controlled (Passive), Commercial-controlled (Active), LQR, and SMC-controlled scenarios, in a *Step Steer* manoeuvre at 150 km/h and with 90 deg steering wheel angle.

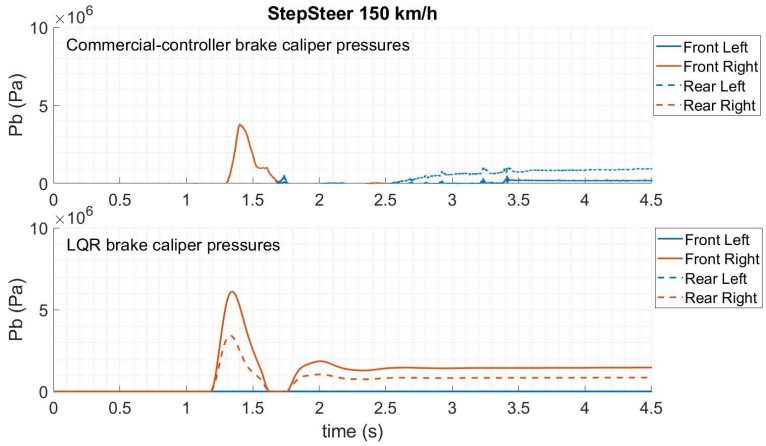

Figure 5.25: Evaluation of the four brake caliper pressures in case of Commercial-controlled and LQR-controlled scenarios, in a *Step Steer* manoeuvre at 150 km/h and with 90 deg steering wheel angle.

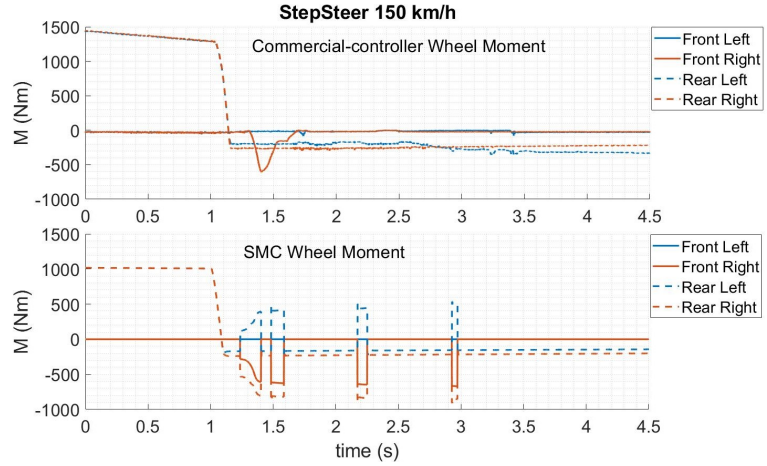

Figure 5.26: Evaluation of the four wheel moments in case of Commercial-controlled and SMC-controlled scenarios, in a *Step Steer* manoeuvre at 150 km/h and with 90 deg steering wheel angle.

Sine Steer A sine path wave of 90 deg on steering wheel is realized by the driver while travelling at 150 km/h, to evaluate responsiveness of the controlling techniques during this test. This manoeuvres allow us to investigate on the correctness of implemented dead-zone on the states errors, since both yaw rate and side-slip consecutively cross 0 values. In the top plot of Figure 5.27 the steer angle imposed by the driver is visible for the different scenarios. For the SMC-Controlled solutions the impact of the steering correction control technique is shown.

Even in this case, the proposed controllers performs quite well respect to the task of tracking the controlled states. In Non-controlled solutions vehicle is unstable, while for LQR and SMC scenarios both vehicle yaw rate and side-slip angle are controlled by active torque distributions effort of Figure 5.28 and Figure 5.29,

exhibiting improved stability performances even respect to Commercial-controlled scenario.

As for *Step Steer* test, LQR and SMC control actions show higher control effort values respect to reference ESP controller. This leads to improved tracking performances of the controlled states, especially for the side slip angle, achieving higher safety margin.

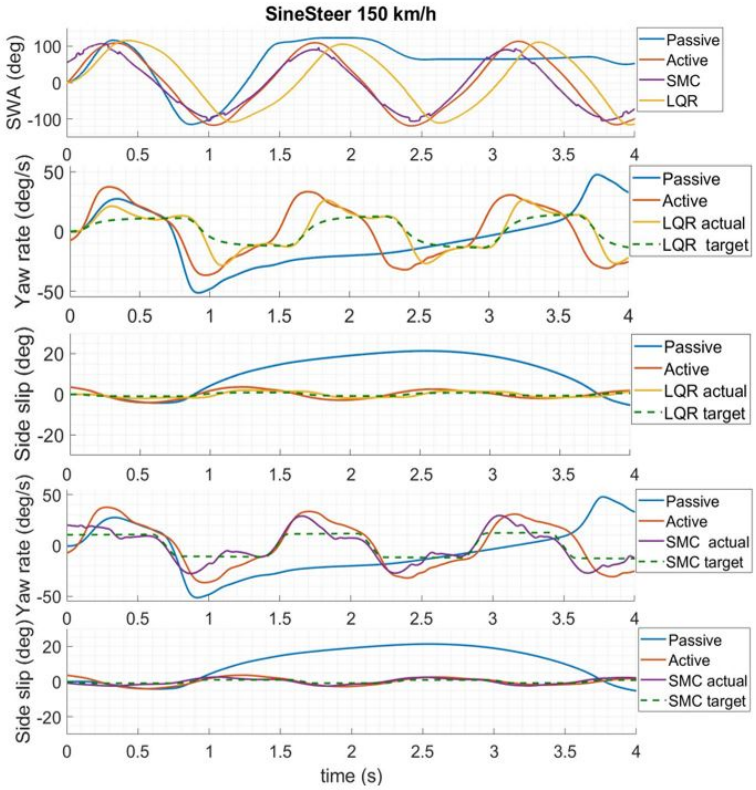

Figure 5.27: Evaluation of the states tracking performances in case of Non-controlled vehicle (Passive), Commercial-controlled vehicle (Active), LQR, and SMC controlled scenarios, in a *Sine Steer* manoeuvre at 150 km/h and a 90 deg of steering wheel angle amplitude.

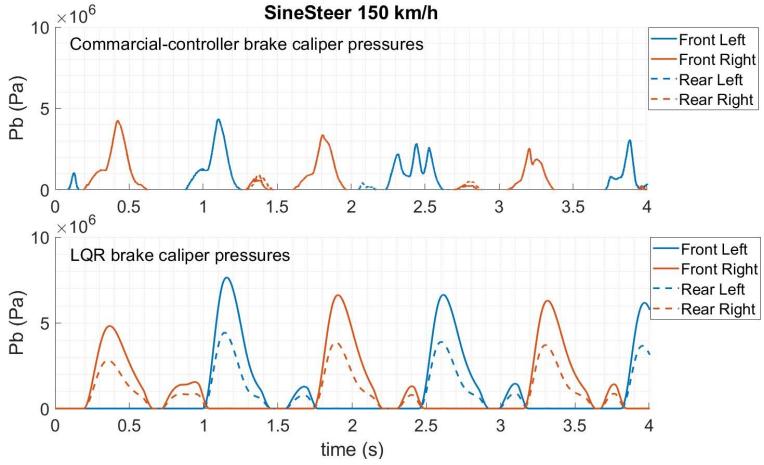

Figure 5.28: Evaluation of the four brake caliper pressures in case of Commercial-controlled vehicle and LQR controlled, in a *Sine Steer* manoeuvre of 150 km/h and 90 deg of steering wheel angle.

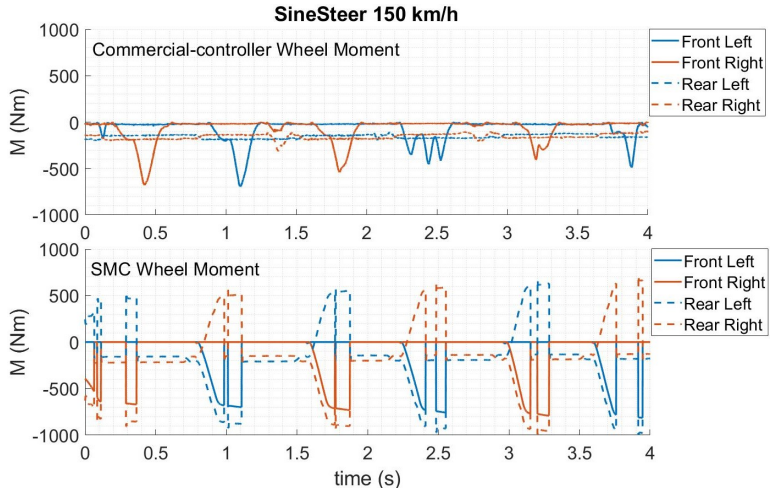

Figure 5.29: Evaluation of the four wheel moments in case of Commercial-controlled vehicle and SMC controlled, in a *Sine Steer* manoeuvre of 150 km/h and 90 deg of steering wheel angle.

Lane change A single Lane-Change manoeuvre test is conducted to subjectively determine vehicle stability aspects. Respect to previous tests, this is the only one which is specified closed-loop by the reference standard (ISO 3888). The vehicle is driven at 150km/h and a steering path is imposed by the pilot to obtain a lateral displacement of about 3 m. Subsequently, another steer command is applied to re-orient the car in the longitudinal direction. Figure 5.30 shows the driving path performed by the vehicle during the manoeuvre and the vehicle longitudinal speed.

It is interesting to note that LQR scenario trajectory exhibits a slight overshoot in the lateral displacement respect to center-line, with a reduced speed respect to other scenarios. SMC, indeed, tracks desired trajectory with a smoother behaviour.

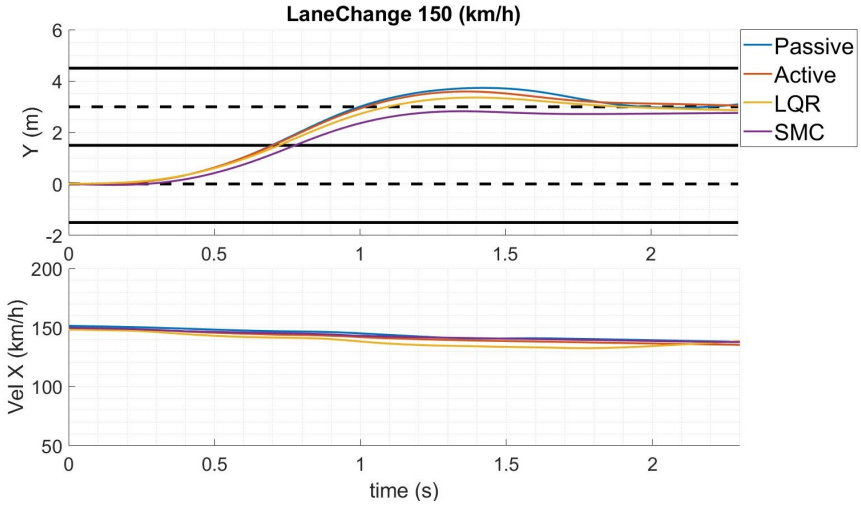

Figure 5.30: Evaluation of the trajectory and longitudinal speed in case of Non-controlled vehicle (Passive), Commercial-controlled vehicle (Active), SMC, and LQR controlled, in a *Lane Change* manoeuvre of 150 km/h and a lateral displacement of about 3 m.

This is due to the fact that sliding control adopts an accelerometric criteria with fixed dead-zones, reducing the control effort when approaching target states. For what concern the speed, the sliding mode solution allows to perform the reference manoeuvre in accordance with the driver intention, maintaining the entrance longitudinal speed by the exploitation of the traction forces of the powertrain.

5.2.3 Conclusion

In this Section a stability vehicle controller based on a tracking LQR was presented aiming at the direct regulation of vehicle's yaw rate and side-slip angle to achieve stability improvements respect to the conventional solution, based on solely yaw rate tracking. The LQR controller is able to apply a yaw moment to the car body with a differential braking technique to stabilize the trajectory. Comparing to standard torque vectoring functionality the target control states are provided in continuous depending on the driver input request of SWA and speed following a reference dynamic model that can be tuned changing the understeering gradient parameters.

This solution ensures the achievement of very good performances thanks to the possibility of use four actuators able to continuously work and optimally manage the individual pressures at the wheels.

As designed, LQR control gain are calculated assuming a constant longitudinal speed value of 80 km/h. Initially, an adaptive approach was tested where various gains corresponding to various vehicle speeds were calculated and then, on-line via look-up tables, the tracking gains were changed according to the longitudinal speed of the car. However, the results obtained showed a deterioration in performance, probably due to a lack of adequate linkage between one condition and the next, resulting in excessive jumps between the various gains. The good results given

by the optimiser shown led to the decision to use only the gain optimized with one longitudinal speed. As future step could be necessary the development of an adaptive control optimised not only with speeds changes but also with cornering stiffness changes.

The simulation campaign consists of a preliminary *off-line test phase*, in which controllers are tuned and validated. *Steering Pad* and *Sine With Dwell* ware fundamental for the definition of the efforts constrains and reference parameters tuning. Tests show that this control results robust in different type of conditions, in steady-state manoeuvres and at limit of handling, for different longitudinal velocities and steering angles. Compared to the uncontrolled vehicle, the lateral stability system allows to achieve more linear response to the driver inputs, ensuring more stable trajectory in all the tests made.

Then, to validate the developed ESC, it underwent a subjective evaluation by a professional test driver, comparing its performances with the ones obtained by a standard torque vectoring system. The results obtained and reported in Table 5.6 showed that a control system with continuous tracking of a dynamic reference model allows higher performance to be achieved with faster and less invasive intervention.

In addition, the tracking and stability capabilities of LQR and SMC strategies are investigated. The controllers share the same algorithm for the control objectives definitions, so the outputs comparability is ensured by the same reference modelling approach. However, the proposed solutions differs from the optimal control effort calculations aspect. In its most common configuration, LQR controller is able to apply a yaw moment to the car body with a differential braking technique to stabilize the trajectory. SMC controller is developed respecting important features to ensure flexibility and portability of the strategy respect to quite different powertrain architectures thanks to the torque allocator used.

In addition, the 2-dimension sliding surface formulation enable the option to apply even steer angle corrections.

The assessment is done in a co-simulation environment exploiting a real-time driving simulator hardware systems, which allows a driver to perform different reference manoeuvres, piloting the vehicle trough steer and pedals interface devices. The manoeuvres are inspired by standard cornering tests, to assess achievement in terms of lateral stability, using a Human in the Loop approach.

Executed cornering manoeuvres could show some gaps between each others, in terms of steering amplitude and rate as well as speed tracking. This is due to the inability of any human driver to assure the perfect repeatability of the tests. However, to mitigate this aspect multiple tests are conducted, comparing the most similar ones.

The *on-line test phase* refer to standard cornering manoeuvre in HiL configuration. Results highlight as both proposed control strategies enable improved performances respect to Non-controlled and Commercial-controlled vehicle scenarios. Indeed, actual yaw rates and side slip angles exhibit lower errors respect to target values using LQR and SMC stability programs solutions.

In particular, in the *Step Steer* manoeuvre (Figure 5.24) is evident how the tracking efforts exhibits different control actions between developed ESP solutions and the Commercial one, achieving better stability and dynamic performance of the car. This is also shown in the *Sine Steer* test of Figure 5.27. Furthermore, the need for stability control is essential: the driver with Non-Controlled vehicle is unable to perform the manoeuvre without losing the control of the car; instead,

the configuration with a ESP ensures to maintain stability and manoeuvrability. One can see the differences between proposed optimal control solution in the *Lane Change* test. In addition to improve the tracking performances of both yaw rate and side-slip angle, this manoeuvre shows also achievements allowed by the exploitation of traction moments. In Figure 5.30, both SMC and LQR assist the driver, enhancing vehicle handling aspects respect to Commercial-controller. However, the sliding approach allows a smoother response of the car to the driver intentions, letting to maintain the target longitudinal vehicle entrance speed and producing desired yaw moment by the usage of traction command and steering, in addition to conventional differential braking technique.

5.3 Control Command Actuation

Improved lateral stability performances of modern vehicles equipped with In-Wheel BW actuators could be achieved by a proper design of the adopted control strategy. The possibility to independently regulates braking efforts delivered at each wheel can lead to increased handling properties during cornering manoeuvres, especially if performed in degraded adherence operative conditions.

In this Section, the low level control command actuation is investigated through the comparison of two different torque allocation methodologies and implemented together with the lateral and longitudinal stability systems presented in the previous Sections.

The assessment of the performances is done through co-simulation activities, imposing to the vehicle specified reference trajectories according to related standards, in order to evaluate the achieved stability improvements.

5.3.1 Torque allocation models

The two allocation logics tested are:

- **Brake pressure splitting logic**: an algorithm developed by me where the target ESC yaw moment is provided to the car by splitting it on the four wheels considering the moment sign and the current force engagement of the wheels;
- **Moore-Penrose pseudo-inverse**: an optimal allocation strategy developed by the PhD student Tommaso Favilli, where the target ESC yaw moment is split on four wheels braking pressures as an optimization between the driver request of acceleration and braking, and the constraint limits of the actuator systems.

Brake pressure splitting logic

The aim of this logic is to ensure that the total moment required is reached: firstly selecting if the right, or left wheel side need to be actuated in accordance to the sign of the input moment; and then defining how much each wheel has to be braked facing the problem of braking pressure saturation limit.

To identify the wheel to be actuated, a selector based on the understeering and oversteering behaviour is adopted: when the vehicle is understeering, it goes to a greater trajectory than that set by the driver. To compensate the error on

the trajectory and linearise the vehicle behaviour to the pilot's input, a braking force must be applied on the inner rear wheel. On the other hand, when the vehicle is oversteering, to compensate the development of the vehicle on a lower trajectory the outer front wheel must be braked (5.40), (5.41), (5.42) and (5.43). In these equations, the M_{bij} symbols represent the brake moment, where index $i \in \{f, r\}$ indicates front or rear wheel, while $j \in \{l, r\}$ indicates left or right wheel, respectively.

$$M_{bfl} = \begin{cases} 0, & right\ \ turn\ \ and\ \ understeering \\ \frac{|M_{yaw}|R_{wf}}{\frac{t_f}{2}\cos\delta}, & right\ \ turn\ \ and\ \ oversteering \end{cases} \tag{5.40}$$

$$M_{brr} = \begin{cases} \frac{|M_{yaw}|R_{wr}}{\frac{t_r}{2}}, & right\ \ turn\ \ and\ \ understeering \\ 0, & right\ \ turn\ \ and\ \ oversteering \end{cases} \tag{5.41}$$

$$M_{bfr} = \begin{cases} \frac{|M_{yaw}|R_{wf}}{\frac{t_f}{2}\cos\delta}, & left\ \ turn\ \ and\ \ oversteering \\ 0, & left\ \ turn\ \ and\ \ understeering \end{cases} \tag{5.42}$$

$$M_{brl} = \begin{cases} 0, & left\ \ turn\ \ and\ \ oversteering \\ \frac{|M_{yaw}|R_{wf}}{\frac{t_r}{2}}, & left\ \ turn\ \ and\ \ understeering \end{cases} \tag{5.43}$$

Thus, it is possible to reduce the lateral slip by adding a longitudinal slip component.

From the torques found, through the rotational balance (5.45) the braking pressure delivered to each wheel P_{bij} are defined (5.44).

$$P_{bij} = \frac{M_{bij}}{(A_c \mu R_{wi})} \tag{5.44}$$

$$I_{\omega ij}\dot{\omega}_i j = -M_{bij} - F_{xij}R_{wi} \tag{5.45}$$

The BBW system saturates the brake calliper pressures to a maximum of $100bar$.

This constraint could limit the braking force of the wheel not ensuring to achieve the moment requested. For this reason, a logic that redistributes the pressure on the wheels is developed, consisting of the following steps:

1. Checking if the wheel reaches the saturation limit;
2. Definition of the pressure quantity by which the saturation limit is exceeded;
3. Subtraction of this quantity from the wheel of the other side, ensuring the allocation of the control yaw moment.

Moore-Penrose pseudo-inverse

The optimal allocation strategy proposed here is based on the Moore-Penrose pseudo-inverse [85]. We would like to accomplish two different tasks: (1) ensure a desired stable lateral behaviour of the vehicle and (2) produce a minimum correction moment, which must be also in accordance with the driver intent and the actuators constraints.

This low-level controller is parametrized in order to be easily applied on different traction architectures. This ensures portability and flexibility of the whole proposed strategy, allowing the application of advanced TV techniques, regardless of vehicle layout.

The followed approach appear efficient, since minimize the norm 2 of the functional cost (5.46), which attempt to stabilize the vehicle lateral behaviour, while minimizing the correction efforts.

$$||T_{\text{cmd-k}} - T_{\text{cmd-k}} * ||_2 = (\sum_{k=1}^{n=4}(T_{\text{cmd-k}} - T_{\text{cmd-k}}{}^*)^2)^{1/2} \tag{5.46}$$

where $k \in \{fl, fr, rl, rr\}$ indicate the wheel (front left, front right, rear left, rear right), y_{k} is the half-track of the corresponding wheel, R_{w} the tire radius, $\text{T}_{\text{cmd-k}}$ and $\text{T}_{\text{cmd-k}}{}^*$ are the torques requested by the driver and by the ESC controller, respectively.

The reference wheel torques is given by (5.47).

$$\begin{bmatrix} \frac{-y_{\text{fl}}}{R_{\text{w}}} & \frac{y_{\text{fr}}}{R_{\text{w}}} & \frac{-y_{\text{rl}}}{R_{\text{w}}} & \frac{y_{\text{rr}}}{R_{\text{w}}} \\ 1 & 1 & 1 & 1 \end{bmatrix} \begin{bmatrix} T_{\text{cmd-fl}} - T_{\text{cmd-fl}}* \\ T_{\text{cmd-fr}} - T_{\text{cmd-fr}}* \\ T_{\text{cmd-rl}} - T_{\text{cmd-rl}}* \\ T_{\text{cmd-rr}} - T_{\text{cmd-rr}}* \end{bmatrix} = \begin{bmatrix} M_{\text{yaw}} \\ 0 \end{bmatrix} \tag{5.47}$$

As one can see, the first row correspond to the task (1), while the second row reflect the task (2). The resolution of (5.47) occur in four sequential steps. In each *k-th* step the value of $\text{T}_{\text{cmd-k}}{}^*$ is checked respect to its upper and lower constrain limits. If it exceeds them, is subsequently saturated at this value. At the *(k+1)-th* steps (5.47) is recalculated, excluding from the system the row related to the *k-th* torque reference, assumed equal to its own limitations.

The algorithm is parameterized respect to the wheels torque constrains, in order to ensure maximum flexibility and portability of the code respect to different vehicle architectures. This ensure that the requested torques are in accordance with the actuators limitations, allowing, in addition, the implementability of advanced torque vectoring techniques. Is the case of the benchmark vehicle investigated in this paper, in which positive and negative efforts could be delivered independently on each wheel, even of the same axis.

5.3.2 Test and results

To evaluate the stability performances allowed by the allocation torque controllers, the uncontrolled vehicle was made perform specific reference manoeuvres and the results obtained were compared with the ones of the vehicle equipped with the ESC, ABS, and *Brake pressure splitting logic*, and with ESC, ABS and *Moor-Penrose pseudo-inverse*. Simulation tests on the proposed vehicle model, implemented in the co-simulation environment of *MATLAB Simulink* and *VI Grade*, could be defined as *Lateral Stability tests*, executed to understand the impact of the ESC system on the vehicle lateral behaviour.

Lateral Stability Test

These simulations campaign are executed in order to asses the effect of the proposed ESC algorithm on lateral stability performances. The test executed is the Double Lane Change manoeuvre [107].

For this manoeuvre, tests are repeated increasing the reference speed, until the vehicle is able to correctly perform the trajectory, supposing availability and unavailability of the proposed controlling method. The improvement are evaluated

observing the maximum speed at which the vehicle executes the imposed steering manoeuvres without leaving the admitted zone and hitting the corners as shown in SubFigure 5.31a.

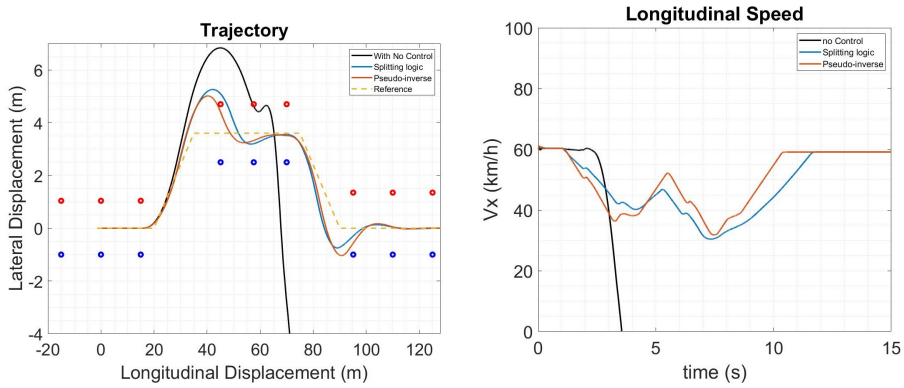

(a) Car trajectory.

(b) Car longitudinal speed.

Figure 5.31: Vehicle trajectory and longitudinal speed in a Double Lane Change manoeuvre, with a longitudinal speed of 60 km/h and a friction of 1, supposing availability and unavailability of the Electronic Stability Control systems.

This Figure shows how the vehicle equipped by the control combined with the pseudo-inverse allocation torque is able to perform the manoeuvre at 60 km/h. Instead, vehicle with ESC and the splitting logic as torque allocator is unable to fulfill test requirements at the same speed. In addition, in SubFigure 5.31b the comparison of the speed during the manoeuvre for the investigated use of cases, shows a lesser vehicle speed reduction in the second phase of the trajectory and a faster return to target speed, due to a better distribution of the vehicle torque values, visible in Figure 5.32. The braking pressure, shown in SubFigure 5.32a, are lower in some cases and the traction torques, shown in SubFigure 5.32b, are distributed on the four wheels.

The assumption to alternatively suppose availability and unavailability of the stability controller is done in order to comparatively asses the simulation outputs of the performed tests. In particular, the results of the tests in which the controller systems are disabled are assumed as a reference baseline for the metrical evaluation of the obtained improvements.

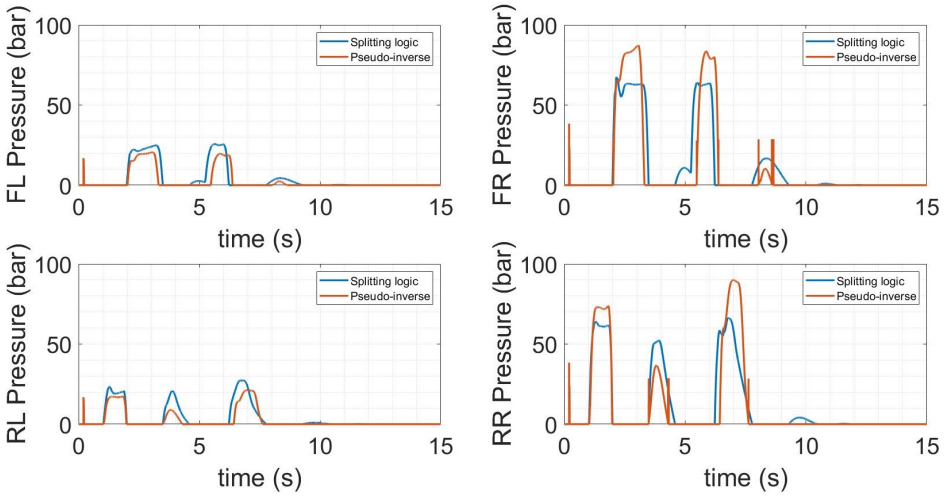

(a) Brake Pressures.

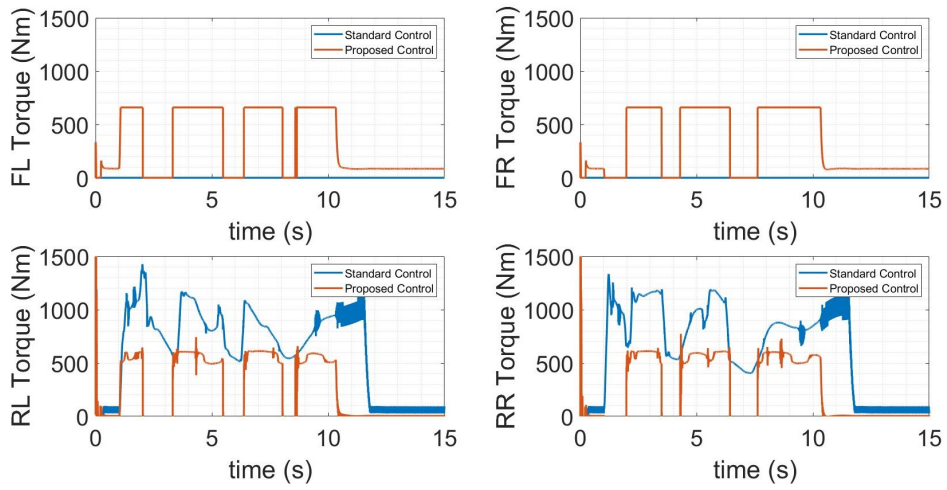

(b) Driving Moments.

Figure 5.32: Braking and driving torque vehicle inputs comparing Standard and Proposed architecture control performances.

5.3.3 Conclusion

Most interesting output of the performed tests campaign concern the dynamical vehicle behaviour improvements allowed by the proposed controllers, both respect to longitudinal and lateral stability.

For the lateral stability, we investigate the performance improvements by observing the result of Double Lane Change. Concerning the Double Lane Change, it can be stated that, looking at the outputs of Figure 5.31a and Table 5.8, the ESC with Moore-Penrose pseudo-inverse strategy can ensure a stable lateral behaviour of the vehicle, by increasing the speed at which the reference trajectory could be executed.

Table 5.8: Maximum vehicle speed during Double Lane Change tests for different adherence conditions

Double-Lane Change		
Adherence	**Configurations**	**Max-speed (km/h)**
1	Splitting	50
	MPp	60
	Passive	40
0.7	Splitting	40
	MPp	45
	Passive	30
0.5	Splitting	30
	MPp	35
	Passive	30

Figure 5.31b and Figure 5.32 show how the Moon-Penrose pseudoinverse torque allocation strategy is able of ensuring desired yaw moment, calculated from the LQR controller implemented in the ESC, integrated with the pedal and steer driver demands. In this way, it's possible to provide stability, safety and passengers comfort.

Summarizing, we can conclude by saying that, in this work, the proposed longitudinal stability controllers are correctly integrated with the lateral stability controller based on tracking LQR and Moore-Penrose torque allocation strategy, in order to accomplish enhanced stability behaviours of the IWM driven vehicle,if compared with conventional activate safety controllers.

In addition, can be said that the proposed lateral stability controller with yaw rate and side slip angle tracking, is correctly integrate with the Moore-Penrose torque allocation strategy, in order to accomplish enhanced stability behaviours of the in wheel actuated vehicle, if compared with a splitting logic activation safety controller.

5.4 Case study application

In this Section, the longitudinal, lateral and torque allocation control algorithms previously shown are integrated together and implemented with the Trajectory Tracking layer to evaluate their beneficial to the case of study autonomous race-car application.

The tests done are off-line simulations, made using the co-simulation environment of Matlab-Simulink and Vi-Grade CRT. The results in terms of lap time shown in Table 5.9 underline a reduction of 0.2 s obtained by the self-driven car with the stability control systems compared with the one without it.

Table 5.9: Case of study results in lap time with and without stability control layer

Lap Time	
Without Stability control layer	151.0 (s)
With Stability control layer	150.8 (s)

This performance improvement is confirmed by Figure 5.33 where one can see

how in some cases the speed and the accelerations of the vehicle with the longitudinal and lateral stability systems can reach higher values compared with the the vehicle not equipped with this additional controls.

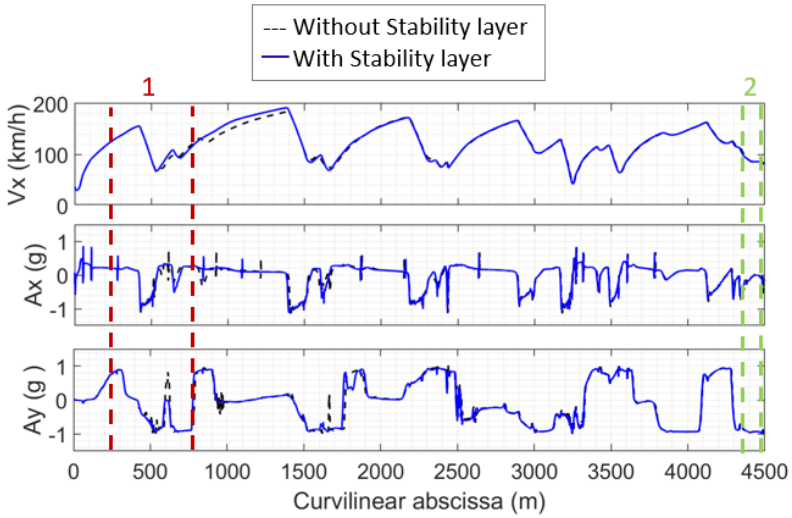

Figure 5.33: Race track comparison between stability controlled and no-controlled vehicle: car speed and accelerations performances.

In particular, in the highlighted sections, 1 and 2, the benefits given by the stability system are greater. In the Figure 5.34, the longitudinal and lateral acceleration of the passive and stability controlled vehicle as function of the path made in section one, together with the braking intensity requested by the longitudinal stability control system are shown, and one can see that by avoiding the wheel locking the ABS improves the stability and allows to start accelerating earlier achieving lower lateral acceleration.

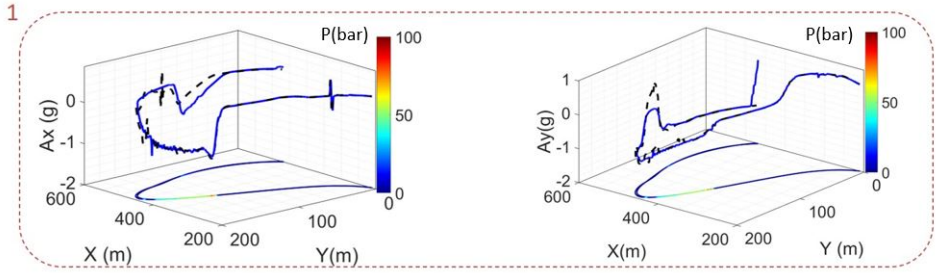

Figure 5.34: Race track comparison between stability controlled and not vehicle: longitudinal stability performances evaluation.

Instead, in the track section 2, the lateral stability control contribution can be evaluated. In the upper part of Figure 5.35, the side slip angle and yaw rate as function of the path are shown in the passive and controlled configurations; and one can see that the side slip angle of the controlled vehicle achieved lower values

than the one of the vehicle without lateral stability system, and the yaw rate shows a smoother behaviour. These characteristics allow to linearise the car responses to the Trajectory Tracking inputs, as it shown in the lower part of Figure 5.35 where lateral acceleration and yaw rate as function of the SWA in the path selected are given. In particular, at the end of the path travelled the car doesn't response to the Trajectory Tracking steering input loosing time and reducing safety.

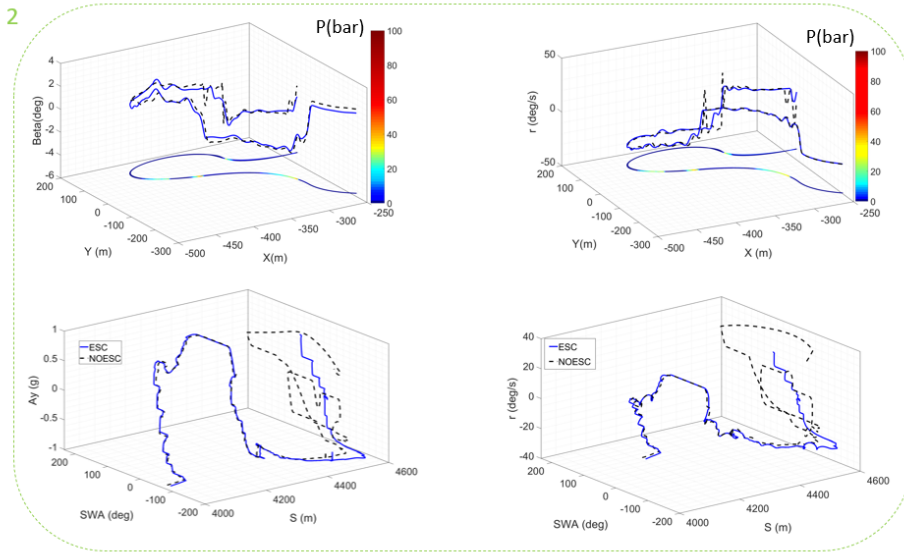

Figure 5.35: Race track comparison between stability controlled and not vehicle: lateral stability performances evaluation.

Chapter 6

Layers integration

In this Chapter, the last work phase is analysed showing the results obtained in terms of performances comparing it with the one obtained by a professional driver. It has involved the integration of the entire architecture developed evaluating the integrations pro and cons. In fact, during the integration step an in depth study and algorithm development was necessary to maintain the same performance that each layer reach independently. Especially, was important to evaluate how the errors made by the single layer have an influence on the good functionality of the entire system.

The real-time test campaign was done to the Meccanica 42 srl static simulator shown in Figure 1.5, with the same setting used by the human driver.

In this case, the Calabogie race track used was no longer flat, as in the off-line test campaign, but its inclination angles are considered, being modelled as in Figure 6.1. Here, positive and negative vertical coordinates along the path are highlighted in meters.

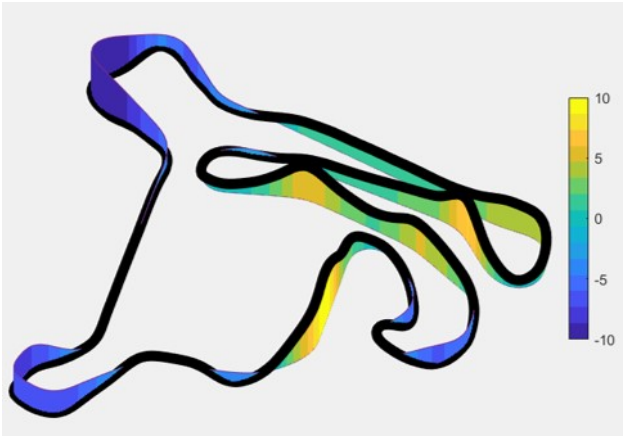

Figure 6.1: Calabogie race-track 3D-model used in simulator test campaign.

6.1 Interface between layers

As said, to ensure a correct integration between the different layers, was being necessary to develop algorithms that permits a correct interface between the control layer, so as to get as close as possible to the performance achieved by the individual logics and to their optimum operation.

6.1.1 Integrals reset

Starting with the State Estimator, how measurements are provided through integration of sensor data signals needs to be explained in more detail.

The State Estimator and Localization developed and shown in Chapter 3, composed by the combination of RNN and UKF, has as inputs measure the signal of the car yaw angle. This signal is obtained by integrated the yaw rate provided by the IMU sensor. As it known, a noisy signal integration as time progresses implies a drift in the estimated value. So, a reset of the integral must be made, taking another signal as reference.

For this intent, the camera measure of its inclination respect the line and the knowledge of the track line position in the world coordinates system are used. In fact, simply subtracting the angle given by the camera to the mid-line tangent of the track for each path segmentation (identified thanks to the position of the vehicle step by step) allows to have a measure of the yaw angle of the car, as show in the Equation 6.1 and Figure 6.2.

$$\theta = \rho - \gamma \tag{6.1}$$

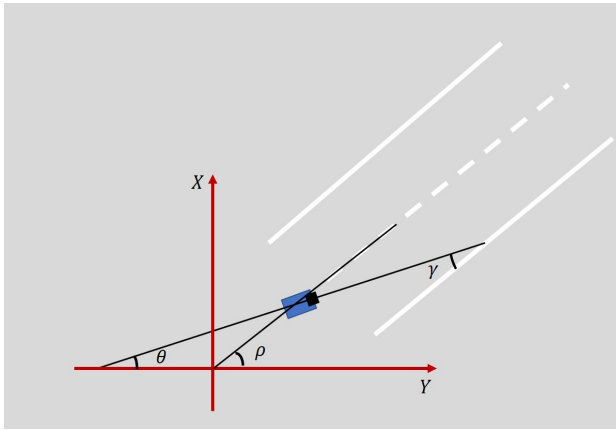

Figure 6.2: Estimation of the car yaw angle by camera sensor measure.

Where with θ, ρ and γ are indicated respectively the yaw angle of the car, the mid-line inclination respect the global coordinate system, and the inclination of the camera respect to the track line.

In addition, to ensure the correctness of the reset value, the integral is only reset when the car is driving on a straight line, i.e. the steering angle is zero, and when the side slip angle is approximately zero, so that the direction of the vehicle speed is directed according to its mean line.

6.1.2 Planned performance maintenance

In this Section, the algorithm developed to allow an efficient interface between the Path Planning and Path Tracking was explained in more details.

Because of the different sample time and independent logic that these two systems have, some consideration need to be made:

- The Path Planning gives as outputs the longitudinal and lateral positions, speeds and accelerations of the car for the following 120 time steps with a sample time of 0.1 s, achieving as inputs the current car positions and speeds respect to the global frame;
- The Path Tracking receives as inputs the next step positions, speeds and accelerations with a sample time of 0.001 s; so, the input values arrived from the Path Planning are the same for the one hundred steps immediately after.

Thus, it was needed something that ensures that the Path Tracking receives the vehicle dynamics behaviour for the steps in which the Path Planning provides constant value due to its sample time. So, considering the car as a point mass vehicle model the speeds and the positions of the car are estimated as follows:

$$\begin{aligned} V_x &= V_{x0} + Dt * Ax_{opt}; \\ V_y &= V_{y0} + Dt * Ay_{opt}; \\ X &= X_0 + Dt * V_x; \\ Y &= Y_0 + Dt * V_y; \end{aligned} \tag{6.2}$$

where V_x, V_y, X, and Y are the longitudinal and lateral car speeds and positions that are provided to the Path Tracking to define the car input commands; V_{x0}, V_{y0}, X_0, and Y_0 are the previous time step target speeds and positions; Dt is the sample time of 0.001 s; and A_{xopt}, and A_{yopt} are the longitudinal and lateral accelerations given by the Path Planning and maintained constant for 0.1 s.

However, it is not sure that this logic gives the correct positions and speeds when the optimization provides its new step values, with the possibility of achieving speeds value too low or too high for the conditions in which the car is. For this reason, a check that the difference of the values calculated by this logic and by the planner is maintained under 0.5 m/s is made at each step. This threshold value was defined by a tuning process and was used as limit above which the next speeds are calculated as the 10% reduction of the difference between the speed given by the planner and the one calculated by the integration algorithm as shown in Equations 6.3.

$$\begin{aligned} V_x &= V_{x0} - (V_{x0} - V_{xopt0}) * 0.1; \\ V_y &= V_{y0} - (V_{y0} - V_{yopt0}) * 0.1; \\ X &= X_0 + Dt * V_x; \\ Y &= Y_0 + Dt * V_y; \end{aligned} \tag{6.3}$$

This additional algorithm, where V_{xopt0}, and V_{yopt0} are the longitudinal and lateral speeds optimized by the planner, allowed to reduce the control noise that the

different sampling times between the two systems were created at the control action (steer, accelerator and brake signals), making possible to improve the operation of both logics and increase vehicle performance. In Figure 6.3, the longitudinal and lateral global speeds optimized by the Path Planning and the ones calculated by this integration logic to be given as inputs to the Path Tracking are shown together with their absolute difference. One can see how the differences between the two speeds remain under the threshold value of 5 m/s, and by the zoom that the this logic ensures to have a continuous speeds signal respect the Path Planning outputs.

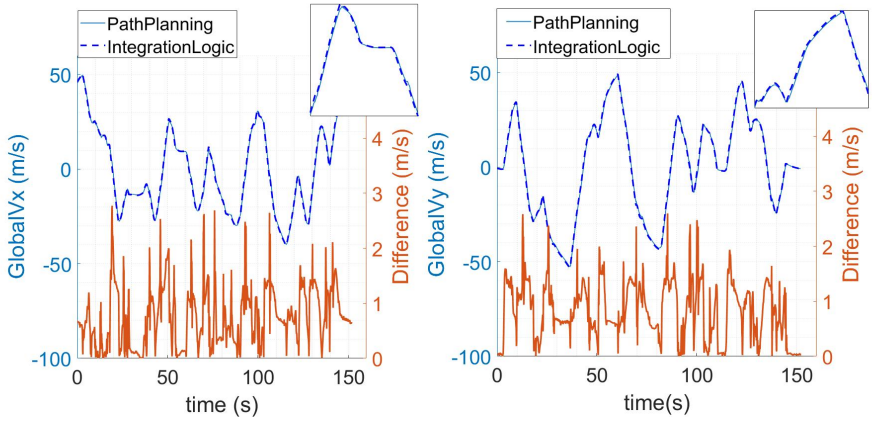

Figure 6.3: Longitudinal and lateral global speeds output from the Path Planner layer and input to the Path Tracking after being modified by the integration algorithm.

6.1.3 Bank angle compensation

If in the off-line tests campaign, the race track is considered flat, in the real-time tests performed to the static simulator, the 3-D model of the Calabogie map, with a mesh grid of $1m$ x $1m$, is used to evaluated the real car performance (other details related to the road data cannot be disclosed for confidentiality reasons).

Due to the selected race layout, the track longitudinal inclination have a great influence on the vehicle dynamics, compromising the optimum performance calculation. In addition, the longitudinal and lateral weight transfers due to the car accelerations have an influence on the vehicle dynamics that can't be neglected.

For these two reasons, a logic that estimate and constraints the car GG-V as function of the pitch and roll of the car is implemented. This was made possible thanks to the way of how the Path Planning work: in fact the constraints equation are link to the track segmentation, making possible to change constraints values depending on where the car is on the path. So, once estimated the pitch and roll of the car as shown in Equation 6.4, where F_{zij} are the normal tyre force calculated as in Equation 6.5, C_p and C_r are tuning scaling coefficients, their values can be considered in the trajectory optimization process.

$$pitch = \frac{mean(F_{zrl} + F_{zrr}) - mean(F_{zfl} + F_{zfr})}{C_p}$$
$$roll = \frac{mean(F_{zrl} + F_{zfl}) - mean(F_{zrr} + F_{zfr})}{C_r} \tag{6.4}$$

$$F_{zij} = \frac{mga_i}{2L} \pm \frac{a_y m h_{cog} a_r}{L t_i} \pm \frac{a_x m h_{cog}}{L} - \frac{{v_x}^2 \rho c_x S}{4} \tag{6.5}$$

Instead to consider the contribution of the race track inclination on the vehicle dynamics, the car pitch and roll every step are calculated using the known 3-D map of the track and providing their values linked to the position of the car in the path.

These values are given to the optimization layer, where are integrated consider that they reduced, or increase the admitted acceleration by the logic shown in Figure 6.4 and Equations 6.6.

$$A_{Xg} = Gsin\phi$$
$$A_{Yg} = -Gsin\theta \tag{6.6}$$

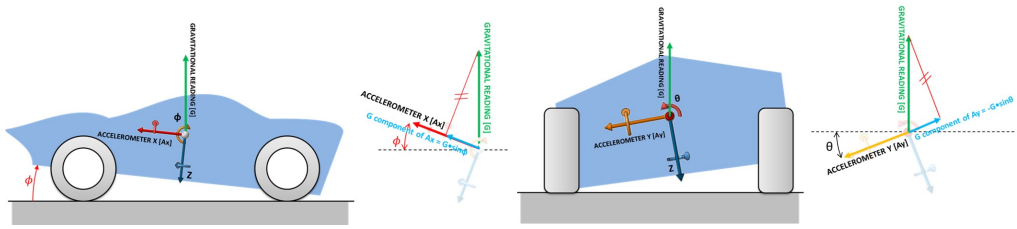

(a) Pitch acceleration component. (b) Roll acceleration component.

Figure 6.4: Additional longitudinal and lateral acceleration components given by the pith and roll angle of the car.

In this way, the performance of the car are improved reducing the time lap.

6.2 Comparison with driver

Thus, considering the additional logic explained in the previous Sections, the entire architecture was integrated together and an evaluation of its performances was made. This is done comparing its results in a flying Calabogie lap and the one obtained by the solely Trajectory Tracking and by a professional driver with the same vehicle and map models.

In Table 6.1 the lap time achieved by the three configurations tested are shown. As said in Chapter 4 the Trajectory Tracking is able to replicate the same performances of the driver. But, the integration of the other layers leads to a worsening of performance, reducing the lap time of about 7 s.

Demonstrating in Chapter 5 that the Stability Control Systems benefit dynamic performance by increasing stability, most of the responsibility for performance reductions lies with the State Estimator.

Table 6.1: Lap time achieved by the full architecture, Trajectory Tracking and driver.

Lap Time	
Driver	150.5 (s)
Trajectory Tracking	150.7 (s)
Trajectory Tracking + State Estimator + Stability Control	157.6 (s)

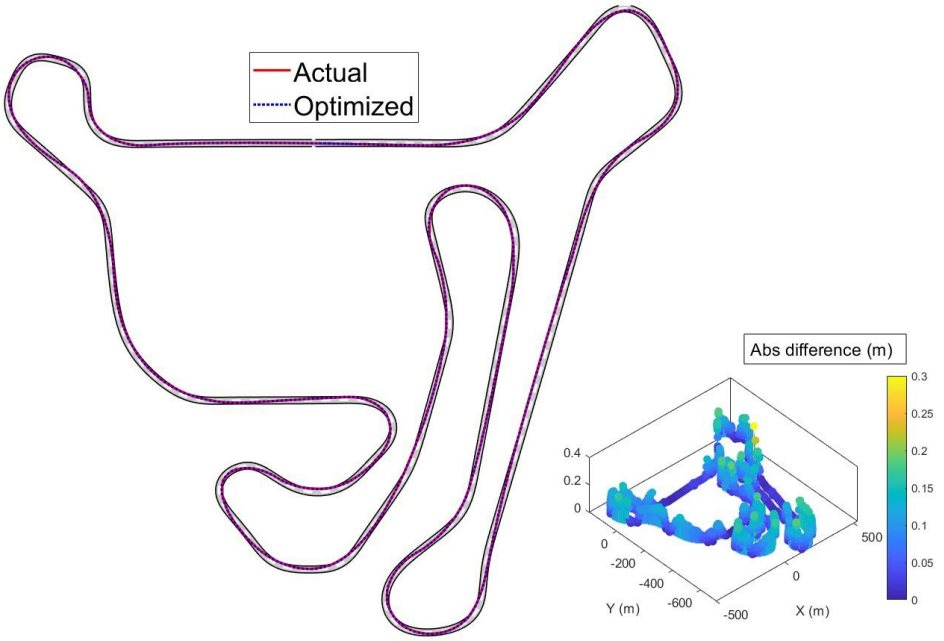

Figure 6.5: Trajectory output from the Path Planner layer and the actual car one.

Furthermore, shown in Figure 6.5 is the consistency between the trajectory optimized by the Trajectory Planner in the first prediction step, and the actual trajectory taken by the car. As one can see, the absolute difference between the normal distances of the corresponding points is very low in the straight sections and increases in the curves, remaining below the value of 0.3 m. Also these errors suggests that the problem lies with the State Estimator. Since as seen in Chapter 3, in the curves the error committed in the estimation of the lateral velocity may have too high spikes. In fact, as it shown on Figure 6.6, even if reduced respect standard speed estimators, the errors made in the side slip angle estimation, during the layer integration, need to be reduced, or being less noisy.

This results in performance deterioration of the trajectory controller which does not ensure that the target states are followed. On the other hand, the integration logic seems to ensure proper consistency between the trajectory optimised by the planner and the one taken as target by the trajectory tracking, even if a more detailed study of the logic to be used could result in a mismatches reduction.

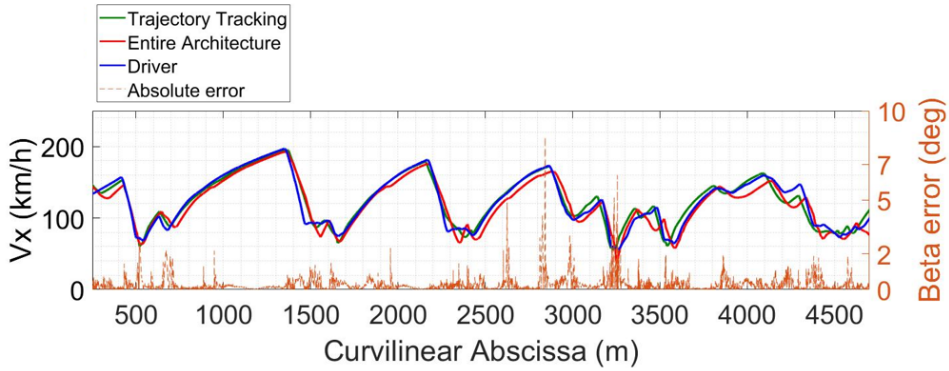

Figure 6.6: Best speed profile obtained by the entire architecture compared with the one of the driver and of the only implementation of the Trajectory Tracking, together with the side slip angle estimation absolute errors.

However, the actual trajectory made by the car ensures good results compared with the actual results obtained by the state of the art.

By the speed profile shown in Figure 6.6, it possible to see that if the Trajectory Tracking have the same acceleration performance, even higher near 3500 m of the path, the architecture have almost always a less acceleration reducing its lap time. Instead, about the decelerations, the architecture replicates the ones of the Trajectory Tracking, that are lower than the driver ones. The inability of the system to achieve the same levels of deceleration of the driver lies in the braking input oscillations shown in Figure 4.9. As mentioned in Chapter 4, the gain used by the trajectory control are necessary to track the correct acceleration but are probably too high to deceleration. Here, small oscillations appeared in the braking state error were amplified. The difference in the performances are shown also in the trajectories comparison given by Figure 6.7. Here, the driver and the tracker of trajectories are almost similar, as seen in Chapter 4, with some discrepancies: in curve 2 the Trajectory Tracking made a larger trajectory which led to a lower speed during deceleration and a slight anticipation of the subsequent acceleration with a higher speed.

Instead, the entire architecture have some discrepancies in all the curves highlighted in the Figure 6.7 with the other two configurations. The planner and the driver kept a trajectory close to the inner kerb reducing the road travelled and increasing the longitudinal speed. In the sections shown, the entire algorithm was not able to face the curve with the right trajectory driving too wide, even going off track in some points. Tests have shown that at these points, the algorithm believes it has a higher lateral speed when approaching the curve than it actually does, and in order to stay within the limits imposed by the GG, it decides to take a wider trajectory than initially calculated. Finding itself then constrained to remain with a certain margin within the track, it results in trajectories with a tighter radius of curvature, reducing speed and increasing lap time. In fact, in general, the trajectory made by the proposed system with respect to the driver and solely tracking layer is wider in all curves, not allowing the car to reach the speeds reached in the other configurations.

However, in the Figures 6.8 where the GG-Vs made by the driver, SubFigure

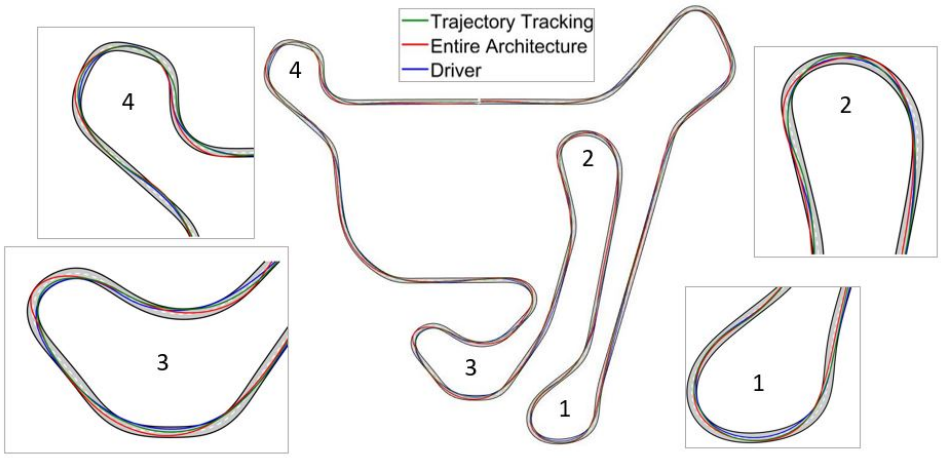

Figure 6.7: Best trajectory obtained by the entire architecture compared with the one of the driver and of the only implementation of the Trajectory Tracking.

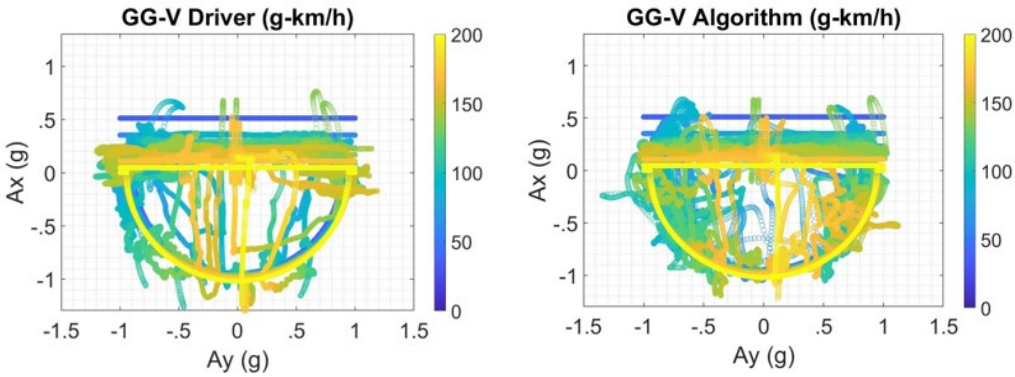

(a) Driver GG-V.

(b) Architecture GG-V.

Figure 6.8: GG-V performances obtained by the entire architecture and driver.

6.8a, and by the entire architecture, SubFigure 6.8b, together with the GG-V constraints implemented in the Path Planning are shown, it is underlined that the vehicle dynamics constraints and performance are repeated most of the times, even if the proposed algorithm shows more transitory behaviour than the driver that drives more at the constraints limits.

6.3 Conclusion

Thus, in this Section the integration of each layer developed and explained in the previous Chapters is shown together with the results obtained in term of lap time performance in a real-time static simulator implementation. Integration has involved the development of some interfacing algorithms to aim at increasing the performance of each individual layer once it has to deal with the performance of other systems.

In order to establish the correct functioning of the proposed architecture, the results obtained were compared with those of a professional driver. From the analysis of these results it was possible to see how the interaction of the various estimation, optimisation and control systems allows a sports car to complete laps of the Calabogie race track autonomously, guaranteeing the on-line operation of all the systems and their proper functioning. However, at the moment, compared to the performance obtained by the driver, there is a deterioration of 7 seconds on the lap time, probably due to a speed estimation which is noisy and not very robust leading in some conditions to an incorrect localization of the vehicle within the track.

Chapter 7

Conclusion

In this PhD study an autonomous driving control architecture was developed to allow a sportive car to drive independently on the Calabogie race track. Because of the constraints imposed by the perception system, the focuses of this research were to improve the current state of functioning of: a Dynamic States Estimator and Vehicle Localization; a Trajectory Planning and Tracking; and Stability Systems. So, the problem is reduced from a dynamic urban area scenario to a static race one.

Thus, the work has involved the development of each single layer independently, after an in-depth study of the state of the art and considering the aim constraints. Then, the systems were integrated and the control architecture functionality was tested.

About the State Estimator and Vehicle Localization layer, it had the aim of improve the actual state estimators functioning. This improvement was necessary in order to guarantee the correct functioning of the following layers, without increasing the cost and using the current available car sensor technologies. At the beginning a state observer based on the UKF algorithm was developed using a double-track vehicle model to predict longitudinal and lateral speeds of the car. Then, due to its estimation errors a RNN was added to work as an additional input measure and reset the UKF integration errors given to high non-linear and unknown dynamic model. This RNN was trained to estimate longitudinal and lateral vehicle speed starting from IMU vehicle accelerations and yaw rate, SWA, and wheel speeds knowledge. In order to avoid long times and high costs of training, the network was trained on a set of predefined manoeuvres trying to cover all the use of case vehicle dynamics. The statistical analysis of the estimation results obtained by the mixed configuration and the only UKF showed that the approach developed ensures to increase the car speed estimation capability, allowing a more robust estimation in front of dynamic condition changes. In this way, it was possible to estimate the car speeds ensuring to not improve the dynamic model of the UKF avoiding a additional time consuming, and reduce the tuning time and costs given by a in-depth training of the RNN.

About the Trajectory Tracking, it was divided into Path Planning and Path Tracking layer both developed to work on-line while the car is running. This ensured real-time optimization of the trajectory taking into account the current dynamic conditions of the car, which are usually not considered in favour of a more accurate modelling of the vehicle dynamics. However, this implies an increase of the calculation time by providing off-line optimization of the trajectory. The

Path Planning uses the point mass model to define the acceleration outputs which ensure the faster trajectory permitted by the speed dependent GG-V limits. These constraints are established by off-line simulations campaign on CRT. The sample time that allows a correct and efficient optimization of the performances with the algorithm implemented was found to be 0.1 s. By the tests made, the Path Planning was shown able to respect this computational cost both in a off-line implementation that in an on-line one with the hardware characteristics shown in Table 1.1. The Path Tracking is based on a LQR with feed-back and feed-forward control actions, where the longitudinal and lateral vehicle dynamics are considered not influencing each other. This controller ensure to consider a more complex vehicle model and a lower sample time, 0.001 s, achieving a more accurate vehicle dynamic control through the steering, accelerator and braking inputs definition as a driver model. The off-line co-simulation tests showed that this Trajectory Tracking improves the car performances respect a standard off-line motion planning reducing the lap time of almost 1 s, and achieves the performance of a professional driver. This configuration allows to open the way to obstacle avoidance implementation, being able to optimize and track the trajectory considering on-line car performances and conditions.

About the Stability Control Systems, a longitudinal and lateral dynamics controller were developed aiming at an improvement of the current standard technologies. The longitudinal stability control composed of EBD, CBC and ABS have involved the development of three different ABS types: two based on the current logics used, and one that tries to overcome the issues of the other ones. The last longitudinal stability control developed has focused to not used longitudinal slip estimation or wheel acceleration derivative because they bring to inaccuracies and less efficient braking effort. In fact, ensuring that each wheel tracks a target speed (the one that allows the 10% of tire slip) lead to a continuous and smooth braking pressures with consequent higher deceleration level. This ABS was possible using the CBA system developed by Meccanica 42 srl which allows to control each wheel independently and with less actuation delay. Passing to the lateral stability control, it aims at increasing passengers safety and vehicle dynamics by tracking the yaw rate and side slip angle given by a steady state single track target vehicle model. Usually, the common ESC systems used TV actuation to track the yaw rate and minimize the side slip angle. Instead, ensuring a reference values of both yaw rate and side slip angle has ensured to control the car in a more efficient way, as was resulted both in subjective that in objective tests made with Human in the Loop interface. In addition, a test campaign to evaluate which is the best strategies to allocate the braking pressure to the four wheels was done. Two strategies were compared: a so called Splitting Logic, that defines which pressure each wheels must provide to achieve the total yaw moment requested by considering the ESC yaw moment sign and the wheels saturation limits; and a Moore-Penrose pseudo-inverse logic that calculates the wheels braking pressure by solving an optimization problem by considering not only the ESC requested moment but also the driver inputs and the actuators constraints. The results obtained in Double Lane Change tests showed how the second strategy ensured to do the manoeuvres with higher speed not reducing the requirements of the driver during the manoeuvre. For this reason, it was decide to implement the Stability Control Systems with: the tracking LQR lateral stability control, the Moore-Penrose pseudo-inverse torque allocation strategy, and the discrete PID ABS.

At this point, all the layers are integrated together implementing some logic strategies to ensure a good interface integration between the systems involved. Then, the architecture was compiled to run in the real-time static simulator placed at Meccanica 42 srl and its performance compared with the one obtained by a professional driver with the same test set-up. The results showed that the architecture is able to allow the car to drive in autonomous the race track in a safety way. However, respect to the driver, the lap time is increased by about 7 s due to a still noisy and not reliable estimation of the vehicle speeds. Anyway, the results obtained were satisfactory from the point of view of the increase in performance achieved compared to the state of the art and the possibility of opening the way to future developments to make autonomous driving more realistic.

So, the next steps involved: an improving of the integration tuning of the layer to ensure the good functionality of each one; a sensitivity analysis on the repeatability of results and on the influence that each layer have on the others; and a real car implementation with dedicated hardware.

Bibliography

[1] 'Eu road safety policy framework 2021-2030 - next steps towards "vision zero"', European Commission Staff Working Document, Tech. Rep., 2019.

[2] 'Taxonomy and definitions for terms related to driving automation systems for on-road motor vehicles', SAE International, Tech. Rep., 2021.

[3] A. T. van Zanten and R. B. GmbH, 'Evolution of Electronic Control Systems for Improving the Vehicle Dynamic Behavior', vol. 2, p. 9, 2002.

[4] A. van Zanten, R. Erhardt, K. Landesfeind and G. Pfaff, 'Vehicle Stabilization by the Vehicle Dynamics Control System ESP', *IFAC Proceedings Volumes*, vol. 33, pp. 95–102, 2000.

[5] T. Litman, 'Implications for Transport Planning', p. 46,

[6] H. Guo, D. Cao, H. Chen, C. Lv, H. Wang and S. Yang, 'Vehicle dynamic state estimation: State of the art schemes and perspectives', *IEEE/CAA Journal of Automatica Sinica*, vol. 5, no. 2, pp. 418–431, Mar. 2018, ISSN: 2329-9266, 2329-9274. DOI: 10.1109/JAS.2017.7510811.

[7] D. Chindamo, B. Lenzo and M. Gadola, 'On the Vehicle Sideslip Angle Estimation: A Literature Review of Methods, Models, and Innovations', *Applied Sciences*, vol. 8, no. 3, p. 355, Mar. 2018, ISSN: 2076-3417. DOI: 10.3390/app8030355.

[8] Weida Wang, Lijuan Yuan, Sheng Tao, Wei Zhang and Tianshu Su, 'Estimation of vehicle side slip angle in nonlinear condition based on the state feedback observer', in *2010 IEEE International Conference on Automation and Logistics*, Shatin, Hong Kong: IEEE, Aug. 2010, pp. 632–636, ISBN: 978-1-4244-8375-4. DOI: 10.1109/ICAL.2010.5585359.

[9] H. Grip, L. Imsland, T. A. Johansen, J. C. KalKkuhl and A. Suissa, 'Vehicle sideslip estimation', *IEEE Control Systems*, vol. 29, no. 5, pp. 36–52, Oct. 2009, ISSN: 1066-033X, 1941-000X. DOI: 10.1109/MCS.2009.934083.

[10] H. Shraim, M. Ouladsine, L. Fridman and M. Romero, 'Vehicle parameter estimation and stability enhancement using sliding modes techniques', *International Journal of Vehicle Design*, vol. 48, no. 3/4, p. 230, 2008, ISSN: 0143-3369, 1741-5314. DOI: 10.1504/IJVD.2008.022578.

[11] J. C. Cadiou, A. E. Hadri and F. Chikhi, 'Non-linear tyre forces estimation based on vehicle dynamics observation in a finite time', vol. 218, p. 14, 2004.

[12] H. Zhang, X. Huang, J. Wang and H. R. Karimi, 'Robust energy-to-peak sideslip angle estimation with applications to ground vehicles', *Mechatronics*, vol. 30, pp. 338–347, Sep. 2015, ISSN: 09574158. DOI: 10.1016/j.mechatronics.2014.08.003.

[13] S.-H. You, J.-O. Hahn and H. Lee, 'New adaptive approaches to real-time estimation of vehicle sideslip angle', *Control Engineering Practice*, vol. 17, no. 12, pp. 1367–1379, Dec. 2009, ISSN: 09670661. DOI: 10.1016/j.conengprac.2009.07.002.

[14] J. Ryu, E. J. Rossetter and J. C. Gerdes, 'Vehicle Sideslip and Roll Parameter Estimation using GPS', p. 8, 2002.

[15] M. Doumiati, A. Victorino, A. Charara and D. Lechner, 'A method to estimate the lateral tire force and the sideslip angle of a vehicle: Experimental validation', in *Proceedings of the 2010 American Control Conference*, Baltimore, MD: IEEE, Jun. 2010, pp. 6936–6942. DOI: 10.1109/ACC.2010.5531319.

[16] Y. Huang, C. Bao, J. Wu and Y. Ma, 'Estimation of Sideslip Angle Based on Extended Kalman Filter', *Journal of Electrical and Computer Engineering*, vol. 2017, pp. 1–9, 2017, ISSN: 2090-0147, 2090-0155. DOI: 10.1155/2017/5301602.

[17] L. Li, G. Jia, X. Ran, J. Song and K. Wu, 'A variable structure extended Kalman filter for vehicle sideslip angle estimation on a low friction road', *Vehicle System Dynamics*, vol. 52, no. 2, pp. 280–308, Feb. 2014, ISSN: 0042-3114, 1744-5159. DOI: 10.1080/00423114.2013.877148.

[18] G. Morrison and D. Cebon, 'Sideslip estimation for articulated heavy vehicles at the limits of adhesion', *Vehicle System Dynamics*, vol. 54, no. 11, pp. 1601–1628, Nov. 2016, ISSN: 0042-3114, 1744-5159. DOI: 10.1080/00423114.2016.1223326.

[19] S. Antonov, A. Fehn and A. Kugi, 'Unscented Kalman filter for vehicle state estimation', *Vehicle System Dynamics*, vol. 49, no. 9, pp. 1497–1520, Sep. 2011, ISSN: 0042-3114, 1744-5159. DOI: 10.1080/00423114.2010.527994.

[20] Q. Cui, R. Ding, B. Zhou and X. Wu, 'Path-tracking of an autonomous vehicle via model predictive control and nonlinear filtering', *Proceedings of the Institution of Mechanical Engineers, Part D: Journal of Automobile Engineering*, vol. 232, no. 9, pp. 1237–1252, Aug. 2018, ISSN: 0954-4070, 2041-2991. DOI: 10.1177/0954407017728199.

[21] G. Cybenkot, 'Approximation by superpositions of a sigmoidal function', *Mathematics of Control, Signals and Systems*, p. 12,

[22] H. Sasaki and T. Nishimaki, 'A Side-Slip Angle Estimation Using Neural Network for a Wheeled Vehicle', in *SAE 2000 World Congress*, Mar. 2000, pp. 2000-01–0695. DOI: 10.4271/2000-01-0695.

[23] S. Melzi, F. Resta and E. Sabbioni, 'Vehicle Sideslip Angle Estimation Through Neural Networks: Application to Numerical Data', in *Volume 2: Automotive Systems, Bioengineering and Biomedical Technology, Fluids Engineering, Maintenance Engineering and Non-Destructive Evaluation, and Nanotechnology*, Torino, Italy: ASMEDC, Jan. 2006, pp. 167–172, ISBN: 978-0-7918-4249-2. DOI: 10.1115/ESDA2006-95376.

[24] S. Srinivasan, I. Sa, A. Zyner, V. Reijgwart, M. I. Valls and R. Siegwart, 'End-to-End Velocity Estimation For Autonomous Racing', *arXiv:2003.06917 [cs]*, Aug. 2020. arXiv: 2003.06917 [cs].

[25] T. Novi, R. Capitani and C. Annicchiarico, 'An integrated ANN-UKF vehicle sideslip angle estimation based on IMU measurements', p. 13, 2016.

[26] N. Dal Bianco, E. Bertolazzi, F. Biral and M. Massaro, 'Comparison of direct and indirect methods for minimum lap time optimal control problems', *Vehicle System Dynamics*, vol. 57, no. 5, pp. 665–696, May 2019, ISSN: 0042-3114, 1744-5159. DOI: 10.1080/00423114.2018.1480048.

[27] M. Montani, L. Ronchi, R. Capitani and C. Annicchiarico, 'A Hierarchical Autonomous Driver for a Racing Car: Real-Time Planning and Tracking of the Trajectory', *Energies*, vol. 14, no. 19, p. 6008, Sep. 2021, ISSN: 1996-1073. DOI: 10.3390/en14196008.

[28] A. Liniger, 'Path Planning and Control for Autonomous Racing', PhD thesis, ETH Zurich, 2018, 136 p. DOI: 10.3929/ETHZ-B-000302942.

[29] A. Liniger, A. Domahidi and M. Morari, 'Optimization-based autonomous racing of 1:43 scale RC cars: OPTIMIZATION-BASED AUTONOMOUS RACING', *Optimal Control Applications and Methods*, vol. 36, no. 5, pp. 628–647, Sep. 2015, ISSN: 01432087. DOI: 10.1002/oca.2123.

[30] F. Christ, A. Wischnewski, A. Heilmeier and B. Lohmann, 'Time-optimal trajectory planning for a race car considering variable tyre-road friction coefficients', *Vehicle System Dynamics*, pp. 1–25, Dec. 2019, ISSN: 0042-3114, 1744-5159. DOI: 10.1080/00423114.2019.1704804.

[31] R. Verschueren, S. De Bruyne, M. Zanon, J. V. Frasch and M. Diehl, 'Towards time-optimal race car driving using nonlinear MPC in real-time', in *53rd IEEE Conference on Decision and Control*, Los Angeles, CA, USA: IEEE, Dec. 2014, pp. 2505–2510. DOI: 10.1109/CDC.2014.7039771.

[32] R. Verschueren, M. Zanon, R. Quirynen and M. Diehl, 'Time-optimal race car driving using an online exact hessian based nonlinear MPC algorithm', in *2016 European Control Conference (ECC)*, Aalborg, Denmark: IEEE, Jun. 2016, pp. 141–147, ISBN: 978-1-5090-2591-6. DOI: 10.1109/ECC.2016.7810277.

[33] B. Alrifaee and J. Maczijewski, 'Real-time Trajectory optimization for Autonomous Vehicle Racing using Sequential Linearization', in *2018 IEEE Intelligent Vehicles Symposium (IV)*, Changshu: IEEE, Jun. 2018, pp. 476–483, ISBN: 978-1-5386-4452-2. DOI: 10.1109/IVS.2018.8500634.

[34] A. Heilmeier, A. Wischnewski, L. Hermansdorfer, J. Betz, M. Lienkamp and B. Lohmann, 'Minimum curvature trajectory planning and control for an autonomous race car', *Vehicle System Dynamics*, pp. 1–31, Jun. 2019, ISSN: 0042-3114, 1744-5159. DOI: 10.1080/00423114.2019.1631455.

[35] R. Lot and N. Dal Bianco, 'The significance of high-order dynamics in lap time simulations', in *The Dynamics of Vehicles on Roads and Tracks*, CRC Press, 2016, pp. 561–570.

[36] P. A. Theodosis and J. C. Gerdes, 'Generating a Racing Line for an Autonomous Racecar Using Professional Driving Techniques', in *ASME 2011 Dynamic Systems and Control Conference and Bath/ASME Symposium on Fluid Power and Motion Control, Volume 2*, Arlington, Virginia, USA: ASMEDC, Jan. 2011, pp. 853–860, ISBN: 978-0-7918-5476-1. DOI: 10.1115/DSCC2011-6097.

[37] G. Perantoni and D. J. Limebeer, 'Optimal control for a Formula One car with variable parameters', *Vehicle System Dynamics*, vol. 52, no. 5, pp. 653–678, May 2014, ISSN: 0042-3114, 1744-5159. DOI: 10.1080/00423114.2014.889315.

[38] M. Gerdts, 'A moving horizon technique for the simulation of automobile test-drives', *ZAMM*, vol. 83, no. 3, pp. 147–162, Mar. 2003, ISSN: 00442267, 15214001. DOI: 10.1002/zamm.200310015.

[39] M. Gerdts, S. Karrenberg, B. Müller-Beßler and G. Stock, 'Generating locally optimal trajectories for an automatically driven car', *Optimization and Engineering*, vol. 10, no. 4, pp. 439–463, Dec. 2009, ISSN: 1389-4420, 1573-2924. DOI: 10.1007/s11081-008-9047-1.

[40] J. P. Timings and D. J. Cole, 'Minimum Maneuver Time Calculation Using Convex Optimization', *Journal of Dynamic Systems, Measurement, and Control*, vol. 135, no. 3, May 2013, ISSN: 0022-0434, 1528-9028. DOI: 10.1115/1.4023400.

[41] M. Montani, D. Vitaliti, R. Capitani and C. Annicchiarico, 'Performance Review of Three Car Integrated ABS Types: Development of a Tire Independent Wheel Speed Control', *Energies*, vol. 13, no. 23, p. 6183, Nov. 2020, ISSN: 1996-1073. DOI: 10.3390/en13236183.

[42] R. Bosch, *Automotive brake systems*. Robert Bentley, 1996.

[43] S. Yoneda, Y. Naitoh and H. Kigoshi, 'Rear Brake Lock-Up Control System of Mitsubishi Starion', in *SAE International Congress and Exposition*, Feb. 1983. DOI: 10.4271/830482.

[44] L. Yu, X. Liu, Z. Xie and Y. Chen, 'Review of Brake-by-Wire System Used in Modern Passenger Car', *International Design Engineering Technical Conferences and Computers and Information in Engineering Conference*, p. 11, 2016.

[45] D. Savitski, V. Ivanov, K. Augsburg, B. Shyrokau, R. Wragge-Morley, T. Pütz and P. Barber, 'The new paradigm of an anti-lock braking system for a full electric vehicle: Experimental investigation and benchmarking', *Proceedings of the Institution of Mechanical Engineers, Part D: Journal of Automobile Engineering*, vol. 230, no. 10, pp. 1364–1377, Sep. 2016, ISSN: 0954-4070, 2041-2991. DOI: 10.1177/0954407015608548.

[46] R. de Castro, R. E. Araújo, M. Tanelli, S. M. Savaresi and D. Freitas, 'Torque blending and wheel slip control in EVs with in-wheel motors', *Vehicle System Dynamics*, vol. 50, no. sup1, pp. 71–94, Jan. 2012, ISSN: 0042-3114, 1744-5159. DOI: 10.1080/00423114.2012.666357.

[47] S. De Pinto, C. Chatzikomis, A. Sorniotti and G. Mantriota, 'Comparison of Traction Controllers for Electric Vehicles With On-Board Drivetrains', *IEEE Transactions on Vehicular Technology*, vol. 66, no. 8, pp. 6715–6727, Aug. 2017, ISSN: 0018-9545, 1939-9359. DOI: 10.1109/TVT.2017.2664663.

[48] B. Moaveni and P. Barkhordari, 'Modeling, identification, and controller design for hydraulic anti-slip braking system', *Proceedings of the Institution of Mechanical Engineers, Part D: Journal of Automobile Engineering*, vol. 233, no. 4, pp. 862–876, Mar. 2019, ISSN: 0954-4070, 2041-2991. DOI: 10.1177/0954407018755611.

[49] J.-C. Wang and R. He, 'Hydraulic anti-lock braking control strategy of a vehicle based on a modified optimal sliding mode control method', *Proceedings of the Institution of Mechanical Engineers, Part D: Journal of Automobile Engineering*, vol. 233, no. 12, pp. 3185–3198, Oct. 2019, ISSN: 0954-4070, 2041-2991. DOI: 10.1177/0954407018820445.

[50] M. Moavenian, 'An adaptive modified fuzzy-sliding mode longitudinal control design and simulation for vehicles equipped with ABS system', p. 13,

[51] D. Tavernini, F. Vacca, M. Metzler, D. Savitski, V. Ivanov, P. Gruber, A. E. Hartavi, M. Dhaens and A. Sorniotti, 'An Explicit Nonlinear Model Predictive ABS Controller for Electro-Hydraulic Braking Systems', *IEEE Transactions on Industrial Electronics*, vol. 67, no. 5, pp. 3990–4001, May 2020, ISSN: 0278-0046, 1557-9948. DOI: 10.1109/TIE.2019.2916387.

[52] A. A. Aly, E.-S. Zeidan, A. Hamed and F. Salem, 'An Antilock-Braking Systems (ABS) Control: A Technical Review', *Intelligent Control and Automation*, vol. 02, no. 03, pp. 186–195, 2011, ISSN: 2153-0653, 2153-0661. DOI: 10.4236/ica.2011.23023.

[53] T. Johansen, I. Petersen, J. Kalkkuhl and J. Ludemann, 'Gain-scheduled wheel slip control in automotive brake systems', *IEEE Transactions on Control Systems Technology*, vol. 11, no. 6, pp. 799–811, Nov. 2003, ISSN: 1063-6536. DOI: 10.1109/TCST.2003.815607.

[54] M. Montani, R. Capitani and C. Annicchiarico, 'Development of a brake by wire system design for car stability controls', *Procedia Structural Integrity*, vol. 24, pp. 137–154, 2019, ISSN: 24523216. DOI: 10.1016/j.prostr.2020.02.013.

[55] M. Montani, R. Capitani, M. Fainello and C. Annicchiarico, 'Use of a driving simulator to develop a brake-by-wire system designed for electric vehicles and car stability controls', in *10th International Munich Chassis Symposium 2019*, P. E. Pfeffer, Ed., Wiesbaden: Springer Fachmedien Wiesbaden, 2020, pp. 663–684, ISBN: 978-3-658-26435-2.

[56] M. Nagai, 'The perspectives of research for enhancing active safety based on advanced control technology', *Vehicle System Dynamics*, vol. 45, no. 5, pp. 413–431, 2007. DOI: 10.1080/00423110701275162. eprint: https://doi.org/10.1080/00423110701275162.

[57] D. Frede, M. Khodabakhshian and D. Malmquist, 'A state-of-the-art survey on vehicular mechatronics focusing on by-wire systems.', p. 67,

[58] N. Navet, F. Simonot-Lion, Y. Qiong Song and C. Wilwert, 'Design of Automotive X-by-Wire Systems', in *The Industrial Communication Technology Handbook*. CRC Press, Feb. 2005, vol. 20050668, pp. 29-1-29–19. DOI: 10.1201/9781420037821.ch29.

[59] D. Gonzalez, J. Perez, V. Milanes and F. Nashashibi, 'A Review of Motion Planning Techniques for Automated Vehicles', *IEEE Transactions on Intelligent Transportation Systems*, vol. 17, no. 4, pp. 1135–1145, Apr. 2016, ISSN: 1524-9050, 1558-0016. DOI: 10.1109/TITS.2015.2498841.

[60] H. Winner, S. Hakuli, F. Lotz and C. Singer, Eds., *Handbook of Driver Assistance Systems*. Cham: Springer International Publishing, 2016. DOI: 10.1007/978-3-319-12352-3.

[61] A. Mangia, B. Lenzo and E. Sabbioni, 'An integrated torque-vectoring control framework for electric vehicles featuring multiple handling and energy-efficiency modes selectable by the driver', *Meccanica*, vol. 56, no. 5, pp. 991–1010, May 2021, ISSN: 0025-6455, 1572-9648. DOI: 10.1007/s11012-021-01317-3.

[62] Ko Sung-Yeon, Ko Ji-Weon, Lee Sang-Moon, Cheon Jea-Seung and Kim Hyunsoo, 'A Study on In-Wheel Motor Control to Improve Vehicle Stability Using Human-in-the-Loop Simulation', *Journal of Power Electronics*, vol. 13, no. 4, pp. 536–45, 2013.

[63] B. Jin, C. Sun and X. Zhang, 'RESEARCH ON LATERAL STABILITY OF FOUR HUBMOTOR- IN-WHEELS DRIVE ELECTRIC VEHICLE', *International Journal on Smart Sensing and Intelligent Systems*, vol. 8, no. 3, pp. 1855–1875, 2015, ISSN: 1178-5608. DOI: 10.21307/ijssis-2017-833.

[64] M. Jalali, S. Khosravani, A. Khajepour, S.-k. Chen and B. Litkouhi, 'Model predictive control of vehicle stability using coordinated active steering and differential brakes', *Mechatronics*, vol. 48, pp. 30–41, Dec. 2017, ISSN: 09574158. DOI: 10.1016/j.mechatronics.2017.10.003.

[65] P. Falcone, H. Eric Tseng, F. Borrelli, J. Asgari and D. Hrovat, 'MPC-based yaw and lateral stabilisation via active front steering and braking', *Vehicle System Dynamics*, vol. 46, no. sup1, pp. 611–628, Sep. 2008, ISSN: 0042-3114. DOI: 10.1080/00423110802018297.

[66] P. Falcone, F. Borrelli, J. Asgari, H. E. Tseng and D. Hrovat, 'Predictive Active Steering Control for Autonomous Vehicle Systems', *IEEE Transactions on Control Systems Technology*, vol. 15, pp. 566–580, May 2007.

[67] O. Barbarisi, G. Palmieri, S. Scala and L. Glielmo, 'LTV-MPC for Yaw Rate Control and Side Slip Control with Dynamically Constrained Differential Braking', *European Journal of Control*, vol. 15, no. 3, pp. 468–479, Jan. 2009, ISSN: 0947-3580. DOI: 10.3166/ejc.15.468-479.

[68] M. Ataei, A. Khajepour and S. Jeon, 'Model Predictive Control for integrated lateral stability, traction/braking control, and rollover prevention of electric vehicles', *Vehicle System Dynamics*, vol. 58, no. 1, pp. 49–73, Jan. 2020, ISSN: 0042-3114. DOI: 10.1080/00423114.2019.1585557.

[69] B. Zhu, Q. Piao, J. Zhao and L. Guo, 'Integrated chassis control for vehicle rollover prevention with neural network time-to-rollover warning metrics', *Advances in Mechanical Engineering*, vol. 8, no. 2, p. 168 781 401 663 267, Feb. 2016, ISSN: 1687-8140, 1687-8140. DOI: 10.1177/1687814016632679.

[70] H. Ohno, T. Suzuki, K. Aoki, A. Takahasi and G. Sugimoto, 'Neural network control for automatic braking control system', *Neural Networks*, vol. 7, no. 8, pp. 1303–1312, Jan. 1994, ISSN: 0893-6080. DOI: 10.1016/0893-6080(94)90011-6.

[71] V. Ćirović, D. Aleksendrić and D. Smiljanić, 'Longitudinal wheel slip control using dynamic neural networks', *Mechatronics*, vol. 23, no. 1, pp. 135–146, Feb. 2013, ISSN: 0957-4158. DOI: 10.1016/j.mechatronics.2012.11.007.

[72] E. Velenis, D. Katzourakis, E. Frazzoli, P. Tsiotras and R. Happee, 'Steady-state drifting stabilization of RWD vehicles', *Control Engineering Practice*, vol. 19, no. 11, pp. 1363–1376, Nov. 2011, ISSN: 0967-0661. DOI: 10.1016/j.conengprac.2011.07.010.

[73] V. F. Dal Poggetto and A. L. Serpa, 'Vehicle rollover avoidance by application of gain-scheduled LQR controllers using state observers', *Vehicle System Dynamics*, vol. 54, no. 2, pp. 191–209, Feb. 2016, ISSN: 0042-3114. DOI: 10.1080/00423114.2015.1125005.

[74] L. Li, G. Jia, J. Chen, H. Zhu, D. Cao and J. Song, 'A novel vehicle dynamics stability control algorithm based on the hierarchical strategy with constrain of nonlinear tyre forces', *Vehicle System Dynamics*, vol. 53, no. 8, pp. 1093–1116, Aug. 2015, ISSN: 0042-3114. DOI: 10.1080/00423114.2015.1025082.

[75] D. Jagga, M. Lv and S. Baldi, 'Hybrid Adaptive Chassis Control for Vehicle Lateral Stability in the Presence of Uncertainty', in *2018 26th Mediterranean Conference on Control and Automation (MED)*, Jun. 2018, pp. 1–6. DOI: 10.1109/MED.2018.8442921.

[76] K. Nam, H. Fujimoto and Y. Hori, 'Lateral Stability Control of In-Wheel-Motor-Driven Electric Vehicles Based on Sideslip Angle Estimation Using Lateral Tire Force Sensors', *IEEE Transactions on Vehicular Technology*, vol. 61, no. 5, pp. 1972–1985, Jun. 2012, ISSN: 1939-9359. DOI: 10.1109/TVT.2012.2191627.

[77] M. Montani, T. Favilli, L. Berzi, R. Capitani, M. Pierini, L. Pugi and C. Annicchiarico, 'Esc on in-wheel motors driven electric vehicle: Handling and stability performances assessment', in *2020 IEEE International Conference on Environment and Electrical Engineering and 2020 IEEE Industrial and Commercial Power Systems Europe (EEEIC/I&CPS Europe)*, IEEE, 2020, pp. 1–6.

[78] Lorenzo Berzi, Tommaso Favilli, Edoardo Locorotondo, Marco Pierini and Luca Pugi, 'Real Time Models of Automotive Mechatronics Systems: Verifications on "Toy Models"', in *Advances in Italian Mechanism Science*, vol. 68, G. Carbone and A. Gasparetto-Springer International Publishing, 2019, pp. 141–148.

[79] J. de Santiago, H. Bernhoff, B. Ekergård, S. Eriksson, S. Ferhatovic, R. Waters and M. Leijon, 'Electrical Motor Drivelines in Commercial All-Electric Vehicles: A Review', *IEEE Transactions on Vehicular Technology*, vol. 61, no. 2, pp. 475–484, Feb. 2012, ISSN: 1939-9359. DOI: 10.1109/TVT.2011.2177873.

[80] R. de Castro, M. Tanelli, R. E. Araújo and S. M. Savaresi, 'Minimum-time manoeuvring in electric vehicles with four wheel-individual-motors', *Vehicle System Dynamics*, vol. 52, no. 6, pp. 824–846, Jun. 2014, ISSN: 0042-3114. DOI: 10.1080/00423114.2014.902973.

[81] C. Feng, N.-g. Ding, Y.-l. He, G.-y. Xu and F. Gao, 'Control allocation algorithm for over-actuated electric vehicles', *Journal of Central South University*, vol. 21, no. 10, pp. 3705–3712, Oct. 2014, ISSN: 2227-5223. DOI: 10.1007/s11771-014-2354-0.

[82] Luca Pugi, Tommaso Favilli, Lorenzo Berzi, Edoardo Locorotondo and Marco Pierini, 'Brake Blending and Optimal Torque Allocation Strategies for Innovative Electric Powertrains', in *Applications in Electronics Pervading Industry, Environment and Society*, vol. 573, S. Saponara and A. De Gloria, Springer International Publishing, 2019, pp. 477–483.

[83] C. LV, J. Zhang, Y. Li and Y. Yuan, 'Regenerative Braking Control Algorithm for an Electrified Vehicle Equipped with a By-Wire Brake System', in *SAE Technical Paper 2014-01-1791*, 2014.

[84] L. Berzi, T. Favilli, M. Pierini, L. Pugi, G. B. Weiß, N. Tobia and M. Ponchant, 'Brake Blending Strategy on Electric Vehicle Co-simulation Between MATLAB Simulink® and Simcenter Amesim™', in *2019 IEEE 5th International Forum on Research and Technology for Society and Industry (RTSI)*, 9, pp. 308–313. DOI: 10.1109/RTSI.2019.8895548.

[85] J. Jin, 'Modified Pseudoinverse Redistribution Methods for Redundant Controls Allocation', *Journal of Guidance, Control, and Dynamics*, vol. 28, no. 5, pp. 1076–1079, Sep. 2005. DOI: 10.2514/1.14992.

[86] S. Julier, J. Uhlmann and H. Durrant-Whyte, 'A new approach for filtering nonlinear systems', in *Proceedings of 1995 American Control Conference - ACC'95*, vol. 3, Seattle, WA, USA: American Autom Control Council, 1995, pp. 1628–1632, ISBN: 978-0-7803-2445-9. DOI: 10.1109/ACC.1995.529783.

[87] M. Guiggiani, *The Science of Vehicle Dynamics*. Dordrecht: Springer Netherlands, 2014. DOI: 10.1007/978-94-017-8533-4.

[88] D. P. Kroese, T. Brereton, T. Taimre and Z. I. Botev, 'Why the Monte Carlo method is so important today', *WIREs Computational Statistics*, vol. 6, no. 6, pp. 386–392, Nov. 2014, ISSN: 1939-5108, 1939-0068. DOI: 10.1002/wics.1314.

[89] 'Gurobi Optimizer Reference Manual', p. 969,

[90] S. Boyd, 'Convex Optimization', *Convex Optimization*, p. 67,

[91] J. Duchi, *Sequential convex programming, notes for ee364b: Convex optimization ii*, 2018.

[92] J. K. Subosits and J. C. Gerdes, 'From the Racetrack to the Road: Real-Time Trajectory Replanning for Autonomous Driving', *IEEE Transactions on Intelligent Vehicles*, vol. 4, no. 2, pp. 309–320, Jun. 2019, ISSN: 2379-8904, 2379-8858. DOI: 10.1109/TIV.2019.2904390.

[93] J. Sergers, *Analysis techniques for racecar data acquisition*. SAE, 2014.

[94] W. F. Milliken, D. L. Milliken *et al.*, *Race car vehicle dynamics*. Society of Automotive Engineers Warrendale, PA, 1995, vol. 400.

[95] H. Pacejka, *Tire and Vehicle Dynamics Ed. 3*. Elsevier Science, 2012.

[96] M. Veneri and M. Massaro, 'A free-trajectory quasi-steady-state optimal-control method for minimum lap-time of race vehicles', *Vehicle System Dynamics*, vol. 58, no. 6, pp. 933–954, 2020.

[97] F. Altche, P. Polack and A. de La Fortelle, 'A simple dynamic model for aggressive, near-limits trajectory planning', in *2017 IEEE Intelligent Vehicles Symposium (IV)*, Los Angeles, CA, USA: IEEE, Jun. 2017, pp. 141–147, ISBN: 978-1-5090-4804-5. DOI: 10.1109/IVS.2017.7995711.

[98] R. Rajamani, 'Vehicle dynamics and control springer', *Science*, pp. 357–384, 2006.

[99] *VI-CarRealTime 18.2 Web Help Documentation*, 2018.

[100] R. Bosch, *Bosch automotive electrics and automotive electronics: systems and components, networking and hybrid drive*. Springer Vieweg., 2014.

[101] *ISO 21994:2007-Passenger cars—Stopping distance at straight-line braking with ABS — Open-loop test method*.

[102] Economic Commission for Europe of the United Nations (UN/ECE), *Uniform provisions concerning the approval of passenger cars with regard to braking*, 2015.

[103] F. Alfatti, C. Annicchiarico and Capitani, 'Vehicle stability controller hil validation on static simulator', in *IOP Proceedings*, 2021, p. 8.

[104] J. Pancik and V. Benes, 'Emulation of wheel speed sensors for automotive electronic control unit', in *Industry 4.0: trends in management of intelligent manufacturing systems*, Springer, 2019, pp. 111–120.

[105] M. Hal, 'Is Vehicle Characterization in Accordance With Standard Test Procedures a Necessary Prerequisite for Validating Computer Models of a Test Vehicle?', 2014. DOI: 10.21427/D76604.

[106] J. J. Breuer, 'Analysis of driver-vehicle-interactions in an evasive manoeuvre-results of'moose test'studies', in *Proc. 16th ESV Conf., Paper*, 1998.

[107] *ISO3888-1:1999-Passenger Cars-Test Track for a Severe Lane-change Manoeuvre: Part 1: Double Lane-change.*

Acronyms

ABS Anti-lock Brake System 13, 14, 15, 16, 17, 57, 58, 59, 60, 60, 62, 64, 66, 66, 67, 68, 69, 71, 72, 94, 98, 112

ADAS Advance Driving Assistant System 2

AI Artificial Intelligence 1,10, 33

ANN Artificial Neural Network 7, 9, 10, 11, 16, 21, 25, 25, 26, 26, 29, 29, 33

BBW Brake By Wire 3, 4, 15, 19, 57, 58, 73, 73, 83, 93

BW By-Wire 1, 12, 16, 17, 92

CAN Controller Area Network 1, 5, 84, 84

CBA Cornering Brake Actuator 7, 19, 58, 59, 60, 72, 73, 112

CBC Cornering Brake Control 13, 58, 72, 112

CRT Car Real Time 5, 19, 21, 24, 25, 47, 48, 58, 63, 66, 72, 73, 78, 78, 97, 112

DDT Dynamic Driving Task 2

DoF Degree of Freedom 5, 11, 18

EBD Electric Brakeforce Distribution 13, 16, 17, 58, 72, 112

EKF Extended Kalman Filter 10

ESC Electronic Stability Control 12, 13, 17, 60, 72, 78, 86, 91, 92, 94, 94, 96, 112

EPS Electric Power Steering 5

ESP Electronic Stability Program 13, 15, 16, 83, 85, 85, 88, 91

EU European Union 1, 15

EV Electric Vehicle 14, 17

GPS Global Positioning System 18, 24

HiL Hardware in the Loop 5, 58, 91

IMU Inertial Measurement Unit 17, 18, 24, 59, 84, 102, 111

IWM In-Wheel Motor 14, 16, 17, 97

KF Kalman Filter 10

LP Linear Programming 12, 35, 36, 38, 43, 55

LQR Linear Quadratic Regulator 11, 12, 13, 16, 44, 44, 46, 46, 73, 73, 77, 78, 85, 85, 87, 89, 91, 97, 112

MPC Model Predictive Control 12, 14, 35, 37

MAE Mean Absolute Error 34
NMPC Non-linear Model Predictive Control 14, 16,57
ODD Operational Design Domain 2
OEDR Object and Event Detection and Response 2
PG Proving Ground 83
PID Proportional Integrative Derivative 13, 14, 15, 57, 63, 64,65, 112
QP Quadratic Programming 12, 55
RMSE Root Mean Square Error 30
RNN Recurrent Neural Network 10, 27, 102, 111
SAE Society of Automotive Engineers 2
SBW Steer By Wire 3, 83
SCP Sequential Convex Programming 12, 35, 41
SMC Sliding Mode Control 14, 73, 78, 83, 85, 85, 87, 89, 91
SWA Steering Wheel Angle 10, 11, 12, 18, 19, 25, 30, 36, 44, 50, 74, 90, 99, 111
SWD Sine With Dwell 78, 81
TV Torque Vectoring 16, 17, 83, 93, 112
UKF Unscented Kalman Filter 6, 10, 11, 21, 22, 25, 29, 30, 31, 34, 102, 111